Chemical Geology 618 (2023) 121221

Contents lists available at ScienceDirect

Chemical Geology

journal homepage: www.elsevier.com/locate/chemgeo

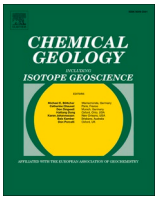

UID: The uranium isotope database

Haoyu Li *, François L.H. Tissot

The Isotoparium, Division of Geological and Planetary Sciences, California Institute of Technology, Pasadena, CA, USA

ARTICLE INFO

Editor: Christian France-Lanord

Keywords:
Uranium isotope
Database
Compilation
$^{238}U/^{235}U$
$\delta^{238}U$

ABSTRACT

As the parent element in the U-Pb and Pb-Pb radiochronometers, uranium (U) was one of the first heavy elements whose isotopic composition was carefully determined. Thought to be constant until the end of the 20th century, the ratio of the long-lived isotopes of U ($^{238}U/^{235}U$) has since been shown to be variable at the permil to sub-permil levels in natural materials. Today, the study of U isotopes has found applications in a variety of fields including geo/cosmochronology, oceanic paleoredox reconstruction, magmatic differentiation, environmental remediation, and forensic studies. With thousands of newly reported U isotopic data each year, a real need exists for a comprehensive U isotope database.

Here, we introduce a global, updatable, U isotope database (UID), which not only contains the most expansive, internally consistent U isotopic dataset to date (14,591 entries from more than 320 papers), but also includes all other sample data from the original publications, as well as the relevant metadata and sample information to facilitate further analysis. The UID is freely accessible and will be updated regularly. All data are normalized to the widely-used CRM-145 standard, and all assumptions used to convert the published data are explicitly detailed in the paper and the database itself. New data can be easily formatted and submitted for incorporation into the database. Using the UID we provide new recommended $\delta^{238}U$ values for certified U standards and geostandards and discuss important applications and future directions for U isotope studies.

1. Introduction

In 1939, Alfred O. Nier reported the first analysis of the isotopic composition of uranium (U), the heaviest primordial element, establishing the $^{238}U/^{235}U$ ratio as 139 (± 1%) (Nier, 1939). Since this pioneering work, the study of U isotopes has found applications in a wide range of scientific fields, including geochemistry, cosmochemistry, nuclear chemistry, and environmental engineering. Today, more than 320 papers reporting $^{238}U/^{235}U$ measurements have been published – most of them in the last two decades – and the U isotope field keeps on rapidly expanding, with on average over 20 new studies and 1270 new data generated each year since 2015 (Fig. 1).

With such numerous data, a real need for a global U isotope database has arisen. In fact, some efforts have been made to collect different subsets of U isotopic data, particularly in the context of paleoredox reconstruction (Tissot and Dauphas, 2015; Zhang et al., 2018a, 2020c; Andersen et al., 2020; Lu et al., 2020; Cao et al., 2020; Chen et al., 2021a; Wei et al., 2021). While these compilations are useful, they usually only focus on specific rock types (organic-rich mudrocks: Lu et al., 2020; carbonates, shales, and iron-rich rocks: Chen et al., 2021a), geological time periods (Permian-Triassic: Zhang et al., 2018a, 2020c; late Neoproterozoic-early Paleozoic: Wei et al., 2021) or event (Shuram excursion: Cao et al., 2020). Even when more global compilations are undertaken (*e.g.*, Tissot and Dauphas, 2015), they rapidly become obsolete as new data gets published, but the compilations are not updated. Beyond the U isotope data, these datasets generally include only a limited amount of relevant information/data for each sample. As a result, when attempting to use these existing compilations, users often lack sufficient related information to contextualize the data.

To address the need for a global U database as well as the short comings of available compilations, we introduce the UID: a comprehensive, updatable, uranium isotope database, in which all $^{238}U/^{235}U$ data published over an 80-year period have been compiled and consistently (and transparently) renormalized relative to the CRM-145 standard. At this writing, the UID, which is freely accessible at: https://isotoparium.org/uid, contains already over 14,000 data point. To preserve the potential for data analysis, all other available metadata from the original publications were also included in the database, such as sample type, concentrations (*e.g.*, major and trace elements), other isotopic data (*e.g.*, $\delta^{98/95}Mo$), or measurement technique.

* Corresponding author.
E-mail address: haoyu.li@caltech.edu (H. Li).

https://doi.org/10.1016/j.chemgeo.2022.121221
Received 10 February 2022; Received in revised form 21 August 2022; Accepted 15 November 2022
Available online 24 November 2022

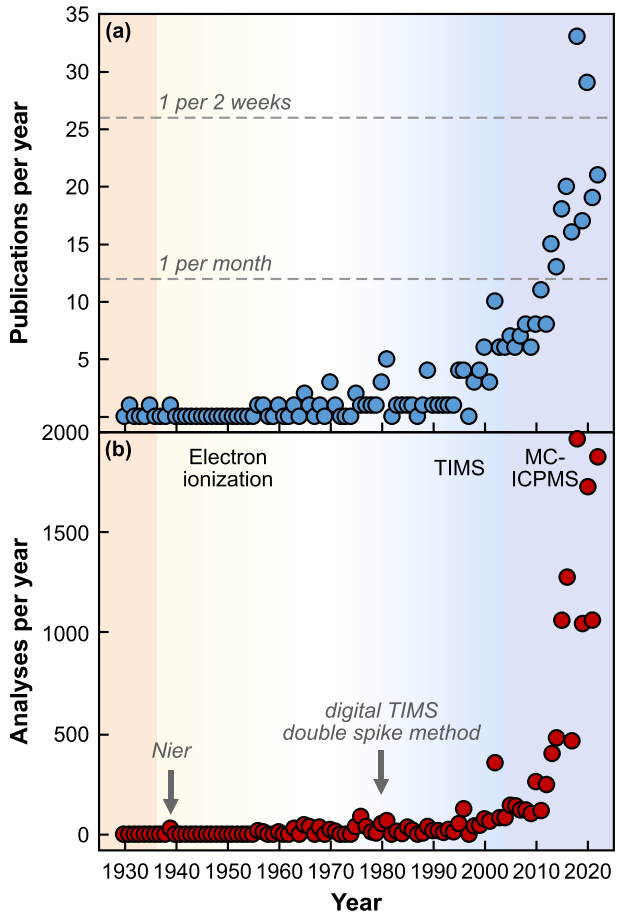

Fig. 1. (a) The number of publications per year reporting $^{238}U/^{235}U$ data through time. The dashed lines represent the number of papers that would be published if one paper on U isotopes was published every month (12 papers) and every two weeks (26 papers). (b) The number of $^{238}U/^{235}U$ analyses published per year. The advent of MC-ICP-MS in the early 2000s made possible to resolve small $^{238}U/^{235}U$ variations and led to the exponential growth of U isotopic studies. (Updated Dec. 2022)

Below, we first briefly review the evolution of U isotope measurements over time before describing the structure and content of the database, as well as the normalization procedures for U isotopic compositions. We then use the UID to provide a compilation of recommended $\delta^{238}U$ values for certified U standards and geostandards (*i.e.*, reference materials). Finally, we conduct a brief review of U isotopic studies according to their various applications and discuss important future directions of research for the field.

2. A brief history of U isotope measurements

Initially motivated by the discovery of the naturally occurring radioactive decay chains of ^{238}U and ^{235}U (at the time known as U_I and AcU, respectively), uranium was amongst the first elements to see its isotopic composition carefully characterized. Using spark-source mass-spectrography, Aston (1931) determined that ^{235}U accounted for at most 2-3 % of U atoms, and Dempster (1935) moved this limit down to only 1 %. The first quantitative determination of the isotopic composition of U, however, was made by Nier (1939) who, using a unique mass spectrometer he had just developed (Nier, 1938), reported in U ore samples a $^{238}U/^{235}U$ ratio of 139 (1% relative error), and a $^{238}U/^{234}U$ of 17,000 (10% relative error). Following this seminal work, early studies of U isotopes mainly focused on ore deposits (Lounsbury, 1956; Senftle et al., 1957; Hamer and Robbins, 1960; Smith, 1961; Rosholt et al., 1963, 1965; Lancelot et al., 1975; Cowan and Adler, 1976), whose unusually high U concentrations enabled high-precision analyses despite the large quantity of U required, which led to the discovery of the first, and so far only, known natural reactor of Oklo (Gabon) (Baudin et al., 1972; Bodu et al., 1972; Neuilly et al., 1972; Lancelot et al., 1975). Although some attempts were made to investigate the U isotopic composition of lunar samples and meteorites, the precision was generally insufficient to resolve any variation (Rosholt and Tatsumoto, 1970, 1971; Tatsumoto and Rosholt, 1970; Shimamura and Lugmair, 1981).

As for other heavy elements, the introduction of digital Thermal Ionization Mass Spectrometer (TIMS) instruments was a transformative technological advance in U isotopic analysis (*e.g.*, Wasserburg et al., 1969). The improved precision and sensitivity of digital instruments enabled permil level precision to be achieved for nanogram quantities of sample U. This development allowed U isotope analysis to grow beyond the study of U-rich materials and to be applied in a wider range of fields. This was particularly important in cosmochemistry, where earlier claims of extremely high ^{235}U excess in meteorites and their inclusions (*e.g.*, Arden, 1977; Tatsumoto and Shimamura, 1980) were then systematically reassessed and found to be the results of analytical artefacts rather than evidence of a high abundance of live ^{247}Cm in the early solar system (Chen and Wasserburg, 1980, 1981a, b, c; Chen, 1988). Using the same instrument, Chen et al. (1986) later determined in a seminal study the U isotope composition of seawater.

The revolution, however, that precipitated U isotope analysis into the age of high-precision (better than ~0.1 ‰, see Tissot and Ibañez-Mejia, 2021), was the appearance in the early 2000s of Multi-Collector Inductively Coupled Plasma Mass Spectrometer (MC-ICP-MS). The ability of MC-ICP-MS instruments to resolve isotopic variations at the sub-permil level marks the start of the field of so-called "stable" U isotopes ($^{238}U/^{235}U$, expressed as $\delta^{238}U$ in δ notation), which is investigating non-radiogenic and non-fissiogenic U isotopic fractionation that occurred during geo(bio)chemical cycles/processes. Initial studies reported resolvable natural U isotopic variations in a range of terrestrial environments (Stirling et al., 2007; Weyer et al., 2008). This discovery challenged the conventional assumption in the field of geochronology of a homogenous and constant $^{238}U/^{235}U$ ratio (assumed to be equal to 137.88, Steiger and Jäger, 1977), and thus highlighted the importance of measuring $^{238}U/^{235}U$ ratios when attempting to obtain high-precision ages via Pb-Pb dating (Amelin et al., 2010, 2011; Brennecka et al., 2010b, 2015; Bouvier et al., 2011a, b; Larsen et al., 2011; Brennecka and Wadhwa, 2012; Connelly et al., 2012; Iizuka et al., 2014; Goldmann et al., 2015; Spivak-Birndorf et al., 2015; Bollard et al., 2017; Tissot et al., 2017; Brennecka et al., 2018; Merle et al., 2020). The prevalence of U isotopic variations in low-temperature surface environments, and in particular the ~1 ‰ heavier U isotope composition of reduced sediments relative to seawater, suggested that U isotopes could be used as a paleoredox proxy to reconstruct the extent of oceanic anoxia. Indeed, the magnitude and direction of these fractionations matched those expected for Nuclear Field Shift effects during exchange reactions between oxidized and reduced U (Bigeleisen, 1996; Schauble, 2007; Abe et al., 2008) and an extensive body of work in both natural and lab-controlled environments soon confirmed that redox reactions could lead to significant U isotopic fractionation in natural materials (Stirling et al., 2007, 2015; Basu et al., 2014, 2015, 2020; Murphy et al., 2014; Stylo et al., 2015b; Wang et al., 2015a; Brown et al., 2016, 2018; Jemison et al., 2018). Today, U is arguably the most widely used paleoredox proxy (see review in Zhang et al., 2020b), and methods are being developed to ensure the most consistent and robust quantitative assessment of marine anoxia using U isotopes (Kipp and Tissot, 2022; Pimentel-Galvan et al., 2022). Because the magnitude of mass-dependent fractionation decreases with increasing temperature, U isotope effects have traditionally been assumed to be negligible at magmatic temperatures. Yet, modern instrumentation enables the resolution of minor $\delta^{238}U$ variations in igneous rocks, and studies have started to investigate the potential of U isotopes as tracers of magmatic processes in bulk rocks (Andersen et al.,

2015; Avanzinelli et al., 2018; Casalini, 2018; Freymuth et al., 2019; Gaschnig et al., 2021; Telus et al., 2012; Tissot et al., 2017), and even single-crystals of accessory minerals (Tissot et al., 2019; Yamamoto et al., 2021). Besides geochemical applications, U isotopes are also used as tracer of U contamination/remediation in environmental engineering (Rademacher et al., 2006; Bopp et al., 2010; Shiel et al., 2013, 2016; Basu et al., 2014, 2015; Murphy et al., 2014; Stylo et al., 2015a; Wang et al., 2015a,b; Brown et al., 2016; Placzek et al., 2016; Dang et al., 2016; Jemison et al., 2018; Lefebvre et al., 2019, 2021, 2022) and have long-standing importance in nuclear chemistry and forensic studies (Lancelot et al., 1975; Sus et al., 1979; De Laeter et al., 1980; Holliger and Devillers, 1981; Joshi et al., 1983; Hamilton and Stevens, 1985; Curtis et al., 1989; Loss et al., 1989; Bros et al., 1996; Hidaka and Holliger, 1998; Hidaka et al., 1999; Boulyga et al., 2000; Ejnik et al., 2000; Fernández-Díaz et al., 2000; Hidaka and Gauthier-Lafaye, 2000; Sobotovich and Bondarenko, 2001; Horan et al., 2002; Howe et al., 2002; Pazukhin and Rudya, 2002; Schramel, 2002; Warneke et al., 2002; Yamamoto et al., 2002; Danesi et al., 2003a, b; Fujikawa et al., 2003; Christensen et al., 2004; Horie et al., 2004; Tamborini, 2004; Al-Zamel et al., 2005; Parrish et al., 2006; Minteer et al., 2007; Kikuchi and Hidaka, 2009; Lloyd et al., 2009; Sahoo et al., 2009; Awudu and Darko, 2011; Marin et al., 2013; Pöml et al., 2013; Tripathi et al., 2013; Meyers et al., 2014; Kikawada et al., 2015; Krachler et al., 2018; Stebelkov et al., 2018; Mishra et al., 2019; Veerasamy et al., 2020).

3. Guide to the UID database

3.1. Data source and general considerations

The UID aims to gather all published $^{238}U/^{235}U$ data, as well as any supporting sample metadata to facilitate data contextualization and interpretation. The UID focuses on $^{238}U/^{235}U$ ratios, so publications only containing ^{234}U data are not included. To the best of our knowledge, all available data was incorporated in the UID. For the sake of completeness, no attempt to screen the resolution or quality of the data was done. If the data were transcribed from tables in the main text or supplements, the table number is given in the UID. For U isotopic data, the UID includes both the original data from publications and the normalized data following the method described in *Section 4.2*. The supporting metadata combines both sample information and geochemical data, which can be quite extensive for some samples.

3.1.1. UID ID

To avoid confusion caused by inconsistent nomenclatures, each sample in the UID is assigned a unique ID along with its original sample name in the publication. The UID ID is composed of three sections separated by hyphens (*e.g.,* 2021-CRM-T001). The first section is the publication year. The second part combines the first initial of the first three authors' surnames (*e.g.,* CRM represents Chen, Romaniello, and McCormick). For papers with fewer than three authors, this section contains the first initial of all authors. In some rare cases where three letters were insufficient to distinguish between articles published in the same year by the same research group, the first initial of the fourth author's surname was added to the second section to ensure the uniqueness of the UID ID. The last section is separated into two components to represent each data point. The letter specifies the sub-database category (S = Standard, T = Terrestrial, M = Meteorite, E = Experimental, F = Forensic, and P = Precision), and the three-digit number denotes the sample number within that category. Using the nomenclature given above, each sample in the UID has a unique identification, with no duplicates.

3.1.2. Methodology

This section gathers information on the standard, spike (if applicable), and mass spectrometric technique used, since the methodology employed influences the achieved precision and data reduction. Detailed information about standards and spikes are described in *Sections 3.2.2 and 3.2.9*. For mass spectrometry, we included the instrument's type (*e.g.,* TIMS, MC-ICP-MS) and model (*e.g.,* NuPlasma, ThermoFisher Neptune), and for ICPMS analyses, details on the desolvating nebulizer (if applicable), and cones combination. The most extensively used instruments for high-precision U isotope measurements in geochemistry are the Neptune and Neptune *Plus* (ThermoFisher) and the Nu Plasma MC-ICP-MS. The range of applications of other types of mass spectrometers are discussed in *Section 5.2.1*, and the abbreviations used in these techniques are listed in Table 1. The sensitivity of measurements can be greatly influenced by sample introduction systems. The highest precision U isotope determinations use liquid sample introduction. Membrane desolvating nebulizer systems can both enhance the sensitivity up to tenfold and significantly reduce solvent-based interferences. Meanwhile, sensitivity is also affected by the cones combination, with the highest sensitivities achieved with a combination of a Jet sample cone and an X-skimmer cone.

3.1.3. Reference

The source publication details are provided for each sample, using a short citation style composed of the author(s) name(s), the year of publication, and the abbreviated journal name. A full version of the bibliography is included in the *Reference* tab of the UID (*Section 3.2.1*).

3.1.4. Assumptions

Because not all studies report U isotope data against the same standard, or in the same way ($\delta^{238}U$ values vs absolute ratios), a clear and transparent normalization algorithm stating what assumptions have been made is critical. In the *Assumptions* columns, we included any original assumptions made by the authors in the original publication, as well as those we made during data normalization. These pertain to the absolute or relative compositions of U reference materials, in house standards or important solar system reservoirs. These assumptions are numbered and summarized in the *Assumptions* tab of the UID (see *Section 3.2.8*). The normalization algorithms are described in *Section 4.2*. Users can easily renormalize the UID data by simply adjusting the input numbers in the *Assumptions* tab of the UID.

3.2. Structure of the database

The UID consists of 10 spreadsheets. The first six, named *Standard*, *Terrestrial*, *Meteorites*, *Experimental*, *Forensic*, and *Precision*, are sub-databases containing the U isotopic data. These categories were chosen to be as independent and unambiguous as possible, and they are non-overlapping, meaning that no data is duplicated between sub-

Table 1
Acronyms for terminologies in technique column

Acronyms	Terminology
MC	Multi-Collector
SC	Single Collector
HR	High Resolution
DF	Double Focusing
Q	Quadrupole
SF	Sector Field
LA	Laser Ablation
FT	Fission Track
SN	Solution Nebulization
DRC	Dynamic Reaction Cell
HEX	Hexapole Collision Cell
ICP	Inductively Coupled Plasma
MS	Mass Spectrometer
SIMS	Secondary-Ion Mass Spectrometer
TIMS	Thermal Ionization Mass Spectrometer
OES	Optical Emission Spectrometer
GRS	Gamma Ray Spectrometer
NAA	Neutron Activation Analysis
SHRIMP	Sensitive High Mass-Resolution Ion Microprobe

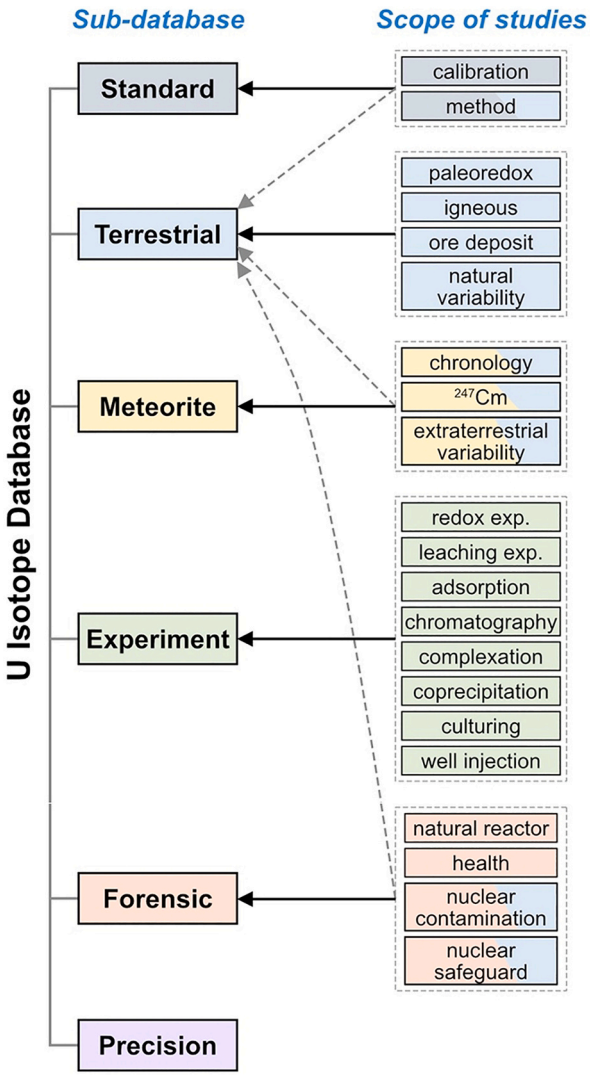

Fig. 2. The UID structure, illustrating the relationships between subdatabases and the scope of U isotopic studies. The solid arrows indicate that the majority of data from papers in a given field of study are distributed to the linked subdatabase, whereas the dash arrows indicate only a minor contribution.

databases (Fig. 2). The remaining four tabs, named *References*, *Assumptions*, *Spike*, and *Constants*, provide supplementary information for the database.

All samples were distributed into the various subdatabases, using a set of standardized criteria based on the sample type and the scope of the study (Fig. 2). This not only minimizes ambiguity, but also allows users to rapidly isolate all publications/data within a major theme (*e.g.,* chronology, paleoredox, forensic etc.), and build custom-compilations for future studies. For each subdatabase, definitions and descriptions of selected data components are included in Table A1-5.

3.2.1. *References*

The *References* table contains the full bibliographic information for publications in the database, including the publication's UID ID, short reference, full reference, DOI link, area of study, the number of U data it reported, the name and email of the corresponding author, and whether the authors of the original publication have reviewed the UID entry. The UID ID is composed of the first two parts of the UID ID of each data point (*e.g.,* 2021-CRM-). The short reference is given as Author-Year-Journal, whereas the full reference includes author(s) name(s), the publication year, the publication's title, the journal/book title, volume number/book chapter, and the article number or pagination where applicable. The DOI links for articles are placed in a separate column for rapid redirection to the publisher's page. The main area of study relevant for the publication is then listed, allowing users to filter the papers based on specific applications. Finally, a summary of the total number of data points in each article is given, and their distribution throughout subdatabases, which will assist users in locating data in subdatabases.

Some studies only display their U isotopic data graphically. These publications are listed at the end of the publication table since they do not have a data table to transcribe and incorporate into the database. In this scenario, only a brief reference, a complete reference, a DOI link, and the area of study are provided. We encourage all researchers to submit such data to the UID to make it more complete and useful to the community.

3.2.2. *Standard*

The *Standard* table contains three types of samples: (i) isotopically certified U standards, (ii) concentration standards, and (iii) other U materials such as metal, compound, reagent, and U-bearing glass. Standard measurements mainly have three purposes: quality control, standard calibration, and method development. In the first scenario, secondary standards are measured alongside unknown samples during an analytical session, and the data is reported to demonstrate the accuracy of the measurements. For standard calibration, on the other hand, the most accurate and precise isotopic compositions of standards are obtained by performing repeated measurements with well-established techniques. We provide recommended $\delta^{238}U$ on these widely used standards by integrating data from these two purposes (*Section 5.1*). Another use of standard analysis is to evaluate the performance of newly developed methods. These data are typically less precise because the tested method is designed for specific applications that may not demand high precision. For method development studies, we incorporated the investigated methodologies and technical innovations in the *Standard* table as well.

3.2.3. *Terrestrial*

The *Terrestrial* table contains U isotope data for virtually all natural solid and liquid terrestrial samples, including common geostandard materials. The only exception is data from the Oklo reactors, which have been included in the Forensic table, along with other data on depleted uranium samples. Solid samples include igneous, sedimentary, metamorphic rocks, and minerals, while liquid samples mainly contain seawaters, lake waters, river waters, and pore waters. This subdatabase includes metadata about the location, age, lithology, concentration, concentration ratio, the isotopic composition of other systems, and other relevant information.

3.2.4. *Meteorite*

The *Meteorite* table contains U isotope data for all extraterrestrial materials including meteorites, their components, and lunar samples. This subdatabase is named meteorite rather than extraterrestrial to avoid confusion during UID assignment for sample in this subdatabase and the *Experimental* subdatabase (as both start with the same letter).

3.2.5. *Experimental*

The *Experimental* table contains all data from lab and field-controlled experiments. For lab-controlled experiments, the table provides the experimental setup information. The field-controlled metadata also includes the locations of the sites.

3.2.6. *Forensic*

The *Forensic* table contains the U isotope data of samples affected by anthropogenic activities, as well as the data from the natural fission reactor of Oklo (Gabon). This table thus gathers all data relevant to nuclear contamination, nuclear safeguard, and health physics studies.

3.2.7. Precision

In MC-ICP-MS studies, it is common practice to report the average value and standard deviation of self-bracketed standard measurements. By definition, such an exercise should return a $\delta^{238}U$ value of 0 (the standard is identical to itself, and no deviation should be found), and the uncertainty can be used to quantify the external reproducibility of the measurements. Indeed, the standard being measured tens of times per analytical sessions, the dispersion in its data is more representative compared to that of the samples, which are only measured a handful of times. We have gathered these data in the *Precision* table, which can be used to assess some aspects of the data quality.

3.2.8. Assumptions

The *Assumptions* spreadsheet contains the assumptions used in the original publications reporting the data, as well as those used for normalization in the database. We divided the assumptions into two categories: assumptions for ^{238}U and assumptions for ^{234}U. For ^{238}U, assumptions pertain to historical name changes (*e.g.,* NBS SRM960 was recertified and renamed NBL CRM-112a in 1987), $^{238}U/^{235}U$ absolute ratios, $\delta^{238}U$ values of standards relative to one another, and alpha activity ratio ($^{233}U/^{238}U$). For ^{234}U, assumptions pertain to the half-lives of ^{234}U and ^{238}U as they determine the $^{234}U/^{238}U$ ratio at secular equilibrium, $^{234}U/^{238}U$ of standards (certified values and $^{234}U/^{238}U$ compositions applied in the publication). How these assumptions play into the data normalization is discussed in *Section 4*.

3.2.9. Spikes

For elements with 4 isotopes or more, the double spike technique (Dodson, 1963) is the gold-standard to achieve high-precision isotopic measurements, as it allows to correct for mass fractionation arising from sample purification and mass spectrometry. While U only has 3 naturally occurring isotopes, the introduction of a man-made ^{233}U-^{236}U double spike in the early 1980s highly improved the precision of U isotopic analysis (Chen and Wasserburg, 1980, 1981b, c). Nowadays, the most widely used double spike is the commercially available IRMM-3636 ($^{233}U/^{236}U = 1.01906(16)$, Verbruggen et al., 2008). Nevertheless, a range of in-house double spikes, with variable U isotopic compositions, have been and/or still are being used (Tatsumoto and Shimamura, 1980; Chen and Wasserburg, 1980, 1981b, c; Shimamura and Lugmair, 1981; Bros et al., 1993; Cheng et al., 2000, 2013; Stirling et al., 2005, 2007; Rademacher et al., 2006; Parrish et al., 2006; Weyer et al., 2008; Bopp et al., 2009, 2010; Amelin et al., 2010; Brennecka et al., 2010b, 2011a, b; Richter et al., 2010; Bouvier et al., 2011b; Shiel et al., 2013; Chernyshev et al., 2014; Holmden et al., 2015; Wang et al., 2015a, 2016; Noordmann et al., 2016; Wei et al., 2018, 2020, 2021). Because the composition of a double-spike is an essential factor controlling the achievable precision of the measurement (Rudge et al., 2009; Marquez and Tissot, 2022), the isotopic composition of the IRMM-3636 and all in-house spikes can be found in the *Spikes* table. A specific abbreviation was given to each spike (*e.g.,* 36CW80): the first two digits represent the enriched isotopes in this spike (*i.e.,* ^{233}U and ^{236}U in this case); the letters in the middle stand for the initials of the authors' last name using the same logic as the UID ID; the last part denotes the year of publication. The U isotopic compositions were converted to $^{i}U/^{236}U$, where i is isotope 233, 234, 235, or 238.

3.2.10. Constants

The *Constants* tab provides a summary of all constants used to homogenize concentration data. In the UID, we report elemental concentrations. This required converting originally published oxide concentrations, which was done by calculating an oxide to element conversion factor (Table C1 in the *Constants* spreadsheet) using the atomic masses from the 2013 IUPAC technical report (Meija et al., 2016). For concentration ratios, Table C2 provides the atomic masses to convert molar ratios to weight ratios. Table C3 shows the abundance of specific isotopes to transform the concentration ratios of the isotopes of two different elements to the elemental ratio. Table C4 shows the atomic masses of uranium isotopes to convert mass fractions of two U isotopes to atomic U isotopic compositions (*Section 4.3*).

3.3. Data retrieval

One of the primary applications of the UID is as a quick-reference library for U isotope research. To help users extract data, a quick search panel is provided right after the sample name (Column F-M in each subdatabase) in which the samples $\delta^{238}U$, $^{238}U/^{235}U$, $\delta^{234}U$, and ($^{234}U/^{238}U$) values are gathered, along with their associated uncertainties. Users can search for specific data in the database using either the scope of studies or sample types. Drop-down menus are available in the subdatabases and reference spreadsheets to implement this functionality. This filtering system uses criteria to subdivide the subdatabases, which are defined based on the properties of each subdatabase (Table 2).

4. Data representation

4.1. Notations for uranium isotopes

The $^{238}U/^{235}U$ data are reported both as absolute ratio and in δ-notation (permil unit, ‰), which is defined as:

$$\delta^{238}U = \left(\frac{{}^{238}U/{}^{235}U_{smp}}{{}^{238}U/{}^{235}U_{std}} - 1 \right) \times 1000 \quad (1)$$

To ensure the internal consistency of the UID, all $\delta^{238}U$ data have been renormalized relative to the CRM-145 standard (a solution made from an aliquot of the CRM-112a metal), and $^{238}U/^{235}U$ ratios are calculated assuming that CRM-145 has the same isotopic compositions as CRM-112a with a $^{238}U/^{235}U$ ratio of 137.837 as reported by the inter-laboratory calibration of Richter et al. (2010).

The $^{234}U/^{238}U$ data are reported as absolute ratios, ($^{234}U/^{238}U$) (the brackets denote activity ratios) and $\delta^{234}U$, the latter two being defined as:

$$\left({}^{234}U/{}^{238}U\right) = \frac{{}^{234}U/{}^{238}U_{smp}}{{}^{234}U/{}^{238}U_{sec.eq}} \quad (2)$$

$$\delta^{234}U = \left[\left({}^{234}U/{}^{238}U\right) - 1\right] \times 1000 \quad (3)$$

In Eq. (2), $^{234}U/^{238}U_{sec.\ eq}$ denotes the secular equilibrium $^{234}U/^{238}U$ ratio, which is the ratio of the decay constants of ^{238}U and ^{234}U, and was calculated here using the recently determined decay constants from Cheng et al. (2013): $\lambda_{238}/\lambda_{234} = (1.55125 \times 10^{-10})/(2.8220 \times 10^{-6}) = 5.4970 \times 10^{-5}$. For both $^{238}U/^{235}U$ and $^{234}U/^{238}U$ data, errors were adjusted to 2SD, or 2SE when applicable.

4.2. Normalization of $^{238}U/^{235}U$ data

The path to data normalization depends on whether the original publication reported $\delta^{238}U$ values or absolute $^{238}U/^{235}U$ ratios. These two scenarios are presented in detail below and summarized in a flowchart in Fig. 3.

4.2.1. When $\delta^{238}U$ is reported in the literature

For studies reporting $\delta^{238}U$ values against standards other than CRM-145, a correction was applied to the originally published data to account for the offset between the U isotopic composition of the standard used in the study and that of the CRM-145. This correction is simply implemented as:

$$\delta^{238}U_{UID} = \delta^{238}U_{CRM145} = \delta^{238}U_{published} + \Delta^{238}U_{STD-CRM145} \quad (4)$$

Table 2
Sorting criteria in the UID and subdatabases

Criteria			Lists
Criterion 1	Criterion 2	Criterion 3	
All Subdatabases			
Scope of study			magmatic, ore deposit, paleoredox, natural variability
			^{247}Cm, chronology, extraterrestrial variability
			adsorption, chromatography, complexation, coprecipitation, culturing, leaching experiment, redox experiment, well injection
			health, natural reactor, nuclear contamination, nuclear safeguard
			method, calibration
Standard Subdatabase			
Purpose			quality control, method development, calibration
Sample type	standard		name of the standard (*e.g.,* CRM-145)
	conc std		Ricca, single elemental standard
	other		compound, metal, reagent, U-bearing glass
Terrestrial Subdatabase			
Sample type	solid	igneous	basalt, basaltic andesite, core sample, glass, granite, granitoids, lamproites, lava, lherzolite, oceanic crust, scoria, shoshonite, tonalite
		sedimentary	carbonate, carbonate-bio, chimney, clay, evaporite, Fe oxide, Fe-Mn curst, Fe-Mn deposit, hydrothermal vein, iron formation, marl, Mn crust, mudrock, mudstone, organic-rich sediments, paleosol, quartzite, reduction spheroid, sandstone, seafloor, sediments, shale, siliciclastic sediments, siltstone, soil
		metamorphic	gneiss, milonite
		mineral	apatite, baddeleyite, monazite, pyrite, titanite, uraninite, xenotime, zircon
		ore	
		reference	name of the geostandard (*e.g.,* BCR-2)
	liquid		groundwater, hydrothermal water, lake water, pore water, river water, seawater
		reference	seawater
Extraterrestrial Subdatabase			
Meteorite classification	chondrite	carbonaceous	CB, CI1, CM2, CR2, CV3
		ordinary	H3, H3-6, H4, H5, H6, L/LL4, L/LL5, L/LL6, L3, L3.10, L4, L5, L6, LL3.6, LL6
		enstatite	EH3, EH4
	achondrite		Acapulcoite, Angrite, Aubrite, Eucrite, Howardite, iron meteorite, primitive, ungrouped
	lunar sample		
Precision Subdatabase			
Sample type			name of the standard (*e.g.,* CRM-145)

where $\delta^{238}U_{UID}$ is the δ^{238}U of the sample relative to CRM-145, $\delta^{238}U_{published}$ is the originally reported δ^{238}U relative to the standard used in the paper, and $\Delta^{238}U_{STD\text{-}CRM145}$ is the δ^{238}U offset between the standard and CRM-145. To ensure the self-consistency of the UID data, we compiled all published high-precision U isotopic measurements of widely (and less-widely) used standards and provide recommended $\Delta^{238}U_{STD\text{-}CRM145}$ values for these materials (Table 3 and *Section 5.1.1*).

In some studies, the authors already corrected the offsets between the standard(s) they used and CRM-145, but sometimes using different $\Delta^{238}U_{STD\text{-}CRM145}$ values (*e.g.,* Bopp et al., 2009, 2010; Dang et al., 2018). Since the δ^{238}U of a specific standard relative to CRM-145 is invariant (provided the standard is homogenous), and to ensure the self-consistency of the UID data, the offset applied in the original publications were undone, and the recommended $\Delta^{238}U_{STD\text{-}CRM145}$ (*Section 5.1.1*) were applied instead.

Because all data is corrected using a unique set of recommended $\Delta^{238}U_{STD\text{-}CRM145}$ values, we did not propagate the uncertainties of these offsets onto the final data. The error on δ^{238}U in the UID is thus the same as that reported in the literature because any conversion discussed above would not influence the measurement uncertainties.

From the δ^{238}U values and their associated errors, the absolute $^{238}U/^{235}U$ ratios in the UID are calculated as:

$$^{238}U/^{235}U_{UID} = \left(\delta^{238}U/1000 + 1\right) \times {}^{238}U/^{235}U_{CRM-145} \quad (5)$$

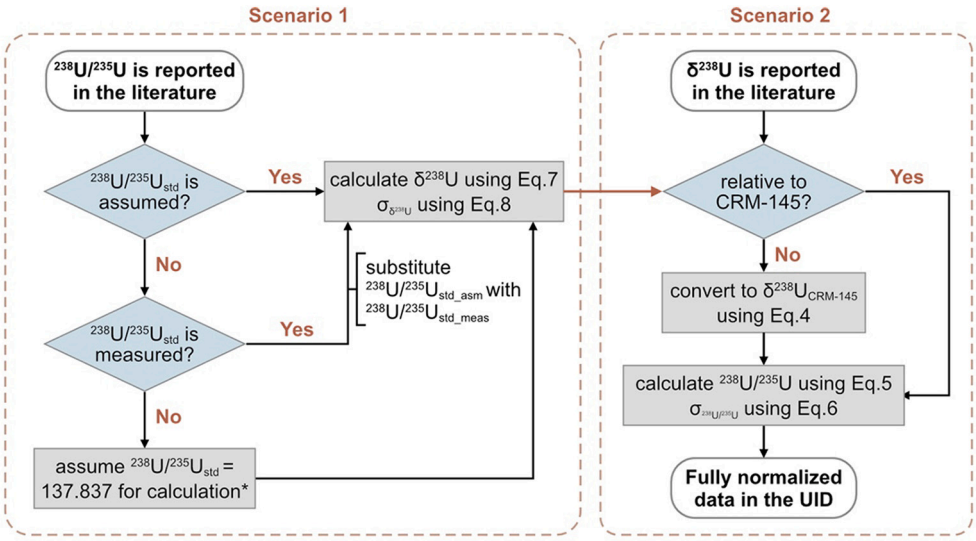

Fig. 3. Summary flowchart of the protocol for the normalization of $^{238}U/^{235}U$ data in the UID. *The $^{238}U/^{235}U_{std}$ comes from Richter et al. (2010). For publications before 2010, the data quality is generally insufficient to resolve the difference between the assumed value and the normalization using the 'consensus' value of 137.88.

$$\sigma_{^{238}U/^{235}U} = \left(\sigma_{\delta^{238}U} \Big/ 1000\right) \times {}^{238}U \Big/ {}^{235}U_{CRM-145} \tag{6}$$

where $^{238}U/^{235}U_{CRM\text{-}145}$ is the absolute $^{238}U/^{235}U$ ratio of CRM-145. In the UID, this value is taken as 137.837 (Richter et al., 2010).

4.2.2. When $^{238}U/^{235}U$ is reported in the literature

For studies reporting absolute $^{238}U/^{235}U$ ratios, the data is first converted to $\delta^{238}U$ values. If an assumption on the standard $^{238}U/^{235}U$ is provided in the original publication, $\delta^{238}U$ and the uncertainty on the sample data are calculated as:

$$\delta^{238}U = \left(\frac{{}^{238}U/{}^{235}U_{smp}}{{}^{238}U/{}^{235}U_{std\_asm}} - 1\right) \times 1000 \tag{7}$$

$$\sigma_{\delta^{238}U} = \left(\frac{\sigma_{^{238}U/^{235}U_{smp}}}{{}^{238}U/{}^{235}U_{std\_asm}}\right) \times 1000 \tag{8}$$

where $^{238}U/^{235}U_{smp}$ and $\sigma_{^{238}U/^{235}U_{smp}}$ are, respectively, the absolute ratio and associated error of the sample presented in the original publication; and $^{238}U/^{235}U_{std\_asm}$ is the absolute ratio of the standard assumed in the original publication. In some cases, the paper reported the $^{238}U/^{235}U$ without any assumption for the absolute ratio of the standard. If a standard with known isotopic composition was measured along with the samples, we used this measurement (*i.e.*, $^{238}U/^{235}U_{std\_meas}$) to substitute $^{238}U/^{235}U_{std\_asm}$ in Eq. (7) and (8). In the absence of a stated $^{238}U/^{235}U$ ratio for the standard, we assumed $^{238}U/^{235}U_{std\_asm} = 137.837$ (Richter et al., 2010). This assumption naturally holds for papers published after 2010. For papers before 2010, the quality of data is generally not good enough to resolve the difference between our calculation and the normalization using 137.88, the consensus ratio from Steiger and Jäger (1977). This additional assumption is clearly stated in the "Assumption for calculation" column for clarification. For each sample, the $\delta^{238}U$ value obtained was then renormalized to CRM-145, and used to recalculate the sample $^{238}U/^{235}U$ ratio and their uncertainty against the $^{238}U/^{235}U$ absolute ratio of CRM-145 using Eq. (5) and (6).

4.2.3. When both $\delta^{238}U$ and $^{238}U/^{235}U$ are reported in the literature

In this case, we used the same normalization strategy as presented in Section 4.2.1. The rationale is that the $\delta^{238}U$ value of a sample relative to a specific standard is invariant regardless of the assumed $^{238}U/^{235}U$ ratio of the standard.

4.2.4. Other circumstances

In addition to $\delta^{238}U$ and $^{238}U/^{235}U$, other notations have been used in the literature to report U isotopic compositions: namely, activity ratios, and epsilon notations. Table 4 lists the frequently used notations and their relationship to $\delta^{238}U$ values. For these notations, we converted them into $\delta^{238}U$ or $^{238}U/^{235}U$ at first, and then used the same approaches mentioned in Section 4.2.1 and 4.2.2 to conduct the normalization.

4.3. Normalization of $^{234}U/^{238}U$ data

While $\delta^{234}U$ and ($^{234}U/^{238}U$) are defined relative to secular equilibrium (*i.e.*, a theoretical value), in practice the majority of high-precision $^{234}U/^{238}U$ measurements are done using the sample-standard bracketing (SSB) method and calculated relative to a U isotopic standard. If the $^{234}U/^{238}U$ composition of the standard used in the paper is clearly stated, we can correct the offset between this value and the certified $^{234}U/^{238}U$ absolute ratio of the standard to ensure the consistency of the UID data. The formulas for this correction are slightly different depending on the information provided in the literature. The flowchart for the normalization protocol is illustrated in Fig. 4.

4.3.1. When $\delta^{234}U$ is reported in the literature

If the $^{234}U/^{238}U$ composition of the standard is stated in the literature, the corrected $\delta^{234}U$ of the samples in the database are calculated using the following formulas:

$$\delta^{234}U = \delta^{234}U_{published} + \delta^{234}U_{std\_cert} - \delta^{234}U_{std\_lit} \tag{9}$$

where $\delta^{234}U_{published}$ is the originally reported $\delta^{234}U$ value; $\delta^{234}U_{std\_lit}$ is δ value of the standard used in the literature; $\delta^{234}U_{std\_cert}$ is δ value of the standard derived from the standard's certificate. For CRM-145 ($^{234}U/^{238}U$ = 0.000052841, New Brunswick Laboratory, 2010), $(^{234}U/^{238}U)_{std\_cert}$ and $\delta^{234}U_{std\_cert}$ are defined as:

$$\left(^{234}U/^{238}U\right)_{std\_cert} = \frac{^{234}U/^{238}U_{std\_cert}}{^{234}U/^{238}U_{sec.eq}} = 0.9613 \tag{10}$$

Table 3
Summary of recommended $\delta^{238}U$ and $^{238}U/^{235}U$ of standards, relative to CRM-145.

Standard	$\delta^{238}U$ (‰)	$^{238}U/^{235}U$	n	MSWD	Comments
NU standards					
CRM-129	−1.709 ± 0.009	137.601 ± 0.001	39	0.60	Batch 1
	−1.48 ± 0.16	137.634 ± 0.021	2	n.a.	Batch 2
IRMM-3184	−1.14 ± 0.15	137.680 ± 0.021	2	n.a.	
IRMM-184	−1.160 ± 0.013	137.677 ± 0.002	15	0.85	
Ricca	−0.220 ± 0.014	137.807 ± 0.002	17	0.79	
Reimep-18a	−0.130 ± 0.005	137.819 ± 0.001	23	9.49[a]	Batch 1
	−0.26 ± 0.01	137.802 ± 0.002	2	n.a.	Batch 2
	0.12 ± 0.07	137.854 ± 0.010	1	n.a.	Batch 3
CRM-112a	−0.001 ± 0.006	137.837 ± 0.001	12	3.04	
CRM-145	0.01 ± 0.04	137.838 ± 0.005	4	n.a.	
SRM-950a	0.046 ± 0.008	137.843 ± 0.001	6	1.77	
EU standards					
U970	−999.9608 ± 0.0003	0.00540 ± 0.00004	1		
CRM-149	−999.5856 ± 0.0001	0.05712 ± 0.00001	1		
U900	−999.30086 ± 0.00004	0.09637 ± 0.00001	8		
U750	−999.7094 ± 0.0003	0.31573 ± 0.00004	4		
U630	−995.985 ± 0.001	0.5534 ± 0.0002	4		
IRMM-074-1	−992.747 ± 0.001	0.9998 ± 0.0003	1		
IRMM-199	−992.746 ± 0.001	0.9999 ± 0.0002	3		
U500	−992.74 ± 0.01	1.001 ± 0.002	46		
U200	−971.28 ± 0.25	3.96 ± 0.03	9		
U100	−934.7 ± 2.8	9.00 ± 0.38	9		
IRMM-2024	−863.77 ± 0.04	18.778 ± 0.005	1		
U050	−862.01 ± 0.94	19.02 ± 0.13	2		
IRMM-187	−846.70 ± 0.05[b]	21.130 ± 0.006	3		
U045	−846.70 ± 0.02	21.130 ± 0.003	9		
IRMM-2029	−835.31 ± 0.05	22.700 ± 0.007	1		
CRM-125	−828.49 ± 0.02	23.640 ± 0.002	9		
IRMM-2027	−826.09 ± 0.05	23.971 ± 0.007	1		
IRMM-2028	−806.93 ± 0.06	26.613 ± 0.008	1		
Reimep-18b	−794.48 ± 0.58	28.329 ± 0.080	1		
IRMM-2023	−785.87 ± 0.03	29.515 ± 0.005	1		
U030	−768.74 ± 0.26	31.876 ± 0.036	19		
IRMM-186	−764.23 ± 0.07	32.498 ± 0.010	1		
IRMM-2026	−717.48 ± 0.08	38.942 ± 0.011	1		
Reimep-18d	−699.1 ± 1.0	41.48 ± 0.14	1		
U020	−651.20 ± 0.62	48.078 ± 0.085	8		
IRMM-2025	−644.99 ± 0.10	48.934 ± 0.013	1		
IRMM-185	−638.251 ± 0.002	49.8624 ± 0.0002	4		
U015	−532.4 ± 8.0	64.5 ± 1.1	3		
U010	−284.81 ± 0.55	98.579 ± 0.076	21		
DU standards					
SPEX U Lot #14-163U	85.09 ± 0.30	149.566 ± 0.041	1		
SPEX CLU2-2Y	93.25 ± 0.56	150.691 ± 0.071	1		
U005	424.96 ± 0.93	196.41 ± 0.13	7		
IRMM-2021	646.90 ± 0.27	227.004 ± 0.037	1		
Reimep-18c	654.5 ± 2.3	228.05 ± 0.31	1		
Inorganic Ventures MSU-100 ppm	927.86 ± 0.92	265.73 ± 0.13	1		
Alfa ICP/DCP	1084.2 ± 3.6	287.28 ± 0.50	1		
Alfa ICP	1084.2 ± 5.3	287.27 ± 0.73	1		
Alfa AA	1085.6 ± 2.9	287.47 ± 0.40	1		
IRMM-183	1256.8 ± 1.2	311.06 ± 0.17	5		
Merck 170360	1643.2 ± 1.9	364.33 ± 0.27	1		
Aldrich AA	1673.1 ± 7.4	368.5 ± 1.0	1		
Assurance U (5% HNO_3)	1861.7 ± 6.3	394.45 ± 0.87	1		
Assurance U (2% HNO_3)	1957.0 ± 4.9	407.58 ± 0.68	1		
SRM-610	2039.8 ± 1.3	419.00 ± 0.19	40		
IRMM-2020	2461.8 ± 1.0	477.17 ± 0.14	1		
Inorganic Ventures CGU1-125mL	2449.8 ± 2.5	475.51 ± 0.34	1		
Perkin-Elmer N9303844	2633.1 ± 2.7	500.78 ± 0.29	1		
SPEX XSTC-3213	2694.9 ± 5.6	509.29 ± 0.78	1		
IRMM-2019	3324.9 ± 1.2	596.13 ± 0.17	1		
U0002	39390 ± 952	5567 ± 131	1		

[a] The MSDW of Reimep-18a represents the potential heterogeneity.
[b] The uncertainty on IRMM-187 represents the analytical error because the three measurements have the same $\delta^{238}U$ value.

Table 4
How published U isotope data are consistently renormalized into the UID

Reported	Expression	Conversion	Approach
$^{235}U/^{238}U$	Absolute atomic ratio	$^{238}U/^{235}U = \frac{1}{^{235}U/^{238}U}$	4.2.2
$(^{238}U/^{235}U)$	Alpha activity ratio	$^{238}U/^{235}U = (^{238}U/^{235}U)/(\lambda_{238}/\lambda_{235})$	4.2.2
$\varepsilon^{238}U$	$\varepsilon^{238}U = \left(\frac{^{238}U/^{235}U_{smp}}{^{238}U/^{235}U_{std}} - 1\right) \times 10000$	$\delta^{238}U = \varepsilon^{238}U/10$	4.2.1
$\delta^{235}U$	$\delta^{235}U = \left(\frac{^{235}U/^{238}U_{smp}}{^{235}U/^{238}U_{std}} - 1\right) \times 1000$	$\delta^{238}U = [1000/(\delta^{235}U + 1000)] \times 1000$	4.2.1
$\varepsilon^{235}U$	$\varepsilon^{235}U = \left(\frac{^{235}U/^{238}U_{smp}}{^{235}U/^{238}U_{std}} - 1\right) \times 10000$	$\delta^{238}U = [1000/(\varepsilon^{235}U/10 + 1000)] \times 1000$	4.2.1

$$\delta^{234}U_{std\_cert} = \left[\left(^{234}U/^{238}U\right)_{std\_cert} - 1\right] \times 1000 = -38.7‰ \quad (11)$$

From the corrected sample $\delta^{234}U$ value, the $^{234}U/^{238}U$ absolute ratio and its associated uncertainty are calculated as:

$$^{234}U/^{238}U = \left(\delta^{234}U/1000 + 1\right) \times {}^{234}U/^{238}U_{sec.eq\_lit} \quad (12)$$

$$\sigma_{^{234}U/^{238}U} = \left(\sigma_{\delta^{234}U}/1000\right) \times {}^{234}U/^{238}U_{sec.eq\_lit} \quad (13)$$

where $^{234}U/^{238}U_{sec.eq\_lit}$ is the absolute $^{234}U/^{238}U$ ratio at secular equilibrium used in the original publication to calculate the $\delta^{234}U$ value. If the original paper did not state the $^{234}U/^{238}U$ at secular equilibrium value used for calculation of $\delta^{234}U$ values, we assumed a value of 5.4970×10^{-5} (Cheng et al., 2013) for publications after 2013, 5.4891×10^{-5} (Cheng et al., 2000) for papers published between 2000 and 2013, and 5.472×10^{-5} (Chen et al., 1986) for papers published before 2000. Once again, we encourage all researchers to submit such missing data to the UID so we can address any erroneous assumptions and make the UID more complete and useful to the community.

To calculate $\delta^{234}U_{UID}$ and $(^{234}U/^{238}U)_{UID}$ in the database, we use the absolute $^{234}U/^{238}U$ ratio and its associated error obtained above (Eq 9 to 13):

$$\left(^{234}U/^{238}U\right)_{UID} = \frac{^{234}U/^{238}U}{^{234}U/^{238}U_{sec.eq}} \quad (14)$$

$$\sigma_{\left(^{234}U/^{238}U\right)} = \frac{\sigma_{^{234}U/^{238}U}}{^{234}U/^{238}U_{sec.eq}} \quad (15)$$

$$\delta^{234}U_{UID} = \left[\left(^{234}U/^{238}U\right) - 1\right] \times 1000 \quad (16)$$

$$\sigma_{\delta^{234}U} = \sigma_{\left(^{234}U/^{238}U\right)} \times 1000 \quad (17)$$

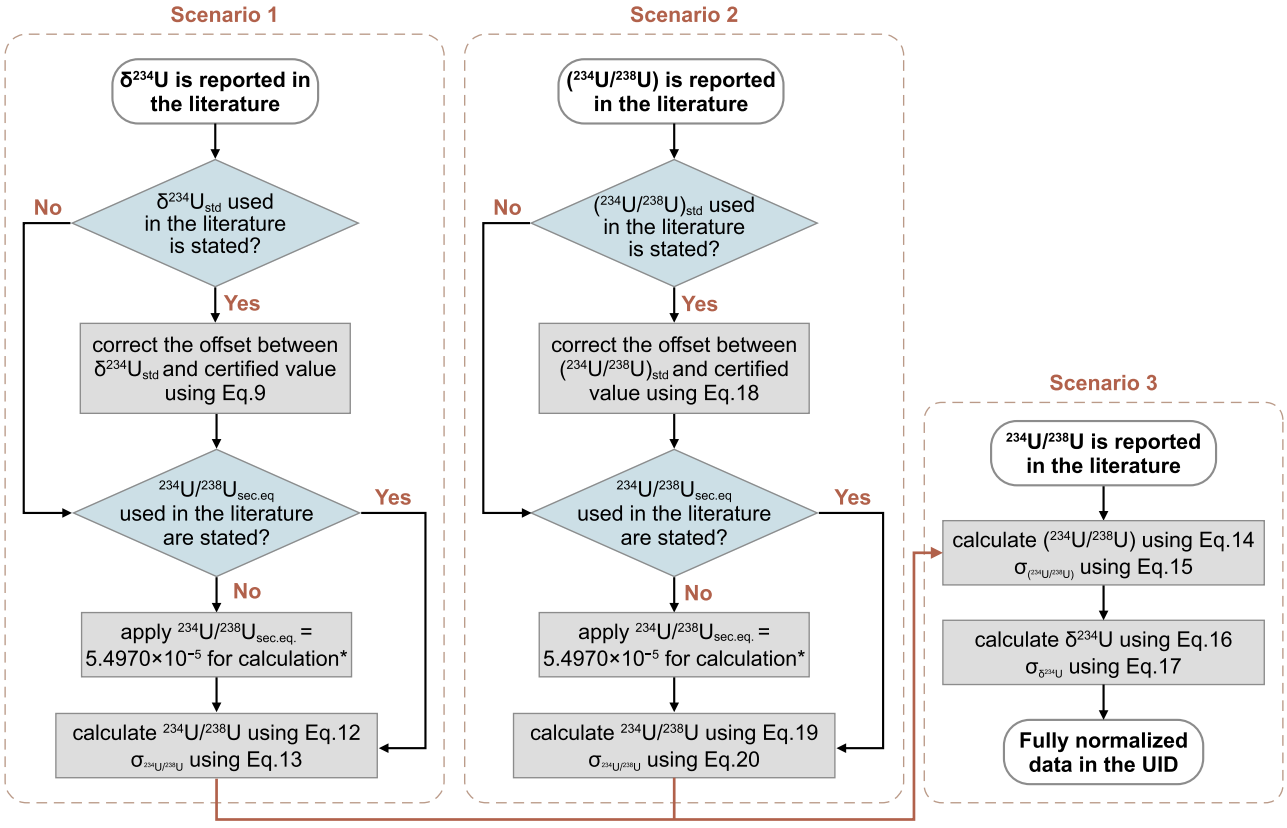

Fig. 4. Summary flowchart of the protocol for the normalization of $^{234}U/^{238}U$ data in the UID. *We apply 5.4970×10^{-5} (Cheng et al., 2013) for publications after 2013, 5.4891×10^{-5} (Cheng et al., 2000) for publications between 2000 and 2013, and 5.472×10^{-5} (Chen et al., 1986) for publications before 2000.

where $^{234}U/^{238}U_{sec.eq}$ is the absolute $^{234}U/^{238}U$ ratio at secular equilibrium. In the UID, this value is taken as 5.4970×10^{-5} (Cheng et al., 2013).

4.3.2. When ($^{234}U/^{238}U$) is reported in the literature

The first task is to correct the reported ($^{234}U/^{238}U$) activity ratio for any difference between the standard composition used in the literature compared to its certified value:

$$\left(^{234}U/^{238}U\right) = \left(^{234}U/^{238}U\right)_{published} + \left(^{234}U/^{238}U\right)_{std\_cert} - \left(^{234}U/^{238}U\right)_{std\_lit} \quad (18)$$

Then, we can calculate the absolute ratio as:

$$^{234}U\Big/^{238}U = \left(^{234}U/^{238}U\right) \times {}^{234}U\Big/^{238}U_{sec.eq\_lit} \quad (19)$$

$$\sigma_{^{234}U/^{238}U} = \sigma_{\left(^{234}U/^{238}U\right)} \times {}^{234}U\Big/^{238}U_{sec.eq\_lit} \quad (20)$$

The definition and the usage of $^{234}U/^{238}U_{sec.eq.\_lit}$ is the same as Section 4.3.1. The subsequent calculations of $\delta^{234}U_{UID}$ and $(^{234}U/^{238}U)_{UID}$, as well as their uncertainties in the database follow Eqs. (14) - (17).

4.3.3. When $^{234}U/^{238}U$ is reported in the literature

Although geochemical studies routinely report $^{234}U/^{238}U$ data as $\delta^{234}U$ and $(^{234}U/^{238}U)$, the $^{234}U/^{238}U$ absolute ratio is a more commonly used notation in nuclear chemistry, method development, and forensic studies. In the latter situation, Eqs. (14)–(17) are directly applied to calculate $\delta^{234}U$ and $(^{234}U/^{238}U)$ and their uncertainties.

4.3.4. When mass fraction is reported in the literature

In some forensic studies, the U isotopic composition is reported as the mass fraction of each U isotope. In this case, we calculate the atomic ratio from the U mass fractions and molar masses, following:

$$\frac{^{i}U}{^{238}U} = \left(f_{m_i}/M_i\right)\Big/\left(f_{m_{238}}/M_{238}\right) \quad (21)$$

$$\sigma_{^{i}U/^{238}U} = \frac{^{i}U}{^{238}U} \times \sqrt{\left(\sigma_{f_{m_i}}\Big/f_{m_i}\right)^2 + \left(\sigma_{f_{m_{238}}}\Big/f_{m_{238}}\right)^2} \quad (22)$$

where i denotes 234 or 235; f_{mi} is the mass fraction of isotope i; M is the atomic mass and σ_{fm} is the uncertainty on mass fraction. When mass ratios are reported, similarly:

$$^{i}U/^{238}U = m_{i/238}/(M_i/M_{238}) \quad (23)$$

$$\sigma_{^{i}U/^{238}U} = \sigma_{m_{i/238}}\Big/(M_i/M_{238}) \quad (24)$$

where $m_{i/238}$ denotes the mass ratio of ^{i}U over ^{238}U ($m_{i/238} = m_i/m_{238}$).

5. Discussion

5.1. $\delta^{238}U$ in uranium standards and geostandards

Measurements of standards and reference materials are key to ensuring data accuracy and comparisons of results from different laboratories. Herein, we use the term 'standard' (or 'isotope standard') only to denote reference materials with certified U isotopic compositions (*e.g.,* CRM-145 and CRM-112a), whereas we use the term 'reference materials' for those other materials that are frequently measured alongside unknown samples but do not have certified U isotopic compositions. 'Reference materials' thus include artificial concentration standards (*e.g.,* ICP single elemental solutions) and natural geostandards. A large number of standards and reference materials are regularly used in U isotope studies, and we used the UID to provide the most up-to-date and reliable recommended $\delta^{238}U$ values for these materials (Figs. 5-8). In these figures, only high-precision measurements are shown (*e.g.,* with uncertainties below 0.10‰ for natural uranium (NU) standards and geostandards), and the data is rank ordered, from lower to higher precision. For standards or reference materials with only a single analysis in the literature, the recommended $\delta^{238}U$ and its error represent the result of said analysis. For well characterized NU standards and geostandards as well as enriched uranium (EU) and depleted uranium (DU) standards (at least 5 analyses), the recommended $\delta^{238}U$ and uncertainties are calculated as weighted average of independent measurements using the following equations:

$$\delta^{238}U_{rec} = \frac{\sum_i \left(\delta^{238}U_i/\sigma_i^2\right)}{\sum_i \left(1/\sigma_i^2\right)} \quad (25)$$

$$2\sigma_{\delta^{238}U}\ (95\%c.i.) = 2 \times \sqrt{\frac{1}{\sum_i 1/{\sigma_i}^2}} \quad (26)$$

where $\delta^{238}U_{rec}$ is the recommended $\delta^{238}U$ in the UID; $\delta^{238}U_i$ and σ_i are the $\delta^{238}U$ value and 1 sigma uncertainty of an independent analysis i, and $2\sigma_{\delta^{238}U}$ is the 2 standard error (*i.e.,* 95% confidence interval) of the recommended $\delta^{238}U$. To assess the adequacy of using an error-weighted average U isotopic composition, reduced-χ^2 statistics (a.k.a., MSWD) were calculated as:

$$\chi^2_{red} = \frac{1}{n-1}\sum_i \frac{\left(\delta^{238}U_i - \delta^{238}U_{rec}\right)^2}{\sigma_i^2} \quad (27)$$

5.1.1. Pure U standards

Fig. 5 summarizes the $\delta^{238}U$ of pure U isotope and concentration standards in the order of increasing $\delta^{238}U$ values. These materials fall in three broad categories: NU, DU, and EU standards. Today, the most widely used U isotope standard is the CRM-145, against which all UID data is normalized. Produced by the New Brunswick Laboratory (NBL), CRM-145 is the solution made from a piece of the CRM-112a U metal. The CRM-112a was initially produced and distributed by the National Bureau of Standard (NBS) as SRM-960 but was recertified and renamed NBL CRM-112a when the Special Nuclear Standard Reference Material (SRM) program was transferred to the NBL CRM (Certified Reference Material) program in 1987. Early papers also frequently used the SRM-950(a), a uranium oxide with indistinguishable $^{238}U/^{235}U$ from SRM-960, but with a distinct $^{234}U/^{238}U$ ratio (Condon et al., 2010; Richter et al., 2010). As a result, the $\delta^{238}U$ values of CRM-112a, CRM-145, SRM-950a, and SRM-960 are considered identical in the UID (an assumption that will be easily relaxed should differences be resolved by future measurements).

In addition to NBL CRM and NBS SRM programs, the Institute for Reference Materials and Measurements (IRMM) has produced two series of U isotopic standards that are currently used for geochemical measurements: IRMM183-187, and REIMEP 18A-D (the latter as part of the Regular European Interlaboratory Measurement Evaluation Programme). Both series contain isotope standards ranging from depleted to low enriched uranium (Richter et al., 2005, 2006).

The homogeneity of these materials is key to their usefulness as standards/reference materials. Among NU standards, IRMM-184, CRM-112a, CRM-145, SRM-950a, SRM-960, and Ricca (concentration standard) exhibit good agreement during interlaboratory comparisons. As already pointed out by Andersen et al. (2017), CRM-129a appears to be heterogeneous, with published $\delta^{238}U$ values clustering around two values: one at ~ -1.5 ‰ (n = 91) (Lau et al., 2016, 2017, 2022; Jost et al., 2017; Lu et al., 2023) and the other one at ~ -1.7 ‰ (n = 1068). Furthermore, while Reimep-18a was until recently considered homogeneous (Andersen et al., 2017), heterogeneity is likely to exist in this standard as well, as $\delta^{238}U$ values in different batches range from -0.26 ‰ (Brüske et al., 2020a) to +0.12 ‰ (Basu et al., 2014). As a result, these

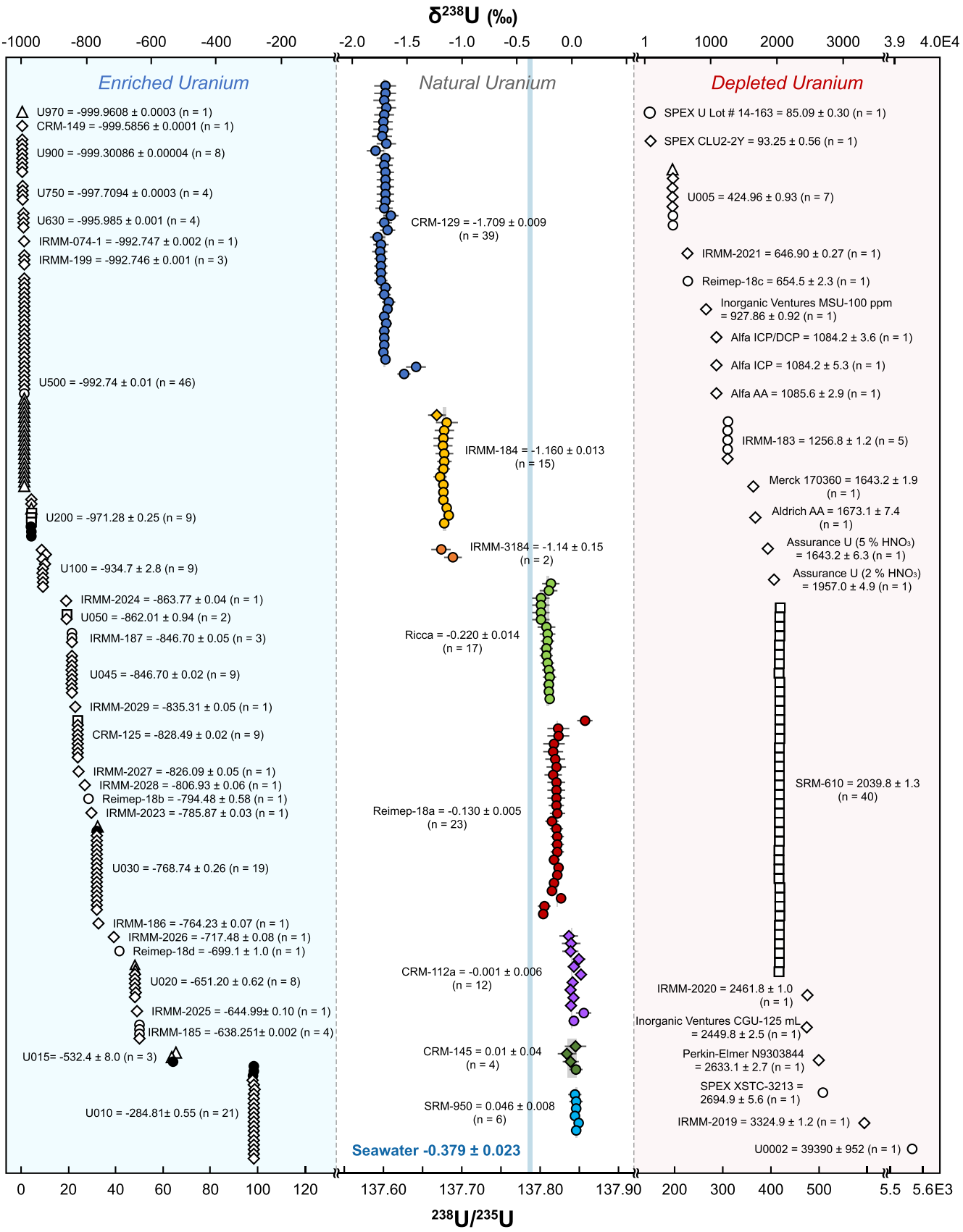

Fig. 5. Summary of U isotopic compositions of certified U isotopic and concentration standards. $\delta^{238}U$ values are renormalized against CRM-145, and absolute ratios ($^{238}U/^{235}U$, lower x-axis) assume a $^{238}U/^{235}U = 137.837$ for CRM-145 (Richter et al., 2010). The symbols denote the data collection technique: circle (MC-ICP-MS), diamond (TIMS), triangle (ICP-MS), square (in-situ techniques), and black circle (other techniques). The blue band shows the U isotopic composition of modern seawater ($\delta^{238}U_{SW}$= -0.379 ± 0.023, Tissot and Dauphas, 2015; Kipp et al., 2022)

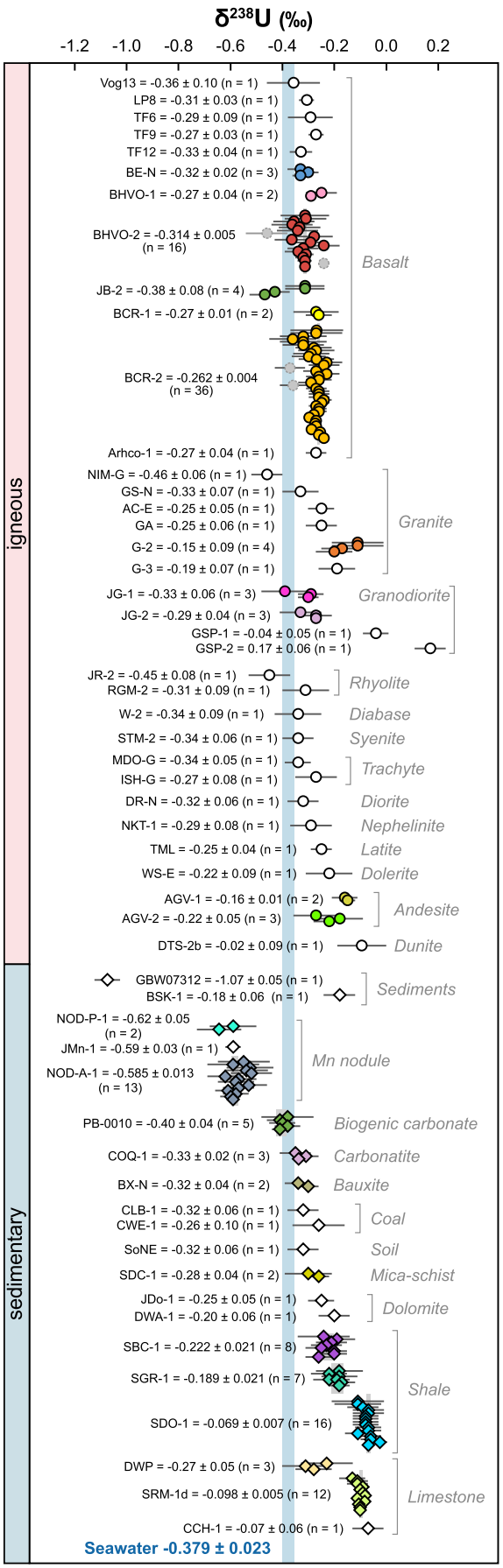

(caption on next page)

Fig. 6. Summary of $\delta^{238}U$ values of rock geostandards. The symbol shapes denote the sample type: circle (igneous), diamond (sedimentary). The blue band shows the U isotopic composition of modern seawater ($\delta^{238}U_{SW}$= -0.379 ± 0.023, Tissot and Dauphas, 2015; Kipp et al., 2022). Geostandards with at least 2 measurements are colored, and the error bands are shown only for those with more than 5 analyses. When n>1, the uncertainties of the recommended $\delta^{238}U$ values are 2 standard deviations. When n=1, the uncertainty represents the analytical error of the single measurement. Grey symbols for BHVO-2 and BCR-2 denote analyses not use in the calculation of the recommended $\delta^{238}U$ values.

isotopically heterogeneous standards are not ideal for interlaboratory comparison. If utilized as secondary standards in future U isotopic investigations, special care must be taken to cross-calibrate the U isotopic composition of the specific batch used.

5.1.2. Geostandards

At this writing, the U isotopic composition of 73 geostandards has been characterized, covering igneous rocks, sedimentary rocks, and U-bearing minerals (Figs. 6–8). Except for two granodiorites data points, $\delta^{238}U$ variations in igneous rocks are generally smaller than in sedimentary rocks, reflecting the importance of low-temperature isotope fractionations in the latter. Although numerous geostandards have been analyzed, only a few of them are well characterized, by multiple laboratories, namely: basalts BCR-2 and BHVO-2, Fe-Mn nodule NOD-A-1, biogenic carbonates PB-0010, shales SBC-1, SGR-1, and SDO-1, limestone SRM-1-d, and uraninites CZ-1. For these, robust recommended $\delta^{238}U$ values, based on these inter-laboratory data, are provided (Fig. 8). Most geostandards have been less studied (measured 5 times, or less), and their $\delta^{238}U$, even when highly precise, will benefit from seeing their accuracy confirmed by future works, which the UID will allow to easily assess as new data becomes available.

5.2. Scope of uranium isotopic studies and future direction

To facilitate searching and finding of data, the data within the UID is distributed between 6 sub-databases (Fig. 2). These categories were chosen to be as independent and unambiguous as possible, and they are non-overlapping, meaning that no data is duplicated between sub-databases. Within each sub-database, publications (and the data they report) are categorized according to their dominant scope/theme of study. This allows one to rapidly isolate all publications/data within a major theme (*e.g.,* chronology, paleoredox, etc.), and build custom-compilations for future studies. Below, we provide a brief review of the state-of-the-art for most of the themes used in the UID, in the order shown on Fig. 2.

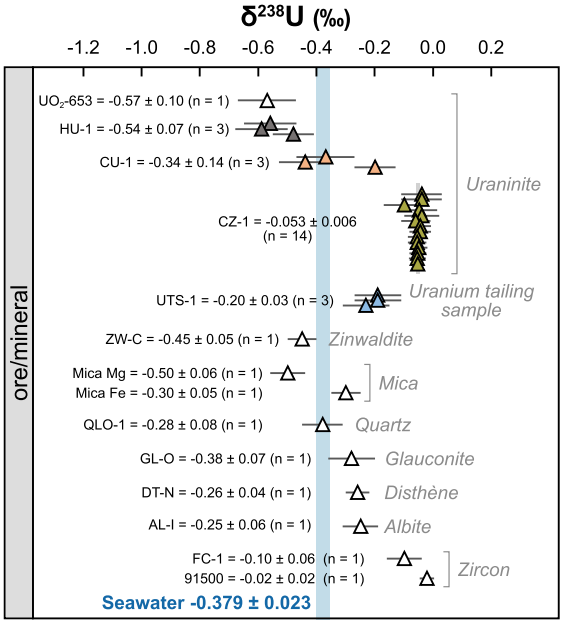

Fig. 7. Summary of $\delta^{238}U$ values of ore and mineral geostandards. The blue band shows the U isotopic composition of modern seawater ($\delta^{238}U_{SW}$= -0.379 ± 0.023, Tissot and Dauphas, 2015; Kipp et al., 2022). Geostandards with at least 2 measurements are colored, and the error bands are shown only for those with more than 5 analyses. When n>1, the uncertainties of the recommended $\delta^{238}U$ values are 2 standard deviations. When n=1, the uncertainty represents the analytical error of the single measurement.

5.2.1. Calibrations and method developments

Many methodologies for U isotopic determination have been established, with remarkable differences in their sensitivity, precision, analysis time, required material mass, and sample preparation processes, among others. The analytical toolbox contains various types of modern spectrometry to fulfill the requirements of a variety of applications, such as inductively-coupled-plasma mass-spectrometry (ICP-MS), TIMS, secondary ion mass spectrometry (SIMS), alpha spectrometry, gamma spectrometry, optical emission spectrometry (OES), optogalvanic spectroscopy (OGS), and neutron activation. As a first-order benchmark to evaluate the precision obtained from specific methods, we used the UID to plot in Fig. 9 the full range (to-date) of analytical precision on $\delta^{238}U$ values achieved by each technique.

ICPMS is the most widely used technique for analyzing U isotopic compositions of small amounts of material in geological, environmental, and forensic studies, taking advantage of the extraordinarily efficient ionization of argon plasma. The instruments used for U isotopic determination are further classified in the ICPMS scheme as MC-ICP-MS, quadrupole ICPMS, and sector-field (SF) ICPMS.

MC-ICP-MS is a well-established technology for high-precision $^{238}U/^{235}U$ determination, as the simultaneous detection of all ion beams alleviates most of the uncertainty stemming from plasma instabilities (relative to single collector instruments). In the geochemistry community, solution-based MC-ICP-MS is currently the most routine approach for analyzing U isotopes (see Tissot and Ibañez-Mejia, 2021, Fig. 2). The performance of this technique can be further improved by employing a double spike (Stirling et al., 2007; Richter et al., 2008; Weyer et al., 2008), introducing samples with membrane desolvating nebulizer systems (*e.g.,* Aridus, DSN-100, and Apex), as well as coupling with multiple ion counting devices for ultra-trace level works (Snow and Friedrich, 2005). Apart from its extensive usage in the field of geochemistry, MC-ICP-MS is also employed in the bulk analysis of environmental samples (*e.g.,* samples collected by safeguards inspectors in the surrounding environment of nuclear facilities) (Buchholz et al., 2007; Boulyga et al., 2016).

Since extensive sample preparation and purification are required beforehand, MC-ICP-MS is rarely suitable for environmental screening and health physics studies, where there is a high demand for the rapid processing of large numbers of samples. In these fields, SF-ICPMS is preferred because isotopic analysis can be performed despite significant and complex matrices. Health physicists have put efforts in developing methods to measure U isotopic ratios in biological samples such as blood (Tolmachyov et al., 2004; Todorov et al., 2009) and urine (Pappas et al., 2003; Gwiazda et al., 2004; Gray et al., 2012; Xiao et al., 2014). Because of the low sample preparation requirements, SF-ICPMS is also applied to environmental samples, such as soil and U-bearing particles (Boulyga et al., 2001; Boulyga and Becker, 2001, 2002; Shinonaga et al., 2008).

Other types of ICPMS are less commonly used for U isotopic analysis. Only a few studies evaluated the ability of quadrupole ICPMS (Oliveira and Sarkis, 2002; Ejnik et al., 2005; Lindahl et al., 2021) and high-resolution (HR) ICPMS (Krystek and Ritsema, 2002; Zhang et al.,

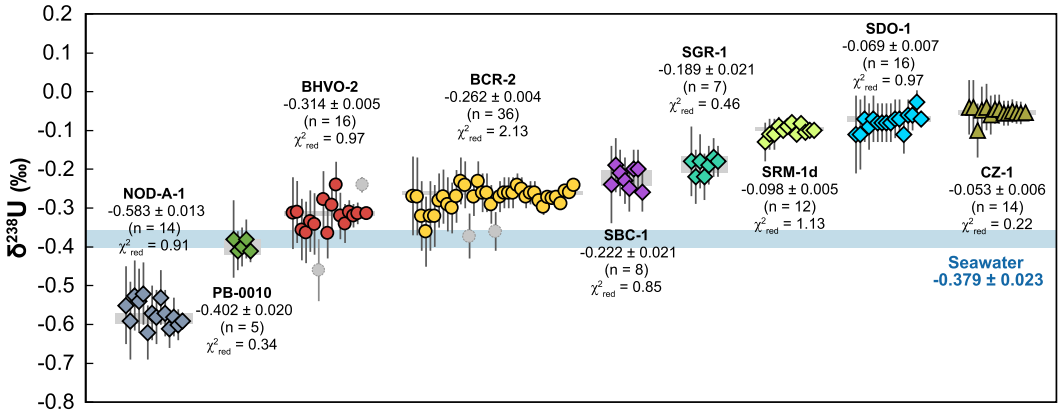

Fig. 8. Summary of $\delta^{238}U$ values of widely used geostandards (with at least 5 measurements). The error bands represent the 95% confidence intervals of the data points. As in Fig. 6 and Fig. 7, symbol shapes denote sample types: circle (igneous), diamond (sedimentary), and triangle (ore/mineral). The grey symbol indicates that the data point meets the selection criterion but is not included in the calculation of recommended $\delta^{238}U$, because of the significant offset relative to other measurements. Within each geostandard, the data are ordered by measurement uncertainty, reflecting the improvement in analytical precision (mostly as a function of time). The blue band shows the U isotopic composition of modern seawater ($\delta^{238}U_{SW}$= -0.379 ± 0.023, Tissot and Dauphas, 2015; Kipp et al., 2022).

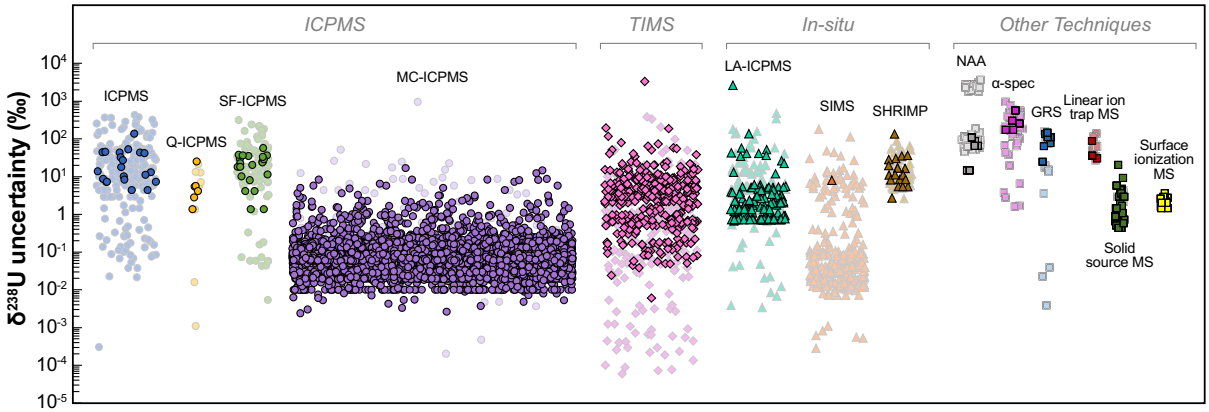

Fig. 9. Compilation of $\delta^{238}U$ uncertainties obtained using different analytical techniques. Uncertainties are those reported in the original studies (2SD, 2SE or 95% CI depending on the study). Dark symbols represent NU samples and light symbols represent EU and DU samples. Symbol shapes denote the types of techniques: circle (ICPMS), diamond (TIMS), and triangle (in-situ techniques), square (other techniques).

2007) to provide fast U isotope data and test their relevance to the study of biological and particle samples.

In addition to liquid sample introduction, ICPMS can be combined with laser ablation (LA) systems, allowing for in-situ isotopic analysis of solid materials, which is especially beneficial for small size samples that lack adequate materials for solution-based measurement. Besides providing spatially resolved data, LA-ICPMS significantly reduces analysis time and does not generate radioactive waste, which are important in forensic studies. LA-ICPMS has thus proven a useful tool to characterize U isotopic compositions in single particles (Boulyga and Prohaska, 2008; Varga, 2008; Pointurier et al., 2011; Kappel et al., 2012, 2013; Pointurier et al., 2013; Claverie et al., 2016; Donard et al., 2017; Varga et al., 2018; Ronzani et al., 2019), highly radioactive materials (Guillong et al., 2007; Günther-Leopold et al., 2008; Stefánka et al., 2008) and biological samples (*e.g.,* flower leaves) (Zoriy et al., 2005). In most natural materials, where U contents are low and isotopic variability is typically limited to sub-permil effects, LA-ICPMS provides insufficient precision to resolve U isotope variations. As a result, the use of laser ablation in geochemistry is still in its infancy, and, to our knowledge, only one recent study has successfully used LA-MC-ICP-MS, in combination with 10^{13} ohm amplifiers, to determine $^{238}U/^{235}U$ ratios in single zircon and titanite grains (Yamamoto et al., 2021).

SIMS is another type of in-situ technique for U isotopic determination (Kips et al., 2007; Lewis et al., 2015; Yomogida et al., 2017). SIMS analysis suffers from higher polyatomic interferences (Ranebo et al., 2009) than LA-ICPMS, but offers a better spatial resolution down to 1 μm (Boulyga et al., 2015). The higher spatial resolution allows for mapping U isotopic compositions in target samples. These maps can be used for preliminary screening in forensic particle analysis to locate and distinguish different types of particles (Tamborini et al., 1998; Betti et al., 1999; Ranebo et al., 2007; Peres et al., 2013). For larger samples like fuel pellets and big particles, SIMS maps are also valuable to detect spatial heterogeneity of U isotope ratios (Tamborini et al., 1998; Kips et al., 2019).

TIMS was the paramount technique for high-precision U isotope measurements before the advent of MC-ICP-MS. Although MC-ICP-MS plays a dominant role in geological and environmental investigations nowadays, TIMS still occupies an important place in studies requiring the determination of absolute U isotope ratios, such as geochronology (*e.g.,* Hiess et al., 2012), nuclear contamination (Taylor et al., 1998; Sahoo et al., 2002, 2004), solution-based single particle analysis (Shinonaga et al., 2008; Kraiem et al., 2012), as well as calibration of certified reference materials, commercially available compounds and reagents (Richter et al., 1999b, 2005, 2006, 2010, 2018; Condon et al., 2010; Mathew et al., 2012; Kraiem et al., 2013; Shibahara et al., 2016; Peńkin et al., 2018). A range of techniques for improving the performance of TIMS were developed, such as employing a cavity source to enhance ionization efficiency (Maden et al., 2018; Trinquier et al., 2019),

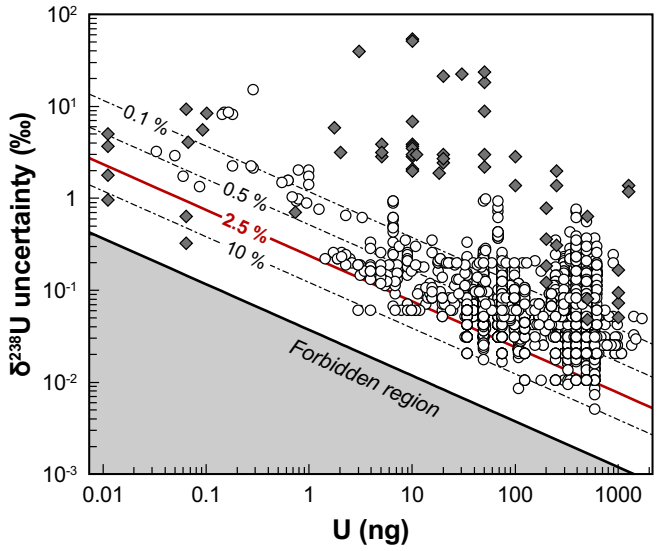

Fig. 10. Relationship between $\delta^{238}U$ uncertainties and mass of U analyzed in nanograms. White circles and grey diamonds are uncertainties of NU samples obtained from MC-ICPMS and TIMS respectively. Uncertainties are those reported in the original studies (2SD, 2SE or 95% CI depending on the study). When the exact mass of U for each sample is not reported, average masses reported in the study are used. Red solid curve and black dash curves represent reference theoretical 2SE (counting statistics and Johnson noise, see Eq. (2) in Tissot et al., 2019, assuming 30 V signal on ^{238}U and use of 10^{11} Ω amplifiers) with ion transmission of 2.5% (typical value for Neptune MC-ICPMS), 0.1%, 0.5%, 10% respectively. Black curve shows precision limit, assuming 100% transmission.

optimizing evaporation protocols (Callis and Abernathey, 1991; Fiedler, 1995; Richter and Goldberg, 2003; Suzuki et al., 2010; Richter et al., 2011; Mathew et al., 2013), and leveraging higher resistance amplifiers or ion counter to improve electronic efficiency (Quemet et al., 2014, 2016).

Other types of spectrometry for U isotope analysis are either preferred in early studies or confined within limited applications. Alpha spectrometry is a conventional technique to determine the activity ratio of U isotopes (Kunzendorf, 1968; Iturbe, 1992; Duarte and Szeles, 1994; Boulyga et al., 2001; Alamelu and Jagadish, 2016). Other techniques including ICP-OES (Zeiri et al., 2021), extractive electrospray ionization mass spectrometry (EESI-MS), passive gamma-ray spectrometry (Nir-El, 2000), glow discharged OGS (Barshick et al., 1995), and neutron activation analysis (Ganapathy, 1978) will not be described in detail here, because they are not commonly employed.

As predicted from counting statistics and Johnson Noise, the precision of U isotope analysis achievable with modern instrumentation is correlated with the total mass of U used for measurements (Fig. 10). For a given instrument (*i.e.*, analytical setup), precision can thus be improved by analyzing more U. The relationship shown in Fig 10 can be used a reference point to design analytical plans based on the available materials and desired precision in future studies.

Besides mass spectrometry, method developments also comprise chemical separation and purification. Chromatography based on the UTEVA resin is well-established nowadays, modified after Horwitz et al. (1992; 1993), with minor differences between labs (*e.g.*, Stirling et al., 2007; Weyer et al., 2008; Tissot and Dauphas, 2015). Recent studies on U chemistry mainly focus on processing special samples, such as high-purity graphite (Metzger et al., 2021) and environmental swipe samples (Metzger et al., 2019), as well as measuring minor isotopes without spike addition (Rovan and Štrok, 2019).

5.2.2. Oceanic paleoredox reconstruction

Reconstructing the oceanic redox history is important to understand the evolution of the Earth's surface conditions, and its interconnection with the appearance and evolution of life. In the past decade, U isotopes have received considerable attention as a paleoredox proxy of marine/seafloor anoxia (see review by Zhang et al., 2020b). Uranium is redox-sensitive and can hold two oxidation states in the terrestrial surface environment: insoluble U(IV) and soluble U(VI) (Langmuir, 1978). In the modern (oxic) ocean, the long residence time of U ($\tau \sim 400$ kyr, Ku et al., 1977; Dunk et al., 2002) results in both homogeneous salinity-normalized concentration (~3.2 ng/g for a salinity of 35 g/L, Chen et al., 1986) and isotopic composition ($\delta^{238}U = -0.379 \pm 0.023$ ‰, Tissot and Dauphas, 2015; Kipp et al., 2022). As U inputs to the ocean are dominated by continental weathering, with an isotopic composition identical to that of the continental crust (-0.30 ± 0.04 ‰, Tissot and Dauphas, 2015; Andersen et al., 2016), the $\delta^{238}U$ of seawater is thus primarily controlled by the isotopic fractionation associated with U removal into different oceanic sinks. The main process fractionating U isotopes during removal is reductive immobilization in anoxic/euxinic settings, which leads to ^{238}U enrichments in reduced sediments. As a result, in periods of expanded marine anoxia, the increased sequestration of U in reduced sediments, would result in lower U concentration and $\delta^{238}U$ value in seawater.

One key aspect when reconstructing past oceanic redox states with U isotopes is to work on a reliable seawater $\delta^{238}U$ archive. Carbonates are the most popular and straightforward archive to date since they tend to directly record the primary seawater $\delta^{238}U$ signal. U(VI) mainly exists as uranyl carbonate complexes $UO_2(CO_3)_3^{4-}$ in seawater, which is incorporated into marine carbonates with no significant isotopic fractionation. This conclusion is supported by both lab-controlled coprecipitation experiments (Chen et al., 2016) and comparison of primary carbonates and modern seawater (Stirling et al., 2007; Weyer et al., 2008; Romaniello et al., 2013; Tissot et al., 2018; Kipp et al., 2022). In just over a decade, more than 60 studies have placed constraints on oceanic anoxia using U isotopes in a variety of carbonates, including limestone, dolomite, biogenic carbonates, and carbonate-rich sediments (Brennecka et al., 2011a; Asael et al., 2013; Romaniello et al., 2013; Andersen et al., 2014, 2018, 2020; Dahl et al., 2014, 2017, 2019; Azmy et al., 2015; Tissot and Dauphas, 2015; Lau et al., 2016, 2017, 2022; Noordmann et al., 2016; Hood et al., 2016, 2018; Elrick et al., 2017, 2022; Jost et al., 2017; Song et al., 2017; White et al., 2018; Zhang et al., 2018a, b, c, 2019a, b, 2020a, b, c, 2022; Phan et al., 2018; Clarkson et al., 2018, 2020, 2021a, b; Bartlett et al., 2018; Wei et al., 2018, 2021; Herrmann et al., 2018; Tissot et al., 2018; Gilleaudeau et al., 2019; Gothmann et al., 2019; Tostevin et al., 2019; Brüske et al., 2020a; Cheng et al., 2020a, 2020b; Li et al., 2020; Lu et al., 2020, 2023; Mänd et al., 2020; Bura-Nakić et al., 2020; Zhao et al., 2020; Cao et al., 2020; Livermore et al., 2020; del Rey et al., 2020, 2022; Bruggmann et al., 2022; Chen et al., 2018a, b, 2021a, b, 2022a, b; Cherry et al., 2022; Dang et al., 2022; Liu et al., 2022; McDonald et al., 2022; Wang et al., 2022). As recently discussed in Kipp and Tissot (2022), perhaps the main uncertainty affecting these reconstructions stems from the way diagenetic transformations alter the primary seawater signal. Studies of modern primary carbonates have shown that early diagenesis leads to non-negligible $\delta^{238}U$ offset between carbonates and seawater (from ~0 to +0.6 ‰; Romaniello et al., 2013; Tissot et al., 2018). Things become even more complicated when using ancient carbonates since the extent of diagenesis varies in different geological settings. In the absence, so far, of a proxy for $\delta^{238}U$ diagenetic offsets, the resulting uncertainty on anoxia reconstructions can have a substantial impact on data interpretations (Kipp and Tissot, 2022).

Shales and organic-rich sediments are another set of widely used sedimentary archives for $\delta^{238}U$ seawater reconstructions (Weyer et al., 2008; Montoya-Pino et al., 2010; Asael et al., 2013; Kendall et al., 2013, 2015, 2020; Holmden et al., 2015; Noordmann et al., 2015; Lu et al., 2017; 2020; Yang et al., 2017; Phan et al., 2018; Wang et al., 2018, 2020; Abshire et al., 2020; Brüske et al., 2020a, b; Cheng et al., 2020b; Cole et al., 2020; Stockey et al., 2020; Dickson et al., 2021, 2022; Pan et al., 2021; Chiu et al., 2022; Dang et al., 2022; Lau et al., 2022; Li et al.,

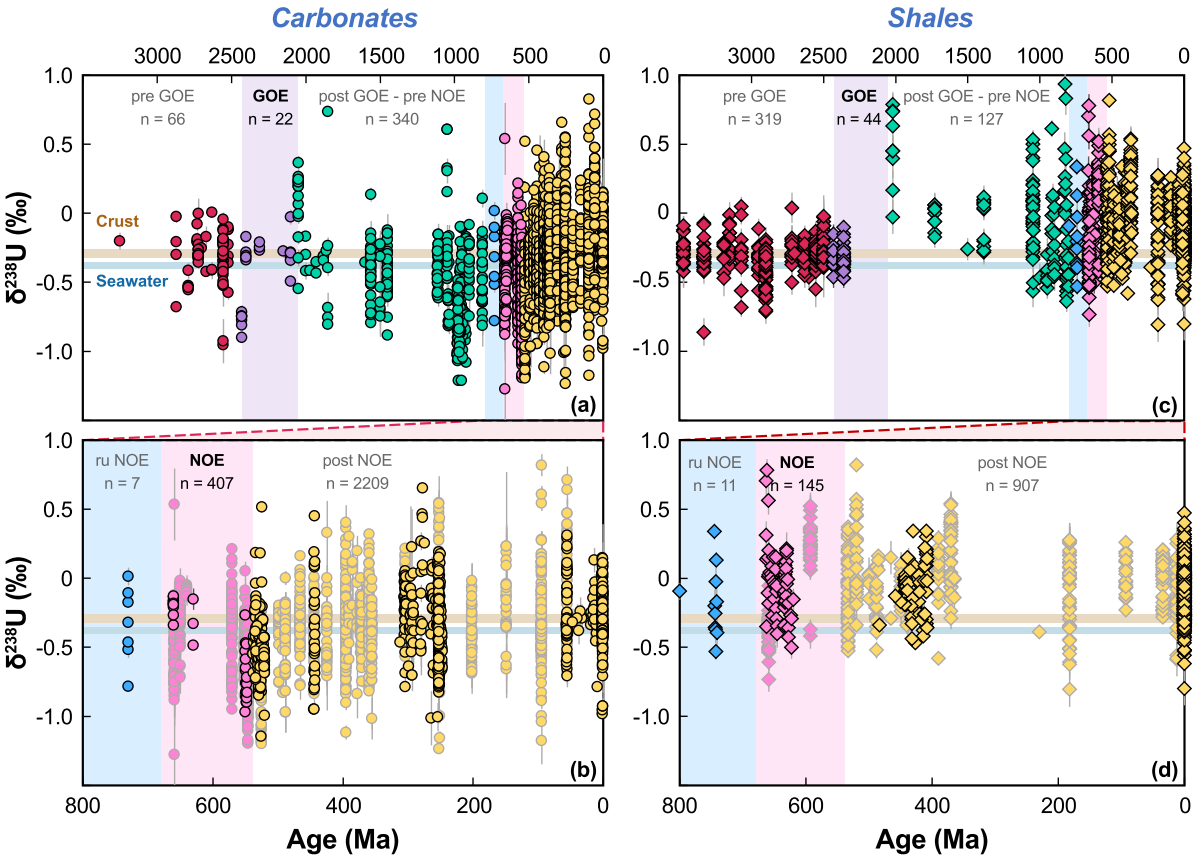

Fig. 11. Compilation of $\delta^{238}U$ values in carbonates (a) from 3500 Ma to present (n = 3132), (b) from 800 Ma to present (n = 2704), and in shales (c) from 3500 Ma to present (n = 1553), (d) from 800 Ma to present (n = 1063). The brown and blue band show $\delta^{238}U$ of continental crust (-0.29 ± 0.03‰) and modern seawater (-0.379 ± 0.023‰) respectively (Tissot and Dauphas, 2015; Kipp et al., 2022). The six geological intervals are pre GOE (3500-2430 Ma), GOE (2430-2060 Ma), post-GOE-pre-NOE (2060-800 Ma), ramp up (ru) NOE (800-680 Ma), NOE (680-540 Ma) and post-NOE (540 Ma-present). In panels (b) and (d), darker symbols denote numerical ages are reported in the original publications, while symbols greyed out denote ages are estimated by the geological periods.

2022; Ostrander et al., 2022). In contrast to marine carbonates, which directly represent seawater, the shale signatures are highly fractionated away from the seawater composition, and the magnitude of the fractionation factor relative to seawater has been shown to depend on environmental controls such as the depositional environments (Andersen et al., 2014), organic carbon and sulfide burial rates (Cole et al., 2020) or the extent of oceanic anoxia (Chen et al., 2021a). Furthermore, shales and organic-rich sediments often consist of both authigenic and detrital components, and the two have to be teased apart, either physically/chemically prior to analysis or through corrections leveraging authigenic U enrichment proxies such as U/Al and U/Th ratios (Asael et al., 2013; Noordmann et al., 2015; Yang et al., 2017; Abshire et al., 2020; Brüske et al., 2020a, b; Kendall et al., 2020; Cole et al., 2020; Stockey et al., 2020). While these added uncertainties certainly complicate $\delta^{238}U$ seawater reconstructions, the record from shales and organic-rich sediments is nonetheless highly valuable, and study of the (co)variations with the carbonate record can provide complementary insights into the U oceanic cycle through time (*e.g.,* Chen et al., 2021a).

Fig. 11 presents the U isotopic data for carbonates and shales from 3500 Ma to the present (panels a and c), with emphasis on the Neoproterozoic and Phanerozoic (panels b and d). Even though there are thousands of data points available for various geological periods, this figure shows that almost all current paleo-redox studies are event-driven, with a particularly strong focus on catastrophic extinction events. Future U isotope studies targeting the current gaps in the record (*i.e.*, between geological events studied so far) will be extremely useful to develop a comprehensive understanding of the redox history through out Earth's history.

Two studies have investigated Fe-Mn crusts, where U is mostly adsorbed on the surface of the samples, as a potential record of seawater $\delta^{238}U$ value (Goto et al., 2014; Wang et al., 2016). In line with adsorption experiments (Brennecka et al., 2011b), these studies found Fe-Mn crusts, from modern back to 80 Myr ago, to be offset from the modern seawater value by ~ 0.24‰, which the authors interpreted as evidence of constant oxygen levels in the ocean during this time interval. The fact that the $^{234}U/^{238}U$ ratios in all samples are widely out of secular equilibrium, and, in many cases, offset towards the modern seawater value, suggests however constant U exchange and equilibration between the Fe-Mn crusts and seawater. This raises serious doubts about the reliability of Fe-Mn crusts as faithful recorders of past seawater $\delta^{238}U$ value and their usefulness in the study of oceanic paleoredox conditions.

It is essential to understand the terrestrial U cycling in paleoredox studies since this proxy is based on the rationale that $\delta^{238}U$ of seawater predominantly reflects the mass balance between riverine input and various sedimentary outputs such as anoxic sediments, euxinic sediments, and biogenic carbonates. While the U isotopic compositions of these sinks have been extensively characterized, those of seawater and rivers are less well constrained (Fig. 12) (Stirling et al., 2007; Andersen et al., 2016; Noordmann et al., 2016). Recently, Kipp et al. (2022) partially addressed this issue by reevaluating the fundamental assumption of homogeneity of the marine U reservoir. They found that subtle $\delta^{238}U$ and $\delta^{234}U$ heterogeneity that correlate with U concentrations exist in modern seawater, and as a result proposed a new-salinity normalized global mean seawater for $\delta^{238}U$ of -0.379 ± 0.023‰ and $\delta^{234}U$ of 145.55 ± 0.28‰.Previous research has shown that substantial variations exist between rivers from different regions, ranging from -0.72 to +0.06‰,

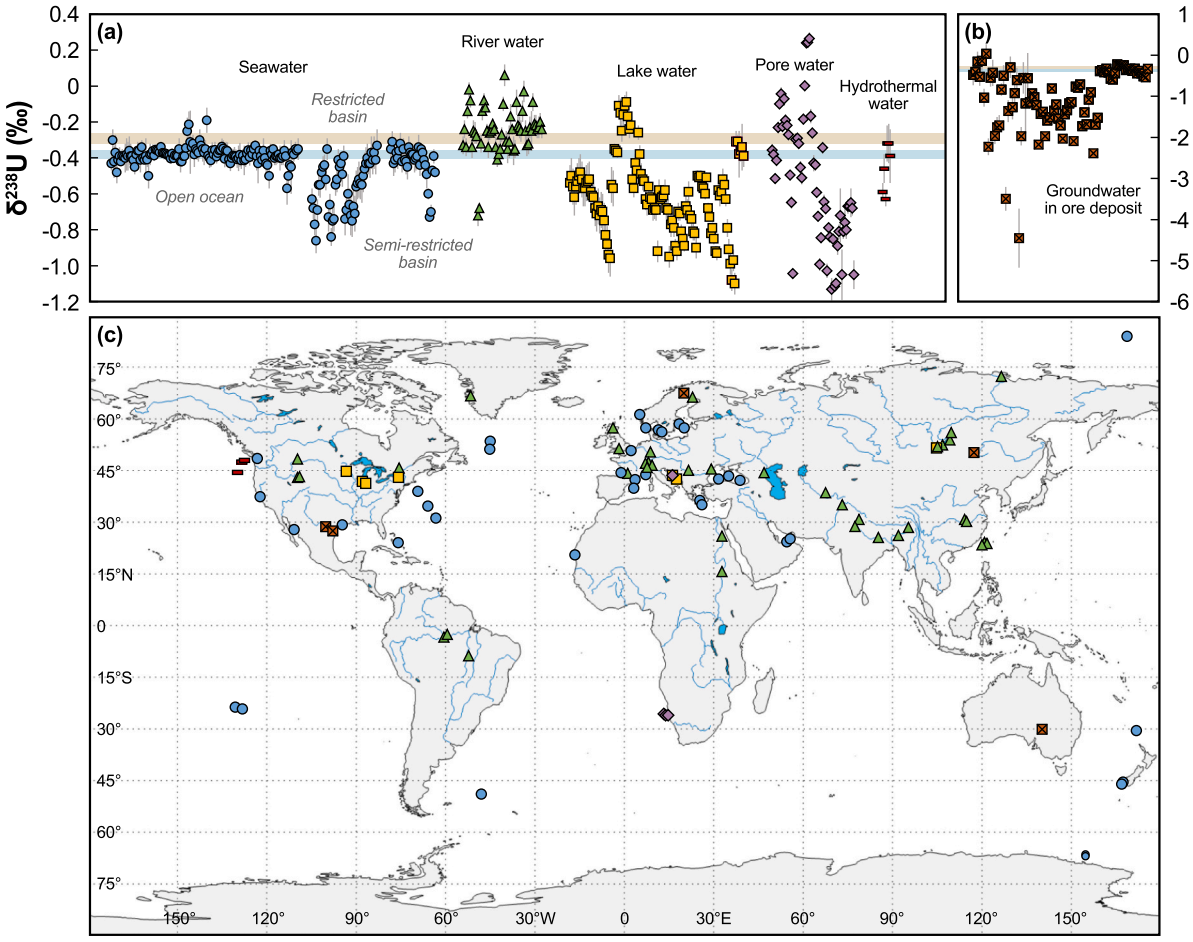

Fig. 12. (a-b) Compilation of $\delta^{238}U$ values in water samples. The symbol shapes denote sample type. The brown and blue band show $\delta^{238}U$ of continental crust (-0.29 ± 0.03‰) and modern seawater (-0.379 ± 0.023‰) respectively (Tissot and Dauphas, 2015; Kipp et al., 2022). (c) World map illustrating the water sample locations. Symbols as in (a) and (b).

and seasonality may affect the riverine $\delta^{238}U$ values (Andersen et al., 2016). In order to establish a tighter constraint on the U budget, an expanded riverine database, both in time and space, is required. Besides the uncertainty on the riverine value, Fig. 12 also reveals other limitations in the data currently available. For instance, the U isotopic composition of groundwater (as an input to the ocean) has not been investigated since previous studies only measured groundwater contaminated by U mines. Furthermore, the $\delta^{238}U$ record of lake water, pore water, and hydrothermal water are extremely limited (< 5 sites for each category). Future characterization of the U isotopic compositions of these reservoirs will provide constraint on the U budget at a finer scale.

Another important issue in the context of the U budget is that U cycling can be dramatically different during expanded marine anoxia. Sparing dissolved U(VI) will significantly shorten the U residence time (*e.g.,* Li et al., 2013), invalidating the assumption of conservative behavior of uranium. This has the potential to shift U isotopic composition from a global to a regional redox indicator (Andersen et al., 2017), and can influence U isotopic fractionation (Chen et al., 2021a).

Finally, detailed studies establishing the reliability of current and future potential archives are needed. Carbonates, for example, frequently experience varying extents of diagenesis, which can significantly alter the primary isotopic composition. More efforts are needed to disentangle the diagenetic signal from the authigenic U composition. Possible directions include developing fine correction protocols for different diagenetic processes and identifying alternative archives that are less affected by and/or more resistant to these alterations. According to recent studies, brachiopod shells can be a promising proxy since they are less impacted by porewater diagenesis (Livermore et al., 2020; del Rey et al., 2020). Finding more applicable archives can help us expand our toolbox when some samples are unavailable.

5.2.3. *Igneous processeses*

High-precision U isotope investigations in igneous systems is a young but growing field. The discovery of $\delta^{238}U$ variations in felsic rocks (Telus et al., 2012), crustal materials (Andersen et al., 2015) and accessory minerals (Hiess et al., 2012), triggered interest in using U isotopes to shed light on high-temperature processes. Since then, several studies have started to explore in more details the potential of U isotopes as tracers of magmatic and other related processes such as crystallization, metasomatism, Soret diffusion, subduction, and sedimentary recycling (Telus et al., 2012; Andersen et al., 2015; Avanzinelli et al., 2018; Casalini, 2018; Livermore et al., 2018; Freymuth et al., 2019; Tissot et al., 2019; Yamamoto et al., 2021; Gaschnig et al., 2021).

Using the classical igneous (I-type) and sedimentary (S-type) granites from the Lachlan Fold Belt, Telus et al. (2012) found a spread in $\delta^{238}U$ from -0.50 ‰ to -0.21 ‰, but without any clear relationship to the nature of the protolith, or tracers of magmatic differentiation (*e.g.,* SiO_2). The lack of positive correlation between U, Fe and Mg isotope data in these samples showed nonetheless that thermal (Soret) diffusion was not the driver of isotope variations for these elements in these rocks.

After Andersen et al. (2015) found that samples from the Mariana arc had lighter U isotope composition than OIBs (by ~0.05 ‰), which were themselves lighter than MORBs (also by ~0.05 ‰), studies started investigating arc systems in more details. These revealed a general trend

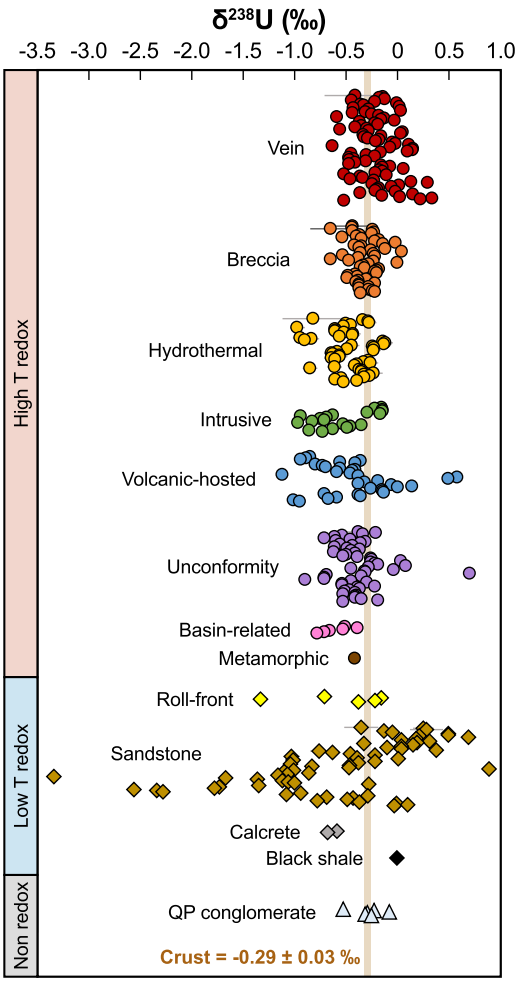

Fig. 13. Compilation of $\delta^{238}U$ values in ore deposits. The symbol shapes represent the sample types: circle (high temperature redox sensitive), diamond (low temperature redox sensitive), and triangle (non-redox sensitive, QP = quartz-pebble). The brown band shows $\delta^{238}U$ value of continental crust (-0.29 ± 0.03‰, Tissot and Dauphas, 2015).

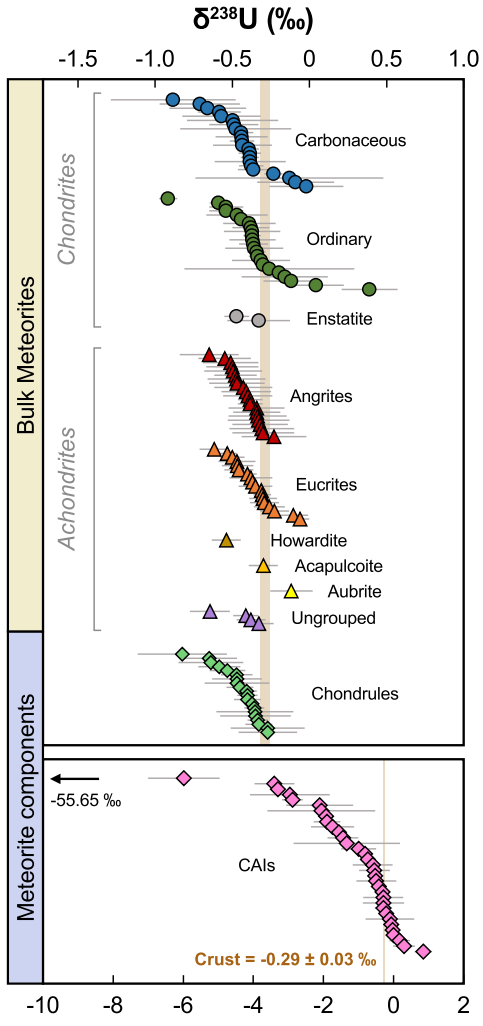

Fig. 14. Compilation of $\delta^{238}U$ of extraterrestrial samples, including bulk meteorites and their components. The symbol shapes represent the sample types: circle (chondrites), triangle (achondrites), and diamond (meteorite components). The brown band shows $\delta^{238}U$ value of continental crust (-0.29 ± 0.03‰, Tissot and Dauphas, 2015).

between $\delta^{238}U$ and Th/U ratios in arc lavas, consistent with the idea (Elliott et al., 1997; Avanzinelli et al., 2012) that the composition of the arc lavas is the result of mixing between low Th/U (and low $\delta^{238}U$) slab-derived fluids and high Th/U (and $\delta^{238}U$) recycled sediments melts into the source of the arc magmas (Andersen et al., 2015; Casalini, 2018; Freymuth et al., 2019). A distinct trend observed in Mount Vesuvius lavas was interpreted to reflect an increase in carbonate sediment recycling, and thus increased CO_2 fluxes to the mantle source of these lavas during the more proactive phases of the volcano (Avanzinelli et al., 2018).

In a recent study of a differentiation sequence in the Kilauea Iki lava lake, Gaschnig et al. (2021) observed only a limited range of U isotope compositions (from -0.38 to -0.20 ‰), and no systematical variations with the extent of differentiation, ruling out this process as a major driver of isotopic variability in such tholeiitic systems. In contrast, correlations of $\delta^{238}U$ with REE patterns and mineral modes in angrites meteorites suggests that a change in the coordination environment of U during incorporation into pyroxene results in cpx-melt U isotope fractionation factor of ~-0.25 ‰ (Tissot et al., 2017).

Some studies have also started exploring the U isotope systematics of pooled mineral fractions (Hiess et al., 2012; Livermore et al., 2018) and single-crystals (Tissot et al., 2019; Yamamoto et al., 2021). We direct the reader to *Section 5.2.5* (chronology) and Tissot and Ibañez-Mejia (2021) for more details on this topic.

While clear $\delta^{238}U$ variations have now been documented in igneous materials, the mechanisms underlying these fractionations at magmatic temperatures are still mostly unknown. The property of minerals incorporating U, temperature, the redox state of the melt, and the extent of crystallization are all potential drivers of isotopic fractionation. More work is needed to systematically assess the contribution as well as the direction and magnitude of U isotopic fractionation resulting from each of these mechanisms. As discussed in more details in Tissot and Ibañez-Mejia (2021), inter-crystal, inter-mineral and inter-rock $^{238}U/^{235}U$ variations could become powerful tools for studying magmatic evolution, provenance, redox, and/or composition. Exploiting the potential of this system will, however, require coordinated efforts to constrain the relationship between the characteristics of the host rock, host mineral, U crystal chemistry/bonding environments, and $\delta^{238}U$ of individual mineral grains, to build a robust interpretative framework for U isotope effects in natural accessory phases and bulk samples.

5.2.4. Ore deposits

Due to their high U concentration, U ore deposits were the preferred target material for early U isotope studies (Nier, 1939; Lounsbury, 1956; Senftle et al., 1957; Hamer and Robbins, 1960; Rosholt et al., 1963,

1965). The discovery in the early 70s of natural 'fossil' fission nuclear reactors with extremely high $^{238}U/^{235}U$ (due to ^{235}U burn-up) in Oklo (Gabon), led to a renewed interest for U isotope studies in ore deposits as a way to search for such reactors (Cowan and Adler, 1976; Richter et al., 1999a; Kirchenbaur et al., 2016). A thorough review of observations and mechanisms of U isotope fractionation in ore deposits can be found in Andersen et al. (2017) and we only provide a brief overview below.

Extensive characterizations of U ore from various deposit types and locations revealed that ore deposits from different geological settings have distinct U isotopic compositions (Fig. 13), opening the possibility to utilize U isotopic composition as a "fingerprint" to distinguish and trace the origins of ore samples (Richter et al., 1999a; Keegan et al., 2008; Bopp et al., 2009; Brennecka et al., 2010a; Uvarova et al., 2014; Kirchenbaur et al., 2016; Placzek et al., 2016; Spano et al., 2017; Keatley et al., 2021). While the majority of U ore deposits studies focus on isotopic heterogeneity between mines, a few studies evaluate U isotopic variations at the smaller scales, such as samples collected from the same mine (Chernyshev et al., 2014; Kirchenbaur et al., 2016) or vein (Keatley et al., 2021), and even coexisting U minerals within single pitchblende (Chernyshev et al., 2014). Besides source fingerprinting, another important aim of U isotope investigations on ore deposits is to understand the mechanisms responsible for U isotopic fractionation in those environments, which are thought to be dominated by low-temperature reduction (Bopp et al., 2009; Brennecka et al., 2010a; Murphy et al., 2014; Uvarova et al., 2014; Keatley et al., 2021), and post-deposition aqueous alteration (Brennecka et al., 2010a; Murphy et al., 2014; Keatley et al., 2021). To confirm the validity of using U isotope to fingerprint the source of U in uranium ore concentrates (uranium oxide U_3O_8, an intermediate product of U ore after mining and chemical processing), a few studies have also investigated the impact of (i) small scale U isotope heterogeneity in the ore material and (ii) the manufacturing processes (Golubev et al., 2013; Spano et al., 2017; Keatley et al., 2021).

5.2.5. High precision chronology

Based on the decay of ^{235}U and ^{238}U to ^{207}Pb and ^{206}Pb with half-lives of 0.703 Gyr and 4.468 Gyr, respectively (Jaffey et al., 1971) the U-Pb/Pb-Pb system is the most widely used high-precision chronometer for dating terrestrial and extraterrestrial samples. Provided knowledge of the $^{238}U/^{235}U$ ratio at present, the dual decay system allows determination of a Pb-Pb age as:

$$\frac{^{207}Pb^*}{^{206}Pb^*} = \frac{^{235}U}{^{238}U} \times \frac{e^{\lambda_{235}t} - 1}{e^{\lambda_{238}t} - 1} \quad (28)$$

where * denotes radiogenic lead, λ_{235} and λ_{238} are decay constants for ^{235}U and ^{238}U, and t is the age of the sample.

For the sake of interlaboratory calibration, and in the absence of resolvable U isotope variations (beside Oklo) in natural materials, a $^{238}U/^{235}U$ consensus value of 137.88 was adopted in the late 70s for Pb-Pb dating (Steiger and Jäger, 1977). This important assumption was, however, overthrown by the discovery of resolvable U isotopic variations in natural samples (*e.g.,* Stirling et al., 2007; Weyer et al., 2008; Bopp et al., 2009; Amelin et al., 2010; Hiess et al., 2012; Tissot and Dauphas, 2015). The impact of these variations on the accuracy of U-Pb and Pb-Pb ages has been extensively discussed (Hiess et al., 2012; Tissot and Dauphas, 2015; Tissot et al., 2017, 2019), and it is now accepted that both U and Pb isotopes need to be measured to obtain both precise and accurate dates.

The impact of U isotope variations is particularly important in early solar system (ESS) chronology, because (i) it took less than 10 Myr from the condensation of the Calcium, Aluminum-rich inclusions (CAIs: the first solids in the solar nebula) to the differentiation of asteroids (Connelly et al., 2017), (ii) the Pb-Pb system is the only high-precision absolute chronometer for such ancient ages, and (iii) small variations in $^{238}U/^{235}U$ results in relatively significant age offsets (~0.15 Myr offset per 0.1‰ variation, Tissot and Dauphas, 2015) compared to the achievable precision of Pb-Pb ages (~0.2-0.5 Myr). Together with the long-lasting search for the short-lived radionuclide ^{247}Cm (*Section 5.2.6*), this has led to a wide characterization of U isotopes in extraterrestrial materials (Fig. 14), from bulk meteorites, including carbonaceous chondrite, ordinary chondrite, enstatite chondrite, achondrites (*e.g.,* angrite, acapulcoite, aubrite, eucrite, and howardite), and ungrouped meteorites (Stirling et al., 2005; Amelin et al., 2010, 2011; Larsen et al., 2011; Bouvier et al., 2011b; Brennecka and Wadhwa, 2012; Connelly et al., 2012; Iizuka et al., 2014; Andersen et al., 2015; Goldmann et al., 2015; Spivak-Birndorf et al., 2015; Tissot et al., 2017), to meteorite components, such as CAIs, chondrules, mineral separates, and meteorite leachates (Stirling et al., 2006; Amelin et al., 2010; Brennecka et al., 2010b, 2015; Bouvier et al., 2011a; Brennecka and Wadhwa, 2012; Connelly et al., 2012; Goldmann et al., 2015; Tissot et al., 2016; Bollard et al., 2017; Shollenberger et al., 2019; Merle et al., 2020). While variability can be resolved in most of these samples at the 0.1 to 0.5 ‰, the largest variations are observed in CAIs, with ^{235}U excesses reaching several ‰ (up to +59‰ in the *Curious Marie* CAI). The U-corrected Pb-Pb ages produced in some of these studies continue to refine the chronology and evolution history of the ESS, for instance establishing the age of the Solar System at ~ 4.567-4.568 Gyr old (Amelin et al., 2010; Bouvier and Wadhwa, 2010; Bouvier et al., 2011a; Connelly et al., 2012), and demonstrating that chondrule formation and reprocessing started contemporaneously with CAI formation and extended for ~ 4 Myr after that (Bollard et al., 2017). In details, however, slight discrepancies between U-corrected Pb-Pb ages and chronometric constraints derived from short-lived chronometers, in particular the Al-Mg system, are the subject of much debate. Indeed, when combined U-Pb and Al-Mg isotopic investigations are conducted on the same CAI and chondrule samples, lower ESS ^{26}Al initials are recorded in chondrules than CAIs, and variable ^{26}Al initials are derived from different chondrules (Bollard et al., 2019). Understanding whether these variations (i) represent a true heterogeneous distribution of ^{26}Al in the ESS, (ii) have chronometric meaning, (iii) are the results of small systematic analytical biases (*e.g.,* isotopic fractionation during sample step leaching), or (iv) are a combination of the above, is a topic of intense research. Another issue in extraterrestrial samples is that the U isotope composition of some meteorite groups are not well-constrained, such as enstatite chondrites, howardites, acapulcoites, or aubrites (Fig. 14), and investigations on meteorite components are also limited to a few meteorites, primarily from the CV group.

Relevant to both extraterrestrial and terrestrial studies, $^{238}U/^{235}U$ variations also exist in the U-bearing minerals commonly used in U-Pb / Pb-Pb chronology, such as zircon, uraninite, apatite, monazite, xenotime, and baddeleyite (Hiess et al., 2012; Livermore et al., 2018). For zircon, the most widely used dating phase, variations have been observed in pooled fractions (100s to 1000s) of comagmatic grains (Hiess et al., 2012; Livermore et al., 2018) as well as in single crystals (Tissot et al., 2019). Recently, variations from -3.5 ±2.2 ‰ to 13.1 ± 3.4 ‰ have also been reported in single grains of titanite using LA-MC-ICP-MS and 10^{13} ohm amplifiers (Yamamoto et al., 2021). As discussed in Tissot and Ibañez-Mejia (2021), while these data clearly indicate the existence of significant mineral specific U isotope fractionations and, more likely for the largest effects, of kinetic isotope fractionations occurring at magmatic temperatures, the exact mecanisms driving U isotope fractionation in magmatic settings remain almost entirely unconstrained.

5.2.6. Search for ^{247}Cm

Curium-247 is short-lived radionuclide which decays into ^{235}U, with a half-life of 15.6 Myr (Tuli, 1995). Both U and Cm belong to the actinides, a group of heavy metal elements produced by the rapid neutron capture process (*r*-process), most likely during neutron-star merger events (Ji et al., 2016; Côté et al., 2021). If ^{247}Cm was present in the early solar system, the ^{247}Cm-^{235}U system would have the potential to

serve as a short-lived *r*-process chronometer (Blake and Schramm, 1973). Since ^{247}Cm is now extinct, the only evidence for the presence of live ^{247}Cm in the ESS would be ^{235}U excesses correlated with Cm/U ratios in ESS materials. An additional complication is that Cm has no stable isotope, and a proxy has to be used, most appropriately Nd (see Tissot et al., 2016 for details).

The findings of early investigations on ^{247}Cm are controversial due to analytical limitations: ^{235}U excesses or depletion up to several tens of percent were reported in meteorites, refractory inclusions and leachates (Arden, 1977; Tatsumoto and Shimamura, 1980). Follow up studies leveraging the "Lunatic I" digital TIMS and the double spike technique showed that lunar and meteoritic materials (and their inclusions) had no excess ^{235}U, within uncertainties, relative to the Earth (Chen and Wasserburg, 1981a, b, c; Chen, 1988). The search for the existence of ^{247}Cm ceased for approximately two decades, and only restarted after the advent of MC-ICP-MS, which achieved 1-2 orders of magnitude higher precision. Stirling et al. (2005, 2006) revisited the U isotopic compositions of bulk meteorites, mineral separates, and meteorite leachates. These initial searches did not find any well-resolved ^{235}U anomalies, but brought down the upper limit on the ESS ^{247}Cm/^{235}U ratio from ~4x10^{-3} (Chen and Wasserburg, 1981a) to ~8 x10^{-5}. In an investigation of CAIs, Brennecka et al. (2010b) found ^{235}U anomalies (up to ~3.5 permil) that correlated broadly with Nd/U and Th/U ratios. This study brought the first evidence of live ^{247}Cm in the ESS, suggesting an ESS ^{247}Cm/^{235}U ratio of (1.2 to 2.4) $\times10^{-4}$. But the origin of these isotopic signatures was rapidly questioned as subsequent studies of CAIs found departure from the apparent correlation between ^{235}U excess and Nd/U ratios (Amelin et al., 2010; Connelly et al., 2012), and instead argued that the observed variations reflected mass-dependent fractionation during condensation of solid CAIs from nebular gas. By targeting fine-grained CAIs, which, due to their volatility-controlled origin, have large Nd/U (and thus Cm/U) ratios, Tissot et al. (2016) was able to find an extremely U-depleted CAI, *Curious Marie*, which also contained a ^{235}U excess (of +59‰) outside the range plausibly explained by evaporation/condensation processes. While more samples would be desirable to populate what is currently essentially a two-points isochron, the discovery of *Curious Marie* confirmed the presence of live ^{247}Cm in the ESS, with an initial ^{247}Cm/^{235}U of (5.6±0.3)×10^{-5} (Tissot et al., 2016; Tang et al., 2017), a value that has become a key constraint to determine the astrophysical site of the *r*-process, and the timing of last injection of *r*-nuclides in the solar system's parental molecular cloud (Ji et al., 2016; Côté et al., 2021).

5.2.7. Experimental studies

Early experimental studies on U isotopes mainly investigated the effect of chemical exchange between reduced and oxidized (typically U(IV)-U(VI)) uranium phases. While the conclusion was that such an approach was not economically viable for large scale ^{235}U enrichment, these studies found (i) a preferential incorporation of heavy U isotopes in the U phase with the lower oxidation state (*i.e.,* reduced U, Shimokaua and Kobayashi, 1970; Florence et al., 1975; Fujii et al., 1989a, b, 2006; Nakanishi et al., 1996), and (ii) that the fractionation of uranium isotopes with odd mass numbers (^{233}U and ^{235}U) did not follow the mass-dependent fractionation line defined by isotopes with even mass numbers (^{234}U and ^{236}U) (Fujii et al., 1989a, b; Nomura et al., 1996). This odd-even staggering pattern was shown to be closely related to the isotope shift in the atomic spectra of U (Gagné et al., 1976, 1977, 1978). The odd-even effect of U isotopes is interpreted as the result of nuclear field shift effects (NFS), which result from the displacement of electronic energy caused by differences in electron density and isotope shape (Bigeleisen, 1996).

NFS, as a mass-independent but volume-dependent effect, prompted a rethinking of equilibrium fractionation theory (Bigeleisen, 1996; Knyazev and Myasoedov, 2001; Schauble, 2007; Yang and Liu, 2016). As mass-dependent fractionation decreases with increasing mass, and NFS effects increase with electron density at the nucleus, NFS effects are most pronounced in heavy elements (*i.e.*, with large nuclei). Today, it is well accepted that NFS effects are the dominant driver of U isotope fractionations in natural materials. Indeed, NFS effect during U redox reactions at room temperature are 3x larger than mass-dependent effects (Bigeleisen, 1996; Schauble, 2007; Abe et al., 2008). Furthermore, while mass-dependent fractionation scales proportionally to 1/T^2, NFS effects scale as 1/T, which implies that their relative contribution to the total isotope fractionation increases in high-T (*e.g.,* igneous) environments, an observation supporting the potential of U isotopes as redox tracers in magmatic environments (Tissot and Ibañez-Mejia, 2021). It is important to point out that NFS effects are equilibrium effects, and that it is not the reduction of U itself that promotes the isotopic fractionation, but the equilibration between oxidized and reduced U that allows the expression of these effects (see next section).

5.2.7.1. Redox experiments. Laboratory-based experiments are important approaches for quantifying the U fractionation associated with specific reaction pathways or environmental conditions. For U, redox reactions have been heavily studied, because of their potential for (1) understanding the role of redox transformation in U cycling near the Earth's surface and (2) developing remediation methods to control contamination in aquifer systems.

Laboratory-controlled redox experiments have primarily focused on U reduction processes, which are further subdivided into biotic and abiotic reduction. There are two major pathways for U biotic reduction: those involving metal-reducing bacteria (Basu et al., 2014; Stylo et al., 2015b) and those involving sulfate-reducing bacteria (Rademacher et al., 2006; Stirling et al., 2015; Stylo et al., 2015a; Dang et al., 2016; Basu et al., 2020). Abiotically, U(VI) can be reduced by various natural reductants such as zerovalent metal, Fe(II)-based reductant, sulfide reductant, and reduced organic matter (Rademacher et al., 2006; Stirling et al., 2007; Stylo et al., 2015b; Brown et al., 2018). During biotic reduction, microbes preferentially incorporate ^{238}U and transfer it into the reduced phase, leading to a lower δ^{238}U (by ~ -1‰) in the remaining U(VI) pool (Basu et al., 2014, 2020; Stirling et al., 2015; Stylo et al., 2015a, b; Dang et al., 2016). One early study reported slightly higher δ^{238}U (by ~+0.2 ‰) in the oxidized U phase during biotic reduction (Rademacher et al., 2006), but this result has since been revisited and attributed (by the same research group, Basu et al., 2014) to U(VI) adsorption onto the surface of bacteria cells overcompensating the U effect of reduction process during the U removal from the solution. In contrast, abiotic reduction experiments using zerovalent metals (Fe^0: Rademacher et al., 2006; Zn^0: Stirling et al., 2007) and organic species (peat: Stylo et al., 2015b) yielded no resolvable U isotopic fractionation. Adding to the initial confusion, most abiotic reduction reactions driven by Fe (II) and/or sulfide reductants, produced detectable U isotopic variations, but in the opposite direction of biotic reduction: ^{238}U is enriched in the remaining U(VI) pool (Stylo et al., 2015b). For a time, these results were interpreted as evidence that only biotic reduction results in significant NFS effects (*i.e.*, ^{238}U enrichments in the reduced phase), and the exciting possibility that U isotopes might be a specific tracer of bioreduction. This hypothesis was disproven by Brown et al. (2018), who showed that preferential sequestration of ^{238}U in the reduced U phases could occur even during abiotic reduction. This study was instrumental as it further showed that the seemingly conflicting literature results discussed above could be easily reconciled in a framework where ^{238}U/^{235}U fractionations reflects a balance between equilibrium (NFS) isotope effects and kinetic isotope fractionation. Indeed, during fast U removal, isotope fractionations are driven by kinetic (mass-dependent) effect, favoring precipitation in the reduced phase of the lighter ^{235}U isotope. In contrast, the expression of full blown NFS effects, with ^{238}U being enriched in the reduced phase, are only possible when U removal from the solution is slow enough that U(VI)-U(IV) isotope equilibration has time to take place. Because the pace of U removal (*i.e.,* reaction rate) is tied to the speciation of aqueous U, which

itself depends on the water chemistry, this study also further supported the conclusion of Chen et al. (2017) that the fractionation factor associated with reductive U removal from the ocean ($\Delta_{reduced\text{-}seawater}$) would likely change over geological times, as a function of the Ca/Mg, pCO_2, and pH of seawater.

In comparison to U reduction, there has been very little research done on U isotopic fractionation during U oxidation. Wang et al. (2015a) used dissolved oxygen to oxidize U(IV) and found a very limited enrichment of ^{238}U in the remaining reduced phase, likely due to a rind effect limiting the development of large isotope fractionations.

5.2.7.2. Well injection. Uranium contamination of groundwater and sediments during the mining and processing of U ores is a major public health concern and developing in-situ remediation techniques is the target of many environmental studies (Wall and Krumholz, 2006). The main approach to mitigate U pollution and decrease [U] in the groundwater is to immobilize aqueous U as a solid phase in the aquifer by changing its mobility (*e.g.,* Ginder-Vogel et al., 2006; Hyun et al., 2009). Since the mobility of U is controlled by its oxidation state and aqueous speciation, the two main methods of U immobilization revolve around the injection of amended groundwater in contaminated sites that promotes either (i) reduction of soluble U(VI) to insoluble U(IV), or (ii) adsorption to the walls of the aquifer through changes in U(VI) speciation.

While the determination of U concentrations is the most common and straightforward approach for monitoring the efficiency of U-contamination remediation methods, it often cannot be used to identify the geochemical processes at play in the aquifer (Jemison et al., 2018). Being able to confirm that the low groundwater U concentrations are the results of the implemented remediation method (reduction vs adsorption) and not some other, non-controlled, parameter is crucial. Uranium isotope variations have emerged as a promising new tool to fingerprint these processes, inspired by the potential revealed by laboratory studies on U isotopic fractionation (Rademacher et al., 2006; Basu et al., 2014; Stylo et al., 2015a; Wang et al., 2015a, b; Dang et al., 2016). In line with

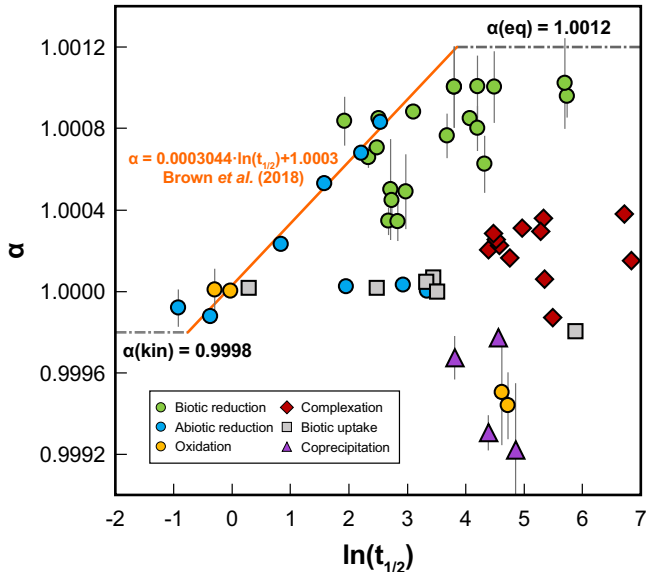

Fig. 15. Relationship between the isotope fractionation factor (α) and half-life of aqueous U(VI) ($t_{1/2}$, in hours) for various U removal reactions. When available, fractionation factors and half-lives are plotted as reported in the original publication. Otherwise, α and $t_{1/2}$ are calculated based on Eqs. (29)–(32). The orange line represents the best fit between α and $t_{1/2}$ from a series of abiotic uranium reductions defined in Brown et al. (2018). The grey dash lines show the limit of kinetic fractionation (0.9998) and equilibrium fractionation (1.0012) respectively.

the early findings of Brennecka et al. (2011b), recent field studies show that only limited $^{238}U/^{235}U$ fractionation is observed during the adsorption-desorption treatment, with ^{235}U being preferentially removed from solution ($\Delta_{adsorbed\text{-}aqueous}$~0 to -0.22 ‰, Shiel et al., 2013; Jemison et al., 2016; Dang et al., 2016). On the contrary, bioremediations that take advantage of metal-reducing bacteria lead to large and clearly resolvable fractionations of opposite direction ($\Delta_{reduced\text{-}aqueous}$ ~ +0.5 to +1.0 ‰; Bopp et al., 2010; Shiel et al., 2016), consistent with the permil effects observed in postmining natural reduction settings (Basu et al., 2015; Brown et al., 2016; Placzek et al., 2016). In a recent oxidation experiment designed to simulate the natural remobilization through U oxidation after remediation, Jemison et al. (2018) showed that a significant $\delta^{238}U$ change was observed, supporting the adequacy of using U isotopes as a monitor of natural redox reactions at mining sites. This conclusion is strengthened by recent reactive transport modeling efforts, which demonstrated that incorporating $\delta^{238}U$ data in the model allows for better interpretation of chemical reactions and groundwater transport processes influencing U cycling (Jemison et al., 2020).

5.2.7.3. Other experimental studies. In addition to redox reactions, lab-controlled experiments have investigated U isotopic fractionation during adsorption, coprecipitation, complexation, weathering, and biotic uptake. U(VI) adsorption onto Mn-oxyhydroxides (birnessite) (Brennecka et al., 2011b) and Fe-hydroxides (goethite) (Dang et al., 2016) under oxic conditions preferentially incorporate ^{235}U into adsorbed phases ($\Delta_{adsorbed\text{-}aqueous}$ ~ -0.20 ‰). Similarly, nonreductive U uptake by freshwater plankton also enriches lighter U isotopes in the biomass ($\Delta_{plankton\text{-}aqueous}$ ~ -0.23 ‰, Chen et al., 2020). As partly discussed above, the aqueous speciation of U, and thus the water chemistry and pH, as well as the nature of the mineral phase (*e.g.*, calcite vs aragonite) were also shown experimentally to influence the degree of isotope fractionation observed in carbonates (Chen et al., 2016, 2017; Brown et al., 2018).

A study investigating U(IV)-U(VI) exchange under near natural aqueous conditions also observed ^{235}U enrichment in U(VI) ($\Delta_{U(VI)\text{-}U(IV)}$ ~ -1.64 ‰, Wang et al., 2015b), slightly larger than, but still broadly consistent with, the ~1.2-1.3 ‰ effects expected from NFS. Under anoxic conditions, a recent study showed that U(IV) can be remobilized by ligands in the near-surface environment, resulting in ^{238}U concentrating in mobilized materials, potentially complicating remediation monitoring or paleo-redox reconstructions (Roebbert et al., 2021).

A few leaching experiments have also been conducted to try to evaluate the influence of weathering and alteration on U isotopic fractionation, as well as to ensure that the minerals used for age determination behave as closed system with regards to U isotopes. The impact of leaching on U isotope fractionation remains, however, unclear. While a systematic enrichment of ^{235}U was observed in the leachates from euxenite (Stirling et al., 2007) and zircon (Hiess et al., 2012), other studies on zircon (Stirling et al., 2007; Livermore et al., 2018) and uraninite (Stirling et al., 2007) found no systematic offset between the leachates and bulk analyses. While the ^{235}U enrichment in successive leaching steps of euxenite and zircon have been interpreted as evidence of the preferential release of weakly bound ^{235}U from the crystal lattice during leaching, these effects could also simply reflect equilibrium U isotope fractionation between the oxidized (soluble) U in the leachates and reduced (insoluble) U in the minerals. More controlled experiments are needed to understand the isotopic impact of leaching on minerals.

Assuming U removal during U reaction experiments can be described as a Rayleigh distillation process, the U isotopic fractionation can be described as:

$$\delta^{238}U = \left(\delta^{238}U_0 + 1000‰\right)\left[\frac{c(t)}{c_0}\right]^{\alpha-1} - 1000‰ \quad (29)$$

where $\delta^{238}U_0$ and c_0 are the initial isotopic composition and

concentration of aqueous U; $\delta^{238}U$ and $c(t)$ are the isotopic composition and concentration at the sampling time t; and α is the U isotopic fractionation factor. Eq. (29) can be rewritten in the following format:

$$ln\left(\delta^{238}U + 1000‰\right) = (\alpha - 1)ln\left[\frac{c(t)}{c_0}\right] + ln\left(\delta^{238}U_0 + 1000‰\right) \quad (30)$$

The α value can be determined by the slope of the linear regression between $ln(\delta^{238}U + 1000‰)$ and $ln[c(t)/c_0]$. Furthermore, in the case of a first-order reaction, the concentration and reaction time are related by the following equation:

$$ln\left[\frac{c(t)}{c_0}\right] = -kt \quad (31)$$

where k is the first-order rate constant, which can be obtained by linear fit between $ln[c(t)/c_0]$ and time. The half-life ($t_{1/2}$) is expressed as:

$$t_{1/2} = ln(2)/k \quad (32)$$

Brown et al. (2018) investigated the relationship between the fractionation factor, α, and the aqueous U(VI) half-life in a series of abiotic reduction. This relationship revealed how the degree of U isotopic fractionation relates to the U removal rate. Using the UID, we expanded this framework to more U removal reactions (Fig. 15), including biotic and abiotic reduction, oxidation, complexation with ligand, biotic U uptake, and U coprecipitation with other mineral phases (Basu et al., 2014, 2020; Stylo et al., 2015a, b; Wang et al., 2015a; Chen et al., 2016; Brown et al., 2018; Roebbert et al., 2021). Only the experiments with first-order reactions rates are included in Fig. 15. We find that most abiotic reduction experiments and some of the biotic reduction and oxidation experiments follow the α-$t_{1/2}$ relationship defined in Brown et al. (2018), with no experiments plotting significantly to the left of this relationship. This observation further supports the proposal by Brown et al. (2018) that when the aqueuous U(VI) half-life is short, the extent of isotopic fractionation represents a balance between equilibrium isotope fractionation (in this case, the mass-independent NFS) and kinetic isotope fractionation. Brown et al. (2018) further hypothesized the necessary half-life to achieve the predicted NFS fractionation of ~1.2 ‰ is ~65 hr. The plateau in isotope fractionation factors observed at ~ 1‰ in biotic reduction experiments with long aqueous U(VI) half-lives supports this proposal. It also reveals that the theoretical maximum NFS effects (~1.2 ‰; Bigeleisen, 1996) is not expressed in any of the currently available experiments, indicating (i) that complete equilibrium between U(VI) and U(IV) is never attained, and/or (ii) in all experiments, another process imparts a small (~0.2‰) negative isotope fractionation. The same mechanism is likely to explain the similar offest to lower fractionation factors that is observed in many of the biotic reduction experiments with aqueous U(VI) half-life lower than 65 hr. More work is needed to further undertsand these effects.

In clear contrast to the redox experiments, other U removal reactions are characterized by small, negigible or negative isotopic fractionations. This indicates that for these reactions, NFS effects are not the dominant driver of isotope fractionation. Instead, and as previous work have proposed, the fractionation factors retrieved from complexation, coprecipitation, and biotic uptake must reflect a stong control of vibrational mass-dependent effects (*e.g.*, during U adsorption) and/or kinetic effects, which both tend to enrich the product of the reaction in the lighter isotopes.

5.2.8. Forensic studies

5.2.8.1. Natural nuclear fission reactor. Under the right conditions, U-rich deposits formed before ~1.8 Ga, when natural ^{235}U abundance was >~3%, could have reached criticality. The only location where such sustained spontaneous fission chain reactions are known to have naturally occurred is in the mine of Oklo, in the Republic of Gabon. These reactors are a series of sandstone-hosted U ore deposits discovered in the 1970's near Oklo and Bangombè, where natural fission events occurred at ~ 1.78 Ga (Bodu, 1972; Neuilly et al., 1972; Roth, 1977). Compared with other types of U deposits (see *Section 5.2.4*), natural nuclear reactors display unusually high $^{238}U/^{235}U$ ratios due to ^{235}U burn-up during self-sustained fission. As a result, U isotopic compositions in Oklo's bulk ore samples or their mineral components are widely used to examine nuclear fission activities (Lancelot et al., 1975; De Laeter et al., 1980; Holliger and Devillers, 1981; Curtis et al., 1989; Loss et al., 1989; Bros et al., 1993, 1996, 2003; Gauthier-Lafaye et al., 1996; Hidaka and Holliger, 1998; Hidaka et al., 1999; Fernández-Díaz et al., 2000; Hidaka and Gauthier-Lafaye, 2000; Horie et al., 2004; Kikuchi and Hidaka, 2009). Natural fission reactors are important for assessing the long-term effects of nuclear waste disposal in geological settings because they are considered as analogues of disposal sites to understand the behavior of radionuclides in natural environment over geological timescales. Hence, numerous isotopic investigations have studied the presence and migration of fissiogenic radionuclides in Oklo's natural nuclear reactors (*e.g.,* Mo, Ru, Pd, Ag, Cd, Sn, Te, Cs, Ba, Tc, Rh and rare earth elements) (Gauthier-Lafaye et al., 1996).

5.2.8.2. Health physics. Depleted uranium, which is predominantly a by-product of nuclear enrichment efforts, has numerous civilian and military applications, including in aeronautics, the shipbuilding industry, radiological protection, chemical manufacturing and armor-piercing ammunitions, due to its high density, hardness, and melting point (Bleise et al., 2003). Internal exposure to DU is a major health concern in humans, especially soldiers, who can be exposed to DU via inhalation of airborne particles from weapon combustion, ingestion of contaminated food and water, penetration by embedded shrapnel, and/or contact on wounds (Bleise et al., 2003). Given that DU has a U isotopic composition significantly different from that of NU (*i.e.,* it is depleted in ^{234}U and ^{235}U), isotopic compositions of urine or blood can be effective diagnostic tools for tracing the source of U exposure. U in urine is the primary focus of isotopic studies on DU exposure since it has historically been used in biomonitoring (Duarte and Szeles, 1994; Ejnik et al., 2000, 2005; Horan et al., 2002; Krystek and Ritsema, 2002; Pappas et al., 2003; Gwiazda et al., 2004; Parrish et al., 2006; Gray et al., 2012; Xiao et al., 2014), while only a few pioneering studies have investigated U isotopes in blood specimen (Tolmachyov et al., 2004; Todorov et al., 2009). These studies successfully identified DU exposure in patients by detecting lower $^{235}U/^{238}U$ ratios urine or blood samples than NU.

5.2.8.3. Nuclear contamination. U isotopes are a useful tool for tracking environmental contaminations produced by anthropogenic nuclear activities such as weapon explosions, power plant accidents, and other contaminations associated with mining or nuclear fuel processing.

Military contamination can cause $^{238}U/^{235}U$ ratios in environmental samples to fluctuate in opposing directions depending on the source of contamination. Contamination from DU munitions causes higher $^{238}U/^{235}U$ ratios in war-zone soils or sediments (Boulyga et al., 2001; Danesi et al., 2003a, b; Al-Zamel et al., 2005; Lloyd et al., 2009). Nuclear weapons and related tests, on the other hand, employed enriched uranium, resulting in lower $^{238}U/^{235}U$ ratios in atmospheric deposits or fallouts (Taylor et al., 1998; Fujikawa et al., 2003; Kikawada et al., 2015; Lewis et al., 2015). Establishing full records of $^{238}U/^{235}U$ in environmental samples over time is thus an efficient method for investigating the existence, sources, or transit of radioactive contamination (Warneke et al., 2002).

Forensic investigations into power plant accidents have focused on the two most catastrophic nuclear energy disasters: the 1986 Chernobyl nuclear power plant accident (Boulyga et al., 2000; Boulyga and Becker, 2001, 2002; Sobotovich and Bondarenko, 2001; Pazukhin and Rudya, 2002; Sahoo et al., 2002, 2004, 2009; Boulyga and Prohaska, 2008; Pöml et al., 2013) and the 2011 Fukushima Daiichi nuclear power plant accident (Shibahara et al., 2016; Mishra et al., 2019; Veerasamy et al.,

2020). Direct measurement of the nuclear fuel from power plant accident reveals enrichment in ^{235}U versus NU (Pöml et al., 2013). When fallout radionuclides from power plants migrated and deposited in neighboring regions, soil samples from polluted areas inherited lower $^{238}U/^{235}U$ ratios than NU (Boulyga et al., 2000; Boulyga and Becker, 2001, 2002; Sobotovich and Bondarenko, 2001; Pazukhin and Rudya, 2002; Sahoo et al., 2002, 2004, 2009; Boulyga and Prohaska, 2008), while those that avoided contamination from the accidents preserved indistinguishable $^{238}U/^{235}U$ compositions relative to NU (Shibahara et al., 2016; Mishra et al., 2019; Veerasamy et al., 2020).

Other nuclear contamination studies are based on the same principle of detecting anomalous $^{238}U/^{235}U$ in sedimentary or water samples near nuclear facilities that produce and process EU (Hamilton and Stevens, 1985; Rodríguez-Alvarez and Sánchez, 1995; Howe et al., 2002; Sahoo et al., 2002; Yamamoto et al., 2002; Christensen et al., 2004; Meyers et al., 2014). And similar investigations have been conducted near mines (Awudu and Darko, 2011) or river systems (Joshi et al., 1983) that were potentially contaminated by radionuclides.

5.2.8.4. Nuclear safeguard. The rapid and precise isotopic characterization of particulate uranium materials is critical for nuclear safeguard applications, such as identifying illicit radioactive material trafficking and detecting the usage of unapproved nuclear materials in nuclear facilities. In-situ characterization of solid nuclear samples is a useful approach for determining the presence and provenance of nuclear materials because U particles have distinct U isotopic fingerprints that are influenced by source materials and manufacturing procedures (Betti et al., 1999; Tamborini, 2004; Varga, 2008; Marin et al., 2013; Hubert et al., 2014; Claverie et al., 2016; Yomogida et al., 2017; Krachler et al., 2018; Stebelkov et al., 2018; Varga et al., 2018; Kips et al., 2019; Ronzani et al., 2019). Aside from direct measurement of U particles (Betti et al., 1999; Varga, 2008; Hubert et al., 2014; Yomogida et al., 2017; Ronzani et al., 2019), fuel pellets (Krachler et al., 2018; Kips et al., 2019) and confiscated illicit U samples (Krachler et al., 2018), some of the nuclear safeguard studies have developed techniques to discover U particles in the mixture of other materials in swipe samples from the environment (Tamborini, 2004) or the surface of nuclear packaging materials (Stebelkov et al., 2018), as a means to identify and prevent undeclared nuclear activities without time-consuming procedures.

6. Conclusion and outlook

This work introduces the UID, a comprehensive, freely accessible, updatable, and internally consistent uranium isotope database. At this writing, the UID contains more than 14,000 data points from approximately 320 publications. We provided a detailed description of our data collection procedure, all additional information entered in the UID, and their coverage as well as the normalization procedure carried out on the data. We took the highest care to make all data coherent, comparable, and back trackable, as well as all adjustments transparent. Adequate metadata are also provided to allow users to select data that are suitable for a particular type of study. The UID will be regularly updated to incorporate newly published uranium isotopes data. With constructive feedback from the community, we expect that the UID can become a reliable resource for the U isotope community, as well as the broader geochemical community.

In the long-term, we hope to the see UID grow from the simple database presented here into a more extensive tool. This includes the development of an online and interactive searchable database with built-in visualization capabilities, as well as a streamlined protocol for data submission, review, and incorporation into the UID. With constructive feedback and involvement from the community, we expect that the UID can become a more community-involved resource, maintained for and by the community, and whose impact will reach far into the broader geochemical community.

CRediT authorship contribution statement

Haoyu Li: Methodology, Formal analysis, Investigation, Data curation, Visualization, Writing – original draft. **François L.H. Tissot:** Conceptualization, Methodology, Supervision, Visualization, Project administration, Writing – review & editing.

Declaration of Competing Interest

The authors declare that they have no conflict of interest.

Data availability

The UID is hosted and freely available on the Isotoparium website: https://isotoparium.org/uid. For security reasons, users can only download the spreadsheets from the website but cannot upload data directly into the database. Future queries about the database should be addressed via email to uid@caltech.edu.

Acknowledgements

This work was supported by grants: NASA grant 80NSSC20K1398 (PI: F.L.H.T., FI: H.L.), as well as NSF grants EAR-1824002 and MGG-2054892, a Packard Fellowship and start-up funds (provided by Caltech) to FLHT.

Appendix A. Supplementary data

Supplementary data to this article can be found online at https://doi.org/10.1016/j.chemgeo.2022.121221.

References

Abe, M., Suzuki, T., Fujii, Y., Hada, M., Hirao, K., 2008. An ab initio molecular orbital study of the nuclear volume effects in uranium isotope fractionations. J. Chem. Phys. 129. https://doi.org/10.1063/1.2992616.

Abshire, M.L., Romaniello, S.J., Kuzminov, A.M., Cofrancesco, J., Severmann, S., Riedinger, N., 2020. Uranium isotopes as a proxy for primary depositional redox conditions in organic-rich marine systems. Earth Planet. Sci. Lett. 529, 115878. https://doi.org/10.1016/j.epsl.2019.115878.

Alamelu, D., Jagadish, Kumar S., 2016. Determination of isotopic composition of uranium samples using alpha spectrometry. J. Radioanal. Nucl. Chem. 310, 541–546. https://doi.org/10.1007/s10967-016-4874-6.

Al-Zamel, A.Z., Bou-Rabee, F., Olszewski, M., Bem, H., 2005. Natural radionuclides and ^{137}Cs activity concentration in the bottom sediment cores from Kuwait Bay. J. Radioanal. Nucl. Chem. 266, 269–276. https://doi.org/10.1007/s10967-005-0903-6.

Amelin, Y., Kaltenbach, A., Iizuka, T., Stirling, C.H., Ireland, T.R., Petaev, M., Jacobsen, S.B., 2010. U-Pb chronology of the Solar System's oldest solids with variable $^{238}U/^{235}U$. Earth Planet. Sci. Lett. 300, 343–350. https://doi.org/10.1016/j.epsl.2010.10.015.

Amelin, Y., Kaltenbach, A., Stirling, C.H., 2011. The U-Pb systematics and cooling rate of plutonic angrite NWA 4590. Lunar and Planetary Science Conference, p. 1682.

Andersen, M.B., Romaniello, S., Vance, D., Little, S.H., Herdman, R., Lyons, T.W., 2014. A modern framework for the interpretation of $^{238}U/^{235}U$ in studies of ancient ocean redox. Earth Planet. Sci. Lett. 400, 184–194. https://doi.org/10.1016/j.epsl.2014.05.051.

Andersen, M.B., Elliott, T., Freymuth, H., Sims, K.W.W., Niu, Y., Kelley, K.A., 2015. The terrestrial uranium isotope cycle. Nature 517, 356–359. https://doi.org/10.1038/nature14062.

Andersen, M.B., Vance, D., Morford, J.L., Bura-Nakić, E., Breitenbach, S.F.M., Och, L., 2016. Closing in on the marine $^{238}U/^{235}U$ budget. Chem. Geol. 420, 11–22. https://doi.org/10.1016/j.chemgeo.2015.10.041.

Andersen, M.B., Stirling, C.H., Weyer, S., 2017. Uranium isotope fractionation. Rev. Mineral. Geochemistry 82, 799–850. https://pubs.geoscienceworld.org/rimg/article/82/1/799-850/302428.

Andersen, M.B., Matthews, A., Vance, D., Bar-Matthews, M., Archer, C., de Souza, G.F., 2018. A 10-fold decline in the deep Eastern Mediterranean thermohaline overturning circulation during the last interglacial period. Earth Planet. Sci. Lett. 503, 58–67. https://doi.org/10.1016/j.epsl.2018.09.013.

Andersen, M.B., Matthews, A., Bar-Matthews, M., Vance, D., 2020. Rapid onset of ocean anoxia shown by high U and low Mo isotope compositions of sapropel S1. Geochemical Perspect. Lett. 15, 10–14. https://doi.org/10.7185/geochemlet.2027.

Arden, J.W., 1977. Isotopic composition of uranium in chondritic meteorites. Nature 269, 788–789. https://doi.org/10.1038/269788a0.

Asael, D., Tissot, F.L.H., Reinhard, C.T., Rouxel, O., Dauphas, N., Lyons, T.W., Ponzevera, E., Liorzou, C., Chéron, S., 2013. Coupled molybdenum, iron and uranium stable isotopes as oceanic paleoredox proxies during the Paleoproterozoic Shunga Event. Chem. Geol. 362, 193–210. https://doi.org/10.1016/j.chemgeo.2013.08.003.

Aston, F.W., 1931. Constitution of Thallium and Uranium. Nature 128, 725. https://doi.org/10.1038/128725a0.

Avanzinelli, R., Prytulak, J., Skora, S., Heumann, A., Koetsier, G., Elliott, T., 2012. Combined ^{238}U- ^{230}Th and ^{235}U- ^{231}Pa constraints on the transport of slab-derived material beneath the Mariana Islands. Geochim. Cosmochim. Acta 92, 308–328. https://doi.org/10.1016/j.gca.2012.06.020.

Avanzinelli, R., Casalini, M., Elliott, T., Conticelli, S., 2018. Carbon fluxes from subducted carbonates revealed by uranium excess at Mount Vesuvius, Italy. Geology 46, 259–262. https://doi.org/10.1130/G39766.1.

Awudu, A.R., Darko, E.O., 2011. ^{234}U/^{238}U and ^{235}U/^{238}U ratios in domestic water from the environs of Obuasi mine in Ghana. J. Radioanal. Nucl. Chem. 287, 129–134. https://doi.org/10.1007/s10967-010-0662-x.

Azmy, K., Kendall, B., Brand, U., Stouge, S., Gordon, G.W., 2015. Redox conditions across the Cambrian-Ordovician boundary: Elemental and isotopic signatures retained in the GSSP carbonates. Palaeogeogr. Palaeoclimatol. Palaeoecol. 440, 440–454. https://doi.org/10.1016/j.palaeo.2015.09.014.

Barshick, C.M., Shaw, R.W., Young, J.P., Ramsay, J.M., 1995. Evaluation of the precision and accuracy of a uranium isotopic analysis using glow discharge optogalvanic spectroscopy. Anal. Chem. 67, 3814–3818. https://doi.org/10.1021/ac00116a033.

Bartlett, R., Elrick, M., Wheeley, J.R., Polyak, V., Desrochers, A., Asmerom, Y., 2018. Abrupt global-ocean anoxia during the Late Ordovician–early Silurian detected using uranium isotopes of marine carbonates. Proc. Natl. Acad. Sci. 115, 5896–5901. https://doi.org/10.1073/pnas.1802438115.

Basu, A., Sanford, R.A., Johnson, T.M., Lundstrom, C.C., Löffler, F.E., 2014. Uranium isotopic fractionation factors during U(VI) reduction by bacterial isolates. Geochim. Cosmochim. Acta 136, 100–113. https://doi.org/10.1016/j.gca.2014.02.041.

Basu, A., Brown, S.T., Christensen, J.N., Depaolo, D.J., Reimus, P.W., Heikoop, J.M., Woldegabriel, G., Simmons, A.M., House, B.M., Hartmann, M., Maher, K., 2015. Isotopic and geochemical tracers for U(VI) reduction and U mobility at an in situ recovery U mine. Environ. Sci. Technol. 49, 5939–5947. https://doi.org/10.1021/acs.est.5b00701.

Basu, A., Wanner, C., Johnson, T.M., Lundstrom, C.C., Sanford, R.A., Sonnenthal, E.L., Boyanov, M.I., Kemner, K.M., 2020. Microbial U Isotope Fractionation Depends on the U(VI) Reduction Rate. Environ. Sci. Technol. 54, 2295–2303. https://doi.org/10.1021/acs.est.9b05935.

Baudin, G., Blain, C., Hagemann, R., Kremer, M., Lucas, M., Merlivat, L., Molina, R., Nief, G., Prost-Marechal, F., Regnaud, F., Roth, E., 1972. Quelques données nouvelles sur les réactions nucléaires en chaîne qui se sont produites dans le gisement d'Oklo. C. R. Acad. Sc. Paris 275, 2291–2294.

Betti, M., Tamborini, G., Koch, L., 1999. Use of secondary ion mass spectrometry in nuclear forensic analysis for the characterization of plutonium and highly enriched uranium particles. Anal. Chem. 71, 2616–2622. https://doi.org/10.1021/ac981184r.

Bigeleisen, J., 1996. Nuclear size and shape effects in chemical reactions. Isotope chemistry of the heavy elements. J. Am. Chem. Soc. 118, 3676–3680. https://doi.org/10.1021/ja954076k.

Blake, J.B., Schramm, D.N., 1973. ^{247}Cm as a Short-lived r-Process Chronometer. Nat. Phys. Sci. 243, 138–140. https://doi.org/10.1038/physci243138a0.

Bleise, A., Danesi, P.R., Burkart, W., 2003. Properties, use and health effects of depleted uranium (DU): A general overview. J. Environ. Radioact. 64, 93–112. https://doi.org/10.1016/S0265-931X(02)00041-3.

Bodu, R., 1972. Sur l'existence d'anomalies isotopiques rencontrées dans l'uranium du Gabon.

Bodu, R., Bouzigues, H., Morin, N., Pfiffelmann, J.-P., 1972. Sur l'existence d'anomalies isotopiques rencontrees dans l'uranium du Gabon. Compte Rendu l'Académie des Sci. 275, 1731–1734.

Bollard, J., Connelly, J.N., Whitehouse, M.J., Pringle, E.A., Bonal, L., Jørgensen, J.K., Nordlund, Å., Moynier, F., Bizzarro, M., 2017. Early formation of planetary building blocks inferred from Pb isotopic ages of chondrules. Sci. Adv. 3. https://doi.org/10.1126/sciadv.1700407.

Bollard, J., Kawasaki, N., Sakamoto, N., Olsen, M., Itoh, S., Larsen, K., Wielandt, D., Schiller, M., Connelly, J.N., Yurimoto, H., Bizzarro, M., 2019. Combined U-corrected Pb-Pb dating and ^{26}Al-^{26}Mg systematics of individual chondrules – Evidence for a reduced initial abundance of 26Al amongst inner Solar System chondrules. Geochim. Cosmochim. Acta 260, 62–83. https://doi.org/10.1016/j.gca.2019.06.025.

Bopp, C.J., Lundstrom, C.C., Johnson, T.M., Glessner, J.J.G., 2009. Variations in ^{238}U/^{235}U in uranium ore deposits: Isotopic signatures of the U reduction process? Geology 37, 611–614. https://doi.org/10.1130/G25550A.1.

Bopp, C.J., Lundstrom, C.C., Johnson, T.M., Sanford, R.A., Long, P.E., Williams, K.H., 2010. Uranium ^{238}U/^{235}U Isotope Ratios as Indicators of Reduction: Results from an in situ Biostimulation Experiment at Rifle, Colorado, U.S.A. Environ. Sci. Technol. 44, 5927–5933. https://doi.org/10.1021/es100643v.

Boulyga, S.F., Becker, J.S., 2001. Determination of uranium isotopic composition and ^{236}U content of soil samples and hot particles using inductively coupled plasma mass spectrometry. Fresenius. J. Anal. Chem. 370, 612–617. https://doi.org/10.1007/s002160100838.

Boulyga, S.F., Becker, J.S., 2002. Isotopic analysis of uranium and plutonium using ICP-MS and estimation of burn-up of spent uranium in contaminated environmental samples. J. Anal. At. Spectrom. 17, 1143–1147. https://doi.org/10.1039/b202196j.

Boulyga, S.F., Prohaska, T., 2008. Determining the isotopic compositions of uranium and fission products in radioactive environmental microsamples using laser ablation ICP-MS with multiple ion counters. Anal. Bioanal. Chem. 390, 531–539. https://doi.org/10.1007/s00216-007-1575-6.

Boulyga, S.F., Becker, J.S., Matusevitch, J.L., Dietze, H.J., 2000. Isotope ratio measurements of spent reactor uranium in environmental samples by using inductively coupled plasma mass spectrometry. Int. J. Mass Spectrom. 203, 143–154. https://doi.org/10.1016/S1387-3806(00)00296-7.

Boulyga, S.F., Testa, C., Desideri, D., Becker, J.S., 2001. Optimisation and application of ICP-MS and alpha-spectrometry for determination of isotopic ratios of depleted uranium and plutonium in samples collected in Kosovo. J. Anal. At. Spectrom. 16, 1283–1289. https://doi.org/10.1039/b103178n.

Boulyga, S., Konegger-Kappel, S., Richter, S., Sangély, L., 2015. Mass spectrometric analysis for nuclear safeguards. J. Anal. At. Spectrom. 30, 1469–1489. https://doi.org/10.1039/c4ja00491d.

Boulyga, S.F., Koepf, A., Konegger-Kappel, S., Macsik, Z., Stadelmann, G., 2016. Uranium isotope analysis by MC-ICP-MS in sub-ng sized samples. J. Anal. At. Spectrom. 31, 2272–2284. https://doi.org/10.1039/c6ja00238b.

Bouvier, A., Wadhwa, M., 2010. The age of the Solar System redefined by the oldest Pb-Pb age of a meteoritic inclusion. Nat. Geosci. 3, 637–641. https://doi.org/10.1038/ngeo941.

Bouvier, A., Brennecka, G.A., Wadhwa, M., 2011a. Absolute Chronology of the First Solids in the Solar System. Work. Form. First Solids Sol. Syst. 4–5.

Bouvier, A., Spivak-Birndorf, L.J., Brennecka, G.A., Wadhwa, M., 2011b. New constraints on early Solar System chronology from Al–Mg and U–Pb isotope systematics in the unique basaltic achondrite Northwest Africa 2976. Geochim. Cosmochim. Acta 75, 5310–5323. Available at: https://doi.org/10.1016/j.gca.2011.06.033.

Brennecka, G.A., Wadhwa, M., 2012. Uranium isotope compositions of the basaltic angrite meteorites and the chronological implications for the early Solar System. Proc. Natl. Acad. Sci. 109, 9299–9303. https://doi.org/10.1073/pnas.1114043109.

Brennecka, G.A., Borg, L.E., Hutcheon, I.D., Sharp, M.A., Anbar, A.D., 2010a. Natural variations in uranium isotope ratios of uranium ore concentrates: Understanding the ^{238}U/^{235}U fractionation mechanism. Earth Planet. Sci. Lett. 291, 228–233. https://doi.org/10.1016/j.epsl.2010.01.023.

Brennecka, G.A., Weyer, S., Wadhwa, M., Janney, P.E., Zipfel, J., Anbar, A.D., 2010b. ^{238}U/^{235}U variations in meteorites: Extant ^{247}Cm and implications for Pb-Pb dating. Science 327, 449–451. https://doi.org/10.1126/science.1180871.

Brennecka, G.A., Herrmann, A.D., Algeo, T.J., Anbar, A.D., 2011a. Rapid expansion of oceanic anoxia immediately before the end-Permian mass extinction. Proc. Natl. Acad. Sci. 108, 17631–17634. https://doi.org/10.1073/pnas.1106039108.

Brennecka, G.A., Wasylenki, L.E., Bargar, J.R., Weyer, S., Anbar, A.D., 2011b. Uranium isotope fractionation during adsorption to Mn-oxyhydroxides. Environ. Sci. Technol. 45, 1370–1375. https://doi.org/10.1021/es103061v.

Brennecka, G.A., Budde, G., Kleine, T., 2015. Uranium isotopic composition and absolute ages of Allende chondrules. Meteorit. Planet. Sci. 50, 1995–2002. https://doi.org/10.1111/maps.12567.

Brennecka, G.A., Amelin, Y., Kleine, T., 2018. Uranium isotope ratios of Muonionalusta troilite and complications for the absolute age of the IVA iron meteorite core. Earth Planet. Sci. Lett. 490, 1–10. https://doi.org/10.1016/j.epsl.2018.03.010.

Bros, R., Turpin, L., Gauthier-Lafaye, F., Holliger, P., Stille, P., 1993. Occurrence of naturally enriched ^{235}U: Implications for plutonium behaviour in natural environments. Geochim. Cosmochim. Acta 57, 1351–1356. https://doi.org/10.1016/0016-7037(93)90072-5.

Bros, R., Carpena, J., Sere, V., Beltritti, A., 1996. Occurrence of Pu and Fissiogenic REE in Hydrothermal Apatites from the Fossil Nuclear Reactor 16 at Oklo (Gabon). Radiochim. Acta 74, 277–282. https://doi.org/10.1524/ract.1996.74.special-issue.277.

Bros, R., Hidaka, H., Kamei, G., Ohnuki, T., 2003. Mobilization and mechanisms of retardation in the Oklo natural reactor zone 2 (Gabon) - Inferences from U, REE, Zr, Mo and Se isotopes. Appl. Geochemistry 18, 1807–1824. https://doi.org/10.1016/S0883-2927(03)00113-6.

Brown, S.T., Basu, A., Christensen, J.N., Reimus, P., Heikoop, J., Simmons, A., WoldeGabriel, G., Maher, K., Weaver, K., Clay, J., DePaolo, D.J., 2016. Isotopic Evidence for Reductive Immobilization of Uranium Across a Roll-Front Mineral Deposit. Environ. Sci. Technol. 50, 6189–6198. https://doi.org/10.1021/acs.est.6b00626.

Brown, S.T., Basu, A., Ding, X., Christensen, J.N., DePaolo, D.J., 2018. Uranium isotope fractionation by abiotic reductive precipitation. Proc. Natl. Acad. Sci. 115, 8688–8693. https://doi.org/10.1073/pnas.1805234115.

Bruggmann, S., Gilleaudeau, G.J., Romaniello, S.J., Severmann, S., Canfield, D.E., Anbar, A.D., Scholz, F., Frei, R., 2022. Uranium isotope cycling on the highly productive Peruvian margin. Chem. Geol. 590, 120705. https://doi.org/10.1016/j.chemgeo.2021.120705.

Brüske, A., Martin, A.N., Rammensee, P., Eroglu, S., Lazarov, M., Albut, G., Schuth, S., Aulbach, S., Schoenberg, R., Beukes, N., Hofmann, A., Nägler, T., Weyer, S., 2020a. The onset of oxidative weathering traced by uranium isotopes. Precambrian Res. 338, 105583. Available at: https://doi.org/10.1016/j.precamres.2019.105583.

Brüske, A., Weyer, S., Zhao, M.Y., Planavsky, N.J., Wegwerth, A., Neubert, N., Dellwig, O., Lau, K.V., Lyons, T.W., 2020b. Correlated molybdenum and uranium isotope signatures in modern anoxic sediments: Implications for their use as paleoredox proxy. Geochim. Cosmochim. Acta 270, 449–474. https://doi.org/10.1016/j.gca.2019.11.031.

Buchholz, B.A., Brown, T.A., Hamilton, T.F., Hutcheon, I.D., Marchetti, A.A., Martinelli, R.E., Ramon, E.C., Tumey, S.J., Williams, R.W., 2007. Investigating uranium isotopic distributions in environmental samples using AMS and MC-ICPMS. Nucl. Instruments Methods Phys. Res. Sect. B Beam Interact. Mater. Atoms 259, 733–738. https://doi.org/10.1016/j.nimb.2007.01.248.

Bura-Nakić, E., Sondi, I., Mikac, N., Andersen, M.B., 2020. Investigating the molybdenum and uranium redox proxies in a modern shallow anoxic carbonate rich marine sediment setting of the Malo Jezero (Mljet Lakes, Adriatic Sea). Chem. Geol. 533, 119441. https://doi.org/10.1016/j.chemgeo.2019.119441.

Callis, E.L., Abernathey, R.M., 1991. High-precision isotopic analyses of uranium and plutonium by total sample volatilization and signal integration. Int. J. Mass Spectrom. Ion Process. 103, 93–105. https://doi.org/10.1016/0168-1176(91)80081-W.

Cao, M., Daines, S.J., Lenton, T.M., Cui, H., Algeo, T.J., Dahl, T.W., Shi, W., Chen, Z., Anbar, A., Zhou, Y., 2020. Comparison of Ediacaran platform and slope $\delta^{238}U$ records in South China: Implications for global-ocean oxygenation and the origin of the Shuram Excursion. Geochim. Cosmochim. Acta 287, 111–124. https://doi.org/10.1016/j.gca.2020.04.035.

Casalini, M., 2018. $^{98}Mo/^{95}Mo$ and $^{238}U/^{235}U$ in Lamproites, shoshonites, and high-K calc-alkaline rocks from Western Alps: Inferences on their genesis. Ital. J. Geosci. 137, 465–477. https://doi.org/10.3301/IJG.2018.20.

Chen, J.H., 1988. ^{238}U, ^{235}U, ^{234}U in Lunar and Terrestrial Samples and the Determination of $\lambda^{238}/\lambda^{234}$. LPSC.

Chen, J.H., Wasserburg, G.J., 1980. A search for isotopic anomalies in uranium. Geophys. Res. Lett. 7, 275–278. https://doi.org/10.1029/GL007i004p00275.

Chen, J.H., Wasserburg, G.J., 1981a. Cm/U, Th/U, and $^{235}U/^{238}U$ in meteorites. Meteoritics 16, 301.

Chen, J.H., Wasserburg, G.J., 1981b. Precise isotopic analysis of uranium in picomole and subpicomole quantities. Anal. Chem. 53, 2060–2067. https://doi.org/10.1021/ac00236a027.

Chen, J.H., Wasserburg, G.J., 1981c. The isotopic composition of uranium and lead in Allende inclusions and meteoritic phosphates. Earth Planet. Sci. Lett. 52, 1–15. https://doi.org/10.1016/0012-821X(81)90202-8.

Chen, J.H., Lawrence Edwards, R., Wasserburg, G.J., 1986. ^{238}U, ^{234}U and ^{232}Th in seawater. Earth Planet. Sci. Lett. 80, 241–251. https://doi.org/10.1016/0012-821X(86)90108-1.

Chen, X., Romaniello, S.J., Herrmann, A.D., Wasylenki, L.E., Anbar, A.D., 2016. Uranium isotope fractionation during coprecipitation with aragonite and calcite. Geochim. Cosmochim. Acta 188, 189–207. https://doi.org/10.1016/j.gca.2016.05.022.

Chen, J., Montañez, I.P., Zhang, S., Isson, T.T., Macarewich, S.I., Planavsky, N.J., Zhang, F., Rauzi, S., Daviau, K., Yao, L., Qi, Y.P., Wang, Y., Fan, J.X., Poulsen, C.J., Anbar, A.D., Shen, S.Z., Wang, X.D., 2022a. Marine anoxia linked to abrupt global warming during Earth's penultimate icehouse. Proc. Natl. Acad. Sci. U. S. A. 119. https://doi.org/10.1073/pnas.2115231119.

Chen, X., Robinson, S.A., Romaniello, S.J., Anbar, A.D., 2022b. 238U/235U in calcite is more susceptible to carbonate diagenesis. Geochim. Cosmochim. Acta 326, 273–287.

Chen, X., Romaniello, S.J., Anbar, A.D., 2017. Uranium isotope fractionation induced by aqueous speciation: Implications for U isotopes in marine $CaCO_3$ as a paleoredox proxy. Geochim. Cosmochim. Acta 215, 162–172. https://doi.org/10.1016/j.gca.2017.08.006.

Chen, X., Romaniello, S.J., Herrmann, A.D., Hardisty, D., Gill, B.C., Anbar, A.D., 2018a. Diagenetic effects on uranium isotope fractionation in carbonate sediments from the Bahamas. Geochim. Cosmochim. Acta 237, 294–311. Available at: https://doi.org/10.1016/j.gca.2018.06.026.

Chen, X., Romaniello, S.J., Herrmann, A.D., Samankassou, E., Anbar, A.D., 2018b. Biological effects on uranium isotope fractionation (238U/235U) in primary biogenic carbonates. Geochim. Cosmochim. Acta 240, 1–10. Available at: https://doi.org/10.1016/j.gca.2018.08.028.

Chen, X., Zheng, W., Anbar, A.D., 2020. Uranium Isotope Fractionation ($^{238}U/^{235}U$) during U(VI) Uptake by Freshwater Plankton. Environ. Sci. Technol. 54, 2744–2752. Available at: https://doi.org/10.1021/acs.est.9b06421.

Chen, X., Romaniello, S.J., McCormick, M., Sherry, A., Havig, J.R., Zheng, W., Anbar, A.D., 2021b. Anoxic depositional overprinting of $^{238}U/^{235}U$ in calcite: When do carbonates tell black shale tales? Geology 49, 1193–1197. Available at: https://doi.org/10.1130/g48949.1.

Chen, X., Tissot, F.L.H., Jansen, M.F., Bekker, A., Liu, C.X., Nie, N.X., Halverson, G.P., Veizer, J., Dauphas, N., 2021a. The uranium isotopic record of shales and carbonates through geologic time. Geochim. Cosmochim. Acta 300, 164–191. https://doi.org/10.1016/j.gca.2021.01.040.

Cheng, H., Edwards, R., Hoff, J., Gallup, C., Richards, D., Asmerom, Y., 2000. The half-lives of uranium-234 and thorium-230. Chem. Geol. 169, 17–33. Available at: https://doi.org/10.1016/S0009-2541(99)00157-6.

Cheng, H., Lawrence, Edwards R., Shen, C.-C., Polyak, V.J., Asmerom, Y., Woodhead, J., Hellstrom, J., Wang, Y., Kong, X., Spötl, C., Wang, X., Calvin, Alexander E., 2013. Improvements in ^{230}Th dating, ^{230}Th and ^{234}U half-life values, and U–Th isotopic measurements by multi-collector inductively coupled plasma mass spectrometry. Earth Planet. Sci. Lett. 371–372, 82–91. https://doi.org/10.1016/j.epsl.2013.04.006.

Cheng, K., Elrick, M., Romaniello, S.J., 2020a. Early mississippian ocean anoxia triggered organic carbon burial and late paleozoic cooling: Evidence from uranium isotopes recorded in marine limestone. Geology 48, 363–367. https://doi.org/10.1130/G46950.1.

Cheng, M., Li, C., Jin, C., Wang, H., Algeo, T.J., Lyons, T.W., Zhang, F., Anbar, A., 2020b. Evidence for high organic carbon export to the early Cambrian seafloor. Geochim. Cosmochim. Acta 287, 125–140. https://doi.org/10.1016/j.gca.2020.01.050.

Chernyshev, I.V., Golubev, V.N., Chugaev, A.V., Baranova, A.N., 2014. $^{238}U/^{235}U$ isotope ratio variations in minerals from hydrothermal uranium deposits. Geochemistry Int. 52, 1013–1029. https://doi.org/10.1134/S0016702914120027.

Cherry, L.B., Gilleaudeau, G.J., Grazhdankin, D.V., Romaniello, S.J., Martin, A.J., Kaufman, A.J., 2022. A diverse Ediacara assemblage survived under low-oxygen conditions. Nat. Commun. 13, 7306. https://doi.org/10.1038/s41467-022-35012-y.

Chiu, C.F., Sweere, T.C., Clarkson, M.O., de Souza, G.F., Hennekam, R., Vance, D., 2022. Co-variation systematics of uranium and molybdenum isotopes reveal pathways for descent into euxinia in Mediterranean sapropels. Earth Planet. Sci. Lett. 585, 117527. https://doi.org/10.1016/j.epsl.2022.117527.

Christensen, J.N., Dresel, P.E., Conrad, M.E., Maher, K., Depaolo, D.T., 2004. Identifying the sources of subsurface contamination at the Hanford site in Washington using high-precision uranium isotopic measurements. Environ. Sci. Technol. 38, 3330–3337. https://doi.org/10.1021/es034700q.

Clarkson, M.O., Stirling, C.H., Jenkyns, H.C., Dickson, A.J., Porcelli, D., Moy, C.M., Von Strandmann, P.P.A.E., Cooke, I.R., Lenton, T.M., 2018. Uranium isotope evidence for two episodes of deoxygenation during Oceanic Anoxic Event 2. Proc. Natl. Acad. Sci. 115, 2918–2923. https://doi.org/10.1073/pnas.1715278115.

Clarkson, M.O., Müsing, K., Andersen, M.B., Vance, D., 2020. Examining pelagic carbonate-rich sediments as an archive for authigenic uranium and molybdenum isotopes using reductive cleaning and leaching experiments. Chem. Geol. 539, 119412. https://doi.org/10.1016/j.chemgeo.2019.119412.

Clarkson, M.O., Hennekam, R., Sweere, T.C., Andersen, M.B., Reichart, G.-J., Vance, D., 2021a. Carbonate associated uranium isotopes as a novel local redox indicator in oxidatively disturbed reducing sediments. Geochim. Cosmochim. Acta 311, 12–28. https://doi.org/10.1016/j.gca.2021.07.025.

Clarkson, M.O., Lenton, T.M., Andersen, M.B., Bagard, M.L., Dickson, A.J., Vance, D., 2021b. Upper limits on the extent of seafloor anoxia during the PETM from uranium isotopes. Nat. Commun. 12, 1–9. https://doi.org/10.1038/s41467-020-20486-5.

Claverie, F., Hubert, A., Berail, S., Donard, A., Pointurier, F., Pécheyran, C., 2016. Improving Precision and Accuracy of Isotope Ratios from Short Transient Laser Ablation-Multicollector-Inductively Coupled Plasma Mass Spectrometry Signals: Application to Micrometer-Size Uranium Particles. Anal. Chem. 88, 4375–4382. https://doi.org/10.1021/acs.analchem.5b04802.

Cole, D.B., Planavsky, N.J., Longley, M., Böning, P., Wilkes, D., Wang, X., Swanner, E.D., Wittkop, C., Loydell, D.K., Busigny, V., Knudsen, A.C., Sperling, E.A., 2020. Uranium Isotope Fractionation in Non-sulfidic Anoxic Settings and the Global Uranium Isotope Mass Balance. Global Biogeochem. Cycles 34, 1–22. Available at: https://doi.org/10.1029/2020GB006649.

Condon, D.J., McLean, N., Noble, S.R., Bowring, S.A., 2010. Isotopic composition ($^{238}U/^{235}U$) of some commonly used uranium reference materials. Geochim. Cosmochim. Acta 74, 7127–7143. Available at: https://doi.org/10.1016/j.gca.2010.09.019.

Connelly, J.N., Bizzarro, M., Krot, A.N., Nordlund, Å., Wielandt, D., Ivanova, M.A., 2012. The absolute chronology and thermal processing of solids in the solar protoplanetary disk. Science 338, 651–655. https://doi.org/10.1126/science.1226919.

Connelly, J.N., Bollard, J., Bizzarro, M., 2017. Pb–Pb chronometry and the early Solar System. Geochim. Cosmochim. Acta 201, 345–363. https://doi.org/10.1016/j.gca.2016.10.044.

Côté, B., Eichler, M., López, A.Y., Vassh, N., Mumpower, M.R., Világos, B., Soós, B., Arcones, A., Sprouse, T.M., Surman, R., Pignatari, M., Peto, M.K., Wehmeyer, B., Rauscher, T., Lugaro, M., 2021. ^{129}I and ^{247}Cm in meteorites constrain the last astrophysical source of solar r-process elements. Science 371, 945–948. https://doi.org/10.1126/science.aba1111.

Cowan, G.A., Adler, H.H., 1976. The variability of the natural abundance of ^{235}U. Geochim. Cosmochim. Acta 40, 1487–1490. https://doi.org/10.1016/0016-7037(76)90087-9.

Curtis, D., Benjamin, T., Gancarz, A., Loss, R., Rosman, K., DeLaeter, J., Delmore, J.E., Maeck, W.J., 1989. Fission product retention in the Oklo natural fission reactors. Appl. Geochemistry 4, 49–62.

Dahl, T.W., Boyle, R.A., Canfield, D.E., Connelly, J.N., Gill, B.C., Lenton, T.M., Bizzarro, M., 2014. Uranium isotopes distinguish two geochemically distinct stages during the later Cambrian SPICE event. Earth Planet. Sci. Lett. 401, 313–326. https://doi.org/10.1016/j.epsl.2014.05.043.

Dahl, T.W., Connelly, J.N., Kouchinsky, A., Gill, B.C., Månsson, S.F., Bizzarro, M., 2017. Reorganisation of Earth's biogeochemical cycles briefly oxygenated the oceans 520 Myr ago. Geochemical Perspect. Lett. 10, 210–220. https://doi.org/10.7185/geochemlet.1724.

Dahl, T.W., Connelly, J.N., Li, D., Kouchinsky, A., Gill, B.C., Porter, S., Maloof, A.C., Bizzarro, M., 2019. Atmosphere-ocean oxygen and productivity dynamics during early animal radiations. Proc. Natl. Acad. Sci. 116, 19352–19361. Available at: https://doi.org/10.1073/pnas.1901178116.

Danesi, P.R., Bleise, A., Burkart, W., Cabianca, T., Campbell, M.J., Makarewicz, M., Moreno, J., Tuniz, C., Hotchkis, M., 2003a. Isotopic composition and origin of uranium and plutonium in selected soil samples collected in Kosovo. J. Environ. Radioact. 64, 121–131.

Danesi, P.R., Markowicz, A., Chinea-Cano, E., Burkart, W., Salbu, B., Donohue, D., Ruedenauer, F., Hedberg, M., Vogt, S., Zahradnik, P., Ciurapinski, A., 2003b. Depleted uranium particles in selected Kosovo samples. J. Environ. Radioact. 64, 143–154. https://doi.org/10.1016/S0265-931X(02)00045-0.

Dang, D.H., Novotnik, B., Wang, W., Bastian, Georg R., Douglas, Evans R., 2016. Uranium isotope fractionation during adsorption, (co)precipitation, and biotic reduction. Environ. Sci. Technol. 50, 12695–12704. https://doi.org/10.1016/j.chemgeo.2021.120644.

Dang, D.H., Evans, R.D., Wang, W., Omanović, D., El Houssainy, A., Lenoble, V., Mullot, J.U., Mounier, S., Garnier, C., 2018. Uranium isotope geochemistry in modern coastal sediments: Insights from Toulon Bay. France. Chem. Geol. 481, 133–145. https://doi.org/10.1016/j.chemgeo.2018.01.032.

Dang, D.H., Wang, W., Gibson, T.M., Kunzmann, M., Andersen, M.B., Halverson, G.P., Evans, R.D., 2022. Authigenic uranium isotopes of late Proterozoic black shale. Chem. Geol. 588, 120644. https://doi.org/10.1016/j.chemgeo.2021.120644.

De Laeter, J.R., Rosman, K.J.R., Smith, C.L., 1980. The Oklo natural reactor: Cumulative fission yields and retentivity of the symmetric mass region fission products. Earth Planet. Sci. Lett. 50, 238–246. https://doi.org/10.1016/0012-821X(80)90135-1.

del Rey, Á., Havsteen, J.C., Bizzarro, M., Dahl, T.W., 2020. Untangling the diagenetic history of uranium isotopes in marine carbonates: A case study tracing the $\delta^{238}U$ composition of late Silurian oceans using calcitic brachiopod shells. Geochim. Cosmochim. Acta 287, 93–110. https://doi.org/10.1016/j.gca.2020.06.002.

del Rey, Á., Rasmussen, C.M.Ø., Calner, M., Wu, R., Asael, D., Dahl, T.W., 2022. Stable ocean redox during the main phase of the Great Ordovician Biodiversification Event. Commun. Earth Environ. 3. https://doi.org/10.1038/s43247-022-00548-w.

Dempster, A.J., 1935. Isotopic Constitution of Uranium. Nature 136, 180. https://doi.org/10.1038/136180a0.

Dickson, A.J., Bagard, M.L., Katchinoff, J.A.R., Davies, M., Poulton, S.W., Cohen, A.S., 2021. Isotopic constraints on ocean redox at the end of the Eocene. Earth Planet. Sci. Lett. 562, 116814. https://doi.org/10.1016/j.epsl.2021.116814.

Dickson, A.J., Idiz, E., Porcelli, D., Murphy, M.J., Celestino, R., Jenkyns, H.C., Poulton, S. W., Hesselbo, S.P., Hooker, J.N., Ruhl, M., van den Boorn, S.H.J.M., 2022. No effect of thermal maturity on the Mo, U, Cd, and Zn isotope compositions of Lower Jurassic organic-rich sediments. Geology 50, 598–602. https://doi.org/10.1130/G49724.1.

Dodson, M.H., 1963. A theoretical study of the use of internal standards for precise isotopic analysis by the surface ionization technique: Part I - General first-order algebraic solutions. J. Sci. Instrum. 40, 289–295. https://doi.org/10.1088/0950-7671/40/6/307.

Donard, A., Pointurier, F., Pottin, A.C., Hubert, A., Pécheyran, C., 2017. Determination of the isotopic composition of micrometric uranium particles by UV femtosecond laser ablation coupled with sector-field single-collector ICP-MS. J. Anal. At. Spectrom. 32, 96–106. https://doi.org/10.1039/c6ja00071a.

Duarte, C.L., Szeles, M.S.-M.F., 1994. An improved method for determination of uranium isotopic composition in urine by alpha spectrometry. J. Radioanal. Nucl. Chem. Artic. 177, 73–79. https://doi.org/10.1007/BF02132411.

Dunk, R.M., Mills, R.A., Jenkins, W.J., 2002. A reevaluation of the oceanic uranium budget for the Holocene. Chem. Geol. 190, 45–67. https://doi.org/10.1016/S0009-2541(02)00110-9.

Ejnik, J.W., Carmichael, A.J., Hamilton, M.M., McDiarmid, M., Squibb, K., Boyd, P., Tardiff, W., 2000. Determination of the isotopic composition of uranium in urine by inductively coupled plasma mass spectrometry. Health Phys. 78, 143–146. https://doi.org/10.1097/00004032-200002000-00003.

Ejnik, J.W., Todorov, T.I., Mullick, F.G., Squibb, K., McDiarmid, M.A., Centeno, J.A., 2005. Uranium analysis in urine by inductively coupled plasma dynamic reaction cell mass spectrometry. Anal. Bioanal. Chem. 382, 73–79. https://doi.org/10.1007/s00216-005-3173-9.

Elliott, T., Plank, T., Zindler, A., White, W., Bourdon, B., 1997. Element transport from slab to volcanic front at the Mariana arc. J. Geophys. Res. Solid Earth 102, 14991–15019. https://doi.org/10.1029/97JB00788.

Elrick, M., Polyak, V., Algeo, T.J., Romaniello, S., Asmerom, Y., Herrmann, A.D., Anbar, A.D., Zhao, L., Chen, Z.Q., 2017. Global-ocean redox variation during the middle-late Permian through Early Triassic based on uranium isotope and Th/U trends of marine carbonates. Geology 45, 163–166. https://doi.org/10.1130/G38585.1.

Elrick, M., Gilleaudeau, G.J., Romaniello, S.J., Algeo, T.J., Morford, J.L., Sabbatino, M., Goepfert, T.J., Cleal, C., Cascales-Miñana, B., Chernyavskiy, P., 2022. Major Early-Middle Devonian oceanic oxygenation linked to early land plant evolution detected using high-resolution U isotopes of marine limestones. Earth Planet. Sci. Lett. 581, 117410. https://doi.org/10.1016/j.epsl.2022.117410.

Fernández-Díaz, M., Quejido, A.J., Crespo, M.T., Del Villar, L.P., Martín-Sánchez, A., Lozano, J.C., 2000. Uranium isotopic data in uraninite spent fuel from the Bangombe natural nuclear reactor (Gabon) and its surroundings. Appl. Radiat. Isot. 53, 91–96. https://doi.org/10.1016/S0969-8043(00)00118-4.

Fiedler, R., 1995. Total evaporation measurements: experience with multi-collector instruments and a thermal ionization quadrupole mass spectrometer. Int. J. Mass Spectrom. Ion Process. 146–147, 91–97. https://doi.org/10.1016/0168-1176(95)04197-S.

Florence, T.M., Batley, G.E., Ekstrom, A., Fardy, J.J., Farrar, Y.J., 1975. Separation of uranium isotopes by uranium(IV)-uranium(VI) chemical exchange. J. Inorg. Nucl. Chem. 37, 1961–1966. https://doi.org/10.1016/0022-1902(75)80925-0.

Freymuth, H., Andersen, M.B., Elliott, T., 2019. Uranium isotope fractionation during slab dehydration beneath the Izu arc. Earth Planet. Sci. Lett. 522, 244–254. https://doi.org/10.1016/j.epsl.2019.07.006.

Fujii, Y., Nomura, M., Okamoto, M., Onitsuka, H., Kawakami, F., Takeda, K., 1989a. An Anomalous Isotope Effect of ^{235}U in U(IV)-U(VI) Chemical Exchange. Zeitschrift für Naturforsch. A 44, 395–398. https://doi.org/10.1515/zna-1989-0507.

Fujii, Y., Nomura, M., Onitsuka, H., Takeda, K., 1989b. Anomalous isotope fractionation in uranium enrichment process. J. Nucl. Sci. Technol. 26, 1061–1064. https://doi.org/10.1080/18811248.1989.9734427.

Fujii, Y., Higuchi, N., Haruno, Y., Nomura, M., Suzuki, T., 2006. Temperature dependence of isotope effects in uranium chemical exchange reactions. J. Nucl. Sci. Technol. 43, 400–406. https://doi.org/10.1080/18811248.2006.9711111.

Fujikawa, Y., Shizuma, K., Endo, S., Fukui, M., 2003. Anomalous $^{235}U/^{238}U$ ratios and metal elements detected in the black rain from the hiroshima A-bomb. Health Phys. 84, 155–162. https://doi.org/10.1097/00004032-200302000-00002.

Gagné, J.M., Van, S.N., Saint-Dizier, J.P., Pianarosa, P., 1976. Isotope shift of ^{234}U, ^{236}U, ^{238}U in Ui. J. Opt. Soc. Am. 66, 1415. Available at. https://doi.org/10.1364/JOSA.66.001415.

Gagné, J.-M., Saint-Dizier, J.-P., Pianarosa, P., 1977. Odd-even staggering of ^{235}U from the 5027 Å line in UI. Opt. Commun. 20, 269–270. https://doi.org/10.1016/0030-4018(77)90349-2.

Gagné, J.-M., Saint-Dizier, J.-P., Pianarosa, P., 1978. Isotope shift ^{238}U-^{233}U from some lines in the UI spectrum. Opt. Commun. 26, 348–350. https://doi.org/10.1016/0030-4018(78)90218-3.

Ganapathy, R., 1978. Reagent grade uranium salts: Isotopic composition by neutron activation. J. Radioanal. Chem. 44, 199–206. https://doi.org/10.1007/BF02517690.

Gaschnig, R.M., Rader, S.T., Reinhard, C.T., Owens, J.D., Planavsky, N., Wang, X., Asael, D., Greaney, A., Helz, R., 2021. Behavior of the Mo, Tl, and U isotope systems during differentiation in the Kilauea Iki lava lake. Chem. Geol. 574, 120239. https://doi.org/10.1016/j.chemgeo.2021.120239.

Gauthier-Lafaye, F., Holliger, P., Blanc, P.L., 1996. Natural fission reactors in the Franceville basin, Gabon: A review of the conditions and results of a "critical event" in a geologic system. Geochim. Cosmochim. Acta 60, 4831–4852. https://doi.org/10.1016/S0016-7037(96)00245-1.

Gilleaudeau, G.J., Romaniello, S.J., Luo, G., Kaufman, A.J., Zhang, F., Klaebe, R.M., Kah, L.C., Azmy, K., Bartley, J.K., Zheng, W., Knoll, A.H., Anbar, A.D., 2019. Uranium isotope evidence for limited euxinia in mid-Proterozoic oceans. Earth Planet. Sci. Lett. 521, 150–157. https://doi.org/10.1016/j.epsl.2019.06.012.

Ginder-Vogel, M., Criddle, C.S., Fendorf, S., 2006. Thermodynamic constraints on the oxidation of biogenic UO_2 by Fe(III) (Hydr)oxides. Environ. Sci. Technol. 40, 3544–3550. https://doi.org/10.1021/es052305p.

Goldmann, A., Brennecka, G., Noordmann, J., Weyer, S., Wadhwa, M., 2015. The uranium isotopic composition of the Earth and the Solar System. Geochim. Cosmochim. Acta 148, 145–158. https://doi.org/10.1016/j.gca.2014.09.008.

Golubev, V.N., Chernyshev, I.V., Chugaev, A.V., Eremina, A.V., Baranova, A.N., Krupskaya, V.V., 2013. U-Pb systems and U isotopic composition of the sandstone-hosted paleovalley Dybryn uranium deposit, Vitim uranium district. Russia. Geol. Ore Depos. 55, 399–410. https://doi.org/10.1134/S1075701513060044.

Gothmann, A.M., Higgins, J.A., Adkins, J.F., Broecker, W., Farley, K.A., McKeon, R., Stolarski, J., Planavsky, N., Wang, X., Bender, M.L., 2019. A Cenozoic record of seawater uranium in fossil corals. Geochim. Cosmochim. Acta 250, 173–190. https://doi.org/10.1016/j.gca.2019.01.039.

Goto, K.T., Anbar, A.D., Gordon, G.W., Romaniello, S.J., Shimoda, G., Takaya, Y., Tokumaru, A., Nozaki, T., Suzuki, K., Machida, S., Hanyu, T., Usui, A., 2014. Uranium isotope systematics of ferromanganese crusts in the Pacific Ocean: Implications for the marine $^{238}U/^{235}U$ isotope system. Geochim. Cosmochim. Acta 146, 43–58. https://doi.org/10.1016/j.gca.2014.10.003.

Gray, P.J., Zhang, L., Xu, H., McDiarmid, M., Squibb, K., Centeno, J.A., 2012. Determination of $^{236}U/^{238}U$ and $^{235}U/^{238}U$ isotope ratios in human urine by inductively coupled plasma mass spectrometry. Microchem. J. 105, 94–100. https://doi.org/10.1016/j.microc.2012.07.004.

Guillong, M., Heimgartner, P., Kopajtic, Z., Günther, D., Günther-Leopold, I., 2007. A laser ablation system for the analysis of radioactive samples using inductively coupled plasma mass spectrometry. J. Anal. At. Spectrom. 22, 399–402. https://doi.org/10.1039/b616364e.

Günther-Leopold, I., Kivel, N., Kobler, Waldis J., Wernli, B., 2008. Characterization of nuclear fuels by ICP mass-spectrometric techniques. Anal. Bioanal. Chem. 390, 503–510. https://doi.org/10.1007/s00216-007-1644-x.

Gwiazda, R.H., Squibb, K., McDiarmid, M., Smith, D., 2004. Detection of depleted uranium in urine of veterans from the 1991 Gulf War. Health Phys. 86, 12–18. https://doi.org/10.1097/00004032-200401000-00004.

Hamer, A.N., Robbins, E.J., 1960. A search for variations in the natural abundance of uranium-235. Geochim. Cosmochim. Acta 19, 143–145. Available at: https://doi.org/10.1016/0016-7037(60)90047-8.

Hamilton, E.I., Stevens, H.E., 1985. Some observations on the geochemistry and isotopic composition of uranium in relation to the reprocessing of nuclear fuels. J. Environ. Radioact. 2, 23–40. https://doi.org/10.1016/0265-931X(85)90023-2.

Herrmann, A.D., Gordon, G.W., Anbar, A.D., 2018. Uranium isotope variations in a dolomitized Jurassic carbonate platform (Tithonian; Franconian Alb, Southern Germany). Chem. Geol. 497, 41–53. https://doi.org/10.1016/j.chemgeo.2018.08.017.

Hidaka, H., Gauthier-Lafaye, F., 2000. Redistribution of fissiogenic and non-fissiogenic REE, Th and U in and around natural fission reactors at Oklo and Bangombe, Gabon. Geochim. Cosmochim. Acta 64, 2093–2108. https://doi.org/10.1016/S0016-7037(00)00364-1.

Hidaka, H., Holliger, P., 1998. Geochemical and neutronic characteristics of the natural fossil fission reactors at Oklo and Bangombé, Gabon. Geochim. Cosmochim. Acta 62, 89–108. https://doi.org/10.1016/S0016-7037(97)00319-0.

Hidaka, H., Holliger, P., Gauthier-Lafaye, F., 1999. Tc/Ru fractionation in the Oklo and Bangombe natural fission reactors, Gabon. Chem. Geol. 155, 323–333. https://doi.org/10.1016/S0009-2541(98)00173-9.

Hiess, J., Condon, D.J., McLean, N., Noble, S.R., 2012. $^{238}U/^{235}U$ Systematics in terrestrial uranium-bearing minerals. Science 335, 1610–1614. https://doi.org/10.1126/science.1215507.

Holliger, P., Devillers, C., 1981. Contribution à l'étude de la température dans les réacteurs fossiles d'Oklo par la mesure du rapport isotopique du lutétium. Earth Planet. Sci. Lett. 52, 76–84. https://doi.org/10.1016/0012-821X(81)90209-0.

Holmden, C., Amini, M., Francois, R., 2015. Uranium isotope fractionation in Saanich Inlet: A modern analog study of a paleoredox tracer. Geochim. Cosmochim. Acta 153, 202–215. https://doi.org/10.1016/j.gca.2014.11.012.

Hood, A.V.S., Planavsky, N.J., Wallace, M.W., Wang, X., Bellefroid, E.J., Gueguen, B., Cole, D.B., 2016. Integrated geochemical-petrographic insights from componentselective $\delta^{238}U$ of Cryogenian marine carbonates. Geology 44, 935–938. https://doi.org/10.1130/G38533.1.

Hood, A.V.S., Planavsky, N.J., Wallace, M.W., Wang, X., 2018. The effects of diagenesis on geochemical paleoredox proxies in sedimentary carbonates. Geochim. Cosmochim. Acta 232, 265–287. https://doi.org/10.1016/j.gca.2018.04.022.

Horan, P., Dietz, L., Durakovic, A., 2002. The quantitative analysis of depleted uranium isotopes in British, Canadian, and U.S. Gulf War veterans. Mil. Med. 167, 620–627. https://doi.org/10.1093/milmed/167.8.620.

Horie, K., Hidaka, H., Gauthier-Lafaye, F., 2004. Isotopic evidence for trapped fissiogenic REE and nucleogenic Pu in apatite and Pb evolution at the Oklo natural reactor. Geochim. Cosmochim. Acta 68, 115–125. https://doi.org/10.1016/S0016-7037(03)00415-0.

Horwitz, E.P., Dietz, M.L., Chiarizia, R., Diamond, H., Essling, A.M., Graczyk, D., 1992. Separation and preconcentration of uranium from acidic media by extraction chromatography. Anal. Chim. Acta 266, 25–37. https://doi.org/10.1016/0003-2670(92)85276-C.

Horwitz, E.P., Chiarizia, R., Dietz, M.L., Diamond, H., Nelson, D.M., 1993. Separation and preconcentration of actinides from acidic media by extraction chromatography. Anal. Chim. Acta 281, 361–372. https://doi.org/10.1016/0003-2670(93)85194-O.

Howe, S.E., Davidson, C.M., McCartney, M., 2002. Determination of uranium concentration and isotopic composition by means of ICP-MS in sequential extracts of sediment from the vicinity of a uranium enrichment plant. J. Anal. At. Spectrom. 17, 497–501. https://doi.org/10.1039/b200270c.

Hubert, A., Claverie, F., Pécheyran, C., Pointurier, F., 2014. Measurement of the isotopic composition of uranium micrometer-size particles by femtosecond laser ablation-inductively coupled plasma mass spectrometry. Spectrochim. Acta - Part B At. Spectrosc. 93, 52–60. https://doi.org/10.1016/j.sab.2013.12.007.

Hyun, S.P., Fox, P.M., Davis, J.A., Campbell, K.M., Hayes, K.F., Long, P.E., 2009. Surface complexation modeling of U(VI) adsorption by aquifer sediments from a former mill tailings site at Rifle, Colorado. Environ. Sci. Technol. 43, 9368–9373. https://doi.org/10.1021/es902164n.

Iizuka, T., Amelin, Y., Kaltenbach, A., Koefoed, P., Stirling, C.H., 2014. U-Pb systematics of the unique achondrite Ibitira: Precise age determination and petrogenetic implications. Geochim. Cosmochim. Acta 132, 259–273. https://doi.org/10.1016/j.gca.2014.02.017.

Iturbe, J.L., 1992. Determination of $^{234}U/^{238}U$ and $^{235}U/^{238}U$ ratios from commercially available uranium compounds by α-spectrometry. J. Radioanal. Nucl. Chem. Lett. 166, 263–272. https://doi.org/10.1007/BF02163832.

Jaffey, A.H., Flynn, K.F., Glendenin, L.E., Bentley, W.C., Essling, A.M., 1971. Precision measurement of half-lives and specific activities of ^{235}U and ^{238}U. Phys. Rev. C 4, 1889–1906. https://doi.org/10.1103/PhysRevC.4.1889.

Jemison, N.E., Johnson, T.M., Shiel, A.E., Lundstrom, C.C., 2016. Uranium isotopic fractionation induced by U(VI) adsorption onto common aquifer minerals. Environ. Sci. Technol. 50, 12232–12240. https://doi.org/10.1021/acs.est.6b03488.

Jemison, N.E., Shiel, A.E., Johnson, T.M., Lundstrom, C.C., Long, P.E., Williams, K.H., 2018. Field Application of $^{238}U/^{235}U$ Measurements To Detect Reoxidation and Mobilization of U(IV). Environ. Sci. Technol. 52, 3422–3430. https://doi.org/10.1021/acs.est.7b05162.

Jemison, N.E., Bizjack, M.T., Johnson, T.M., Druhan, J.L., 2020. Influence of physical and chemical hydrology on bioremediation of a U-contaminated aquifer informed by reactive transport modeling incorporating $^{238}U/^{235}U$ ratios. Geochim. Cosmochim. Acta 269, 303–328. https://doi.org/10.1016/j.gca.2019.10.031.

Ji, A.P., Frebel, A., Chiti, A., Simon, J.D., 2016. R-process enrichment from a single event in an ancient dwarf galaxy. Nature 531, 610–613. https://doi.org/10.1038/nature17425.

Joshi, L.U., Zingde, M.D., Desai, B.N., 1983. Radiochemical determination of uranium and studies of $^{234}U/^{238}U$ and $^{235}U/^{238}U$ activity ratios in estuarine sediments of mindola river. J. Radioanal. Chem. 76, 97–104. https://doi.org/10.1007/BF02519659.

Jost, A.B., Bachan, A., van de Schootbrugge, B., Lau, K.V., Weaver, K.L., Maher, K., Payne, J.L., 2017. Uranium isotope evidence for an expansion of marine anoxia during the end-Triassic extinction. *Geochemistry*. Geophys. Geosystems 18, 3093–3108. https://doi.org/10.1002/2017GC006941.

Kappel, S., Boulyga, S.F., Prohaska, T., 2012. Direct uranium isotope ratio analysis of single micrometer-sized glass particles. J. Environ. Radioact. 113, 8–15. https://doi.org/10.1016/j.jenvrad.2012.03.017.

Kappel, S., Boulyga, S.F., Dorta, L., Günther, D., Hattendorf, B., Koffler, D., Laaha, G., Leisch, F., Prohaska, T., 2013. Evaluation strategies for isotope ratio measurements of single particles by LA-MC-ICPMS. Anal. Bioanal. Chem. 405, 2943–2955. https://doi.org/10.1007/s00216-012-6674-3.

Keatley, A.C., Dunne, J.A., Martin, T.L., Nita, D.C., Andersen, M.B., Scott, T.B., Richards, D.A., Awbery, R.P., 2021. Uranium isotope variation within vein-type uranium ore deposits. Appl. Geochemistry 131, 104977. https://doi.org/10.1016/j.apgeochem.2021.104977.

Keegan, E., Richter, S., Kelly, I., Wong, H., Gadd, P., Kuehn, H., Alonso-Munoz, A., 2008. The provenance of Australian uranium ore concentrates by elemental and isotopic analysis. Appl. Geochemistry 23, 765–777. https://doi.org/10.1016/j.apgeochem.2007.12.004.

Kendall, B., Brennecka, G.A., Weyer, S., Anbar, A.D., 2013. Uranium isotope fractionation suggests oxidative uranium mobilization at 2.50Ga. Chem. Geol. 362, 105–114. https://doi.org/10.1016/j.chemgeo.2013.08.010.

Kendall, B., Komiya, T., Lyons, T.W., Bates, S.M., Gordon, G.W., Romaniello, S.J., Jiang, G., Creaser, R.A., Xiao, S., McFadden, K., Sawaki, Y., Tahata, M., Shu, D., Han, J., Li, Y., Chu, X., Anbar, A.D., 2015. Uranium and molybdenum isotope evidence for an episode of widespread ocean oxygenation during the late ediacaran period. Geochim. Cosmochim. Acta 156, 173–193. https://doi.org/10.1016/j.gca.2015.02.025.

Kendall, B., Wang, J., Zheng, W., Romaniello, S.J., Over, D.J., Bennett, Y., Xing, L., Kunert, A., Boyes, C., Liu, J., 2020. Inverse correlation between the molybdenum and uranium isotope compositions of Upper Devonian black shales caused by changes in local depositional conditions rather than global ocean redox variations. Geochim. Cosmochim. Acta 287, 141–164. https://doi.org/10.1016/j.gca.2020.01.026.

Kikawada, Y., Suzuki, H., Yamauchi, R., Oia, T., Hirose, K., 2015. $^{235}U/^{238}U$ Isotope Ratios in Monthly Atmospheric Deposits Collected at Akita, Japan in 1977 and 1978. Procedia Earth Planet. Sci. 15, 675–679. https://doi.org/10.1016/j.proeps.2015.08.083.

Kikuchi, M., Hidaka, H., 2009. In-situ U-Pb analyses of highly altered zircon from sediments overlying the Bangombé natural fission reactor. Gabon. Geosci. J. 13, 257–264. https://doi.org/10.1007/s12303-009-0025-1.

Kipp, M.A., Li, H., Ellwood, M.J., John, S., Middag, R., Adkins, J.F., Tissot, F.L.H., 2022. ^{238}U, ^{235}U and ^{234}U in seawater and deep-sea corals: A high-precision reappraisal. Geochim. Cosmochim. Acta 336, 231–248. https://doi.org/10.1016/j.gca.2022.09.018.

Kipp, M.A., Tissot, F.L.H., 2022. Inverse methods for consistent quantification of seafloor anoxia using uranium isotope data from marine sediments. Earth Planet. Sci. Lett. 577. https://doi.org/10.1016/j.epsl.2021.117240.

Kips, R., Leenaers, A., Tamborini, G., Betti, M., Van Den Berghe, S., Wellum, R., Taylor, P., 2007. Characterization of uranium particles produced by hydrolysis of UF_6 using SEM and SIMS. Microsc. Microanal. 13, 156–164. https://doi.org/10.1017/S1431927607070341.

Kips, R., Weber, P.K., Kristo, M.J., Jacobsen, B., Ramon, E.C., 2019. Microscale Isotopic Variation in Uranium Fuel Pellets with Implications for Nuclear Forensics. Anal. Chem. 91, 11598–11605. https://doi.org/10.1021/acs.analchem.9b01737.

Kirchenbaur, M., Maas, R., Ehrig, K., Kamenetsky, V.S., Strub, E., Ballhaus, C., Münker, C., 2016. Uranium and Sm isotope studies of the supergiant Olympic Dam Cu-Au-U-Ag deposit, South Australia. Geochim. Cosmochim. Acta 180, 15–32. https://doi.org/10.1016/j.gca.2016.01.035.

Knyazev, D.A., Myasoedov, N.F., 2001. Specific effects of heavy nuclei in chemical equilibrium. Sep. Sci. Technol. 36, 1677–1696. https://doi.org/10.1081/SS-100104758.

Krachler, M., Varga, Z., Nicholl, A., Wallenius, M., Mayer, K., 2018. Spatial distribution of uranium isotopes in solid nuclear materials using laser ablation multi-collector ICP-MS. Microchem. J. 140, 24–30. https://doi.org/10.1016/j.microc.2018.03.038.

Kraiem, M., Richter, S., Erdmann, N., Kühn, H., Hedberg, M., Aregbe, Y., 2012. Characterizing uranium oxide reference particles for isotopic abundances and uranium mass by single particle isotope dilution mass spectrometry. Anal. Chim. Acta 748, 37–44. https://doi.org/10.1016/j.aca.2012.08.030.

Kraiem, M., Essex, R.M., Mathew, K.J., Orlowicz, G.J., Soriano, M.D., 2013. Re-certification of the CRM 125-A UO_2 fuel pellet standard for uranium isotopic composition. Int. J. Mass Spectrom. 352, 37–43. https://doi.org/10.1016/j.ijms.2013.05.007.

Krystek, P., Ritsema, R., 2002. Determination of uranium in urine - Measurement of isotope ratios and quantification by use of inductively coupled plasma mass spectrometry. Anal. Bioanal. Chem. 374, 226–229. https://doi.org/10.1007/s00216-002-1424-6.

Ku, T.L., Knauss, K.G., Mathieu, G.G., 1977. Uranium in open ocean: concentration and isotopic composition. Deep. Res. 24, 1005–1017. Available at: https://doi.org/10.1016/0146-6291(77)90571-9.

Kunzendorf, H., 1968. Determination of the isotopic composition of natural and slightly enriched uranium by alpha-spectrometry. Nucl. Instruments Methods 63, 152–156. Available at: https://doi.org/10.1016/0029-554X(68)90320-0.

Lancelot, J.R., Vitrac, A., Allegre, C.J., 1975. The Oklo natural reactor: Age and evolution studies by U-Pb and Rb-Sr systematics. Earth Planet. Sci. Lett. 25, 189–196. https://doi.org/10.1016/0012-821X(75)90195-8.

Langmuir, D., 1978. Uranium solution-mineral equilibria at low temperatures with applications to sedimentary ore deposits. Geochim. Cosmochim. Acta 42, 547–569. https://doi.org/10.1016/0016-7037(78)90001-7.

Larsen, K.K., Trinquier, A., Paton, C., Schiller, M., Wielandt, D., Ivanova, M.A., Connelly, J.N., Nordlund, Å., Krot, A.N., Bizzarro, M., 2011. Evidence for magnesium isotope heterogeneity in the solar protoplanetary disk. Astrophys. J. Lett. 735. https://doi.org/10.1088/2041-8205/735/2/L37.

Lau, K.V., Maher, K., Altiner, D., Kelley, B.M., Kump, L.R., Lehrmann, D.J., Silva-Tamayo, J.C., Weaver, K.L., Yu, M., Payne, J.L., 2016. Marine anoxia and delayed Earth system recovery after the end-Permian extinction. Proc. Natl. Acad. Sci. 113, 2360–2365. https://doi.org/10.1073/pnas.1515080113.

Lau, K.V., Hancock, L.G., Severmann, S., Kuzminov, A., Cole, D.B., Behl, R.J., Planavsky, N.J., Lyons, T.W., 2022. Variable local basin hydrography and productivity control the uranium isotope paleoredox proxy in anoxic black shales. Geochim. Cosmochim. Acta 317, 433–456. https://doi.org/10.1016/j.gca.2021.10.011.

Lau, K.V., Macdonald, F.A., Maher, K., Payne, J.L., 2017. Uranium isotope evidence for temporary ocean oxygenation in the aftermath of the Sturtian Snowball Earth. Earth Planet. Sci. Lett. 458, 282–292. https://doi.org/10.1016/j.epsl.2016.10.043.

Lefebvre, P., Noël, V., Lau, K.V., Jemison, N.E., Weaver, K.L., Williams, K.H., Bargar, J.R., Maher, K., 2019. Isotopic Fingerprint of Uranium Accumulation and Redox Cycling in Floodplains of the Upper Colorado River Basin. Environ. Sci. Technol. 53, 3399–3409. https://doi.org/10.1021/acs.est.8b05593.

Lefebvre, P., Gourgiotis, A., Mangeret, A., Sabatier, P., Le Pape, P., Diez, O., Louvat, P., Menguy, N., Merrot, P., Baya, C., Zebracki, M., Blanchart, P., Malet, E., Jézéquel, D., Reyss, J.-L., Bargar, J.R., Gaillardet, J., Cazala, C., Morin, G., 2021. Diagenetic formation of uranium-silica polymers in lake sediments over 3,300 years. Proc. Natl. Acad. Sci. 118, 1–9. https://doi.org/10.1073/pnas.2021844118.

Lefebvre, P., Le Pape, P., Mangeret, A., Gourgiotis, A., Sabatier, P., Louvat, P., Diez, O., Mathon, O., Hunault, M.O.J.Y., Baya, C., Darricau, L., Cazala, C., Bargar, J.R., Gaillardet, J., Morin, G., 2022. Uranium sorption to organic matter and long-term

accumulation in a pristine alpine wetland. Geochim. Cosmochim. Acta 338, 322–346. https://doi.org/10.1016/j.gca.2022.10.018.
Lewis, L.A., Knight, K.B., Matzel, J.E., Prussin, S.G., Zimmer, M.M., Kinman, W.S., Ryerson, F.J., Hutcheon, I.D., 2015. Spatially-resolved analyses of aerodynamic fallout from a uranium-fueled nuclear test. J. Environ. Radioact. 148, 183–195. https://doi.org/10.1016/j.jenvrad.2015.04.006.
Li, W., Czaja, A.D., Van Kranendonk, M.J., Beard, B.L., Roden, E.E., Johnson, C.M., 2013. An anoxic, Fe(II)-rich, U-poor ocean 3.46 billion years ago. Geochim. Cosmochim. Acta 120, 65–79. https://doi.org/10.1016/j.gca.2013.06.033.
Li, Z., Cao, M., Loyd, S.J., Algeo, T.J., Zhao, H., Wang, X., Zhao, L., Chen, Z.Q., 2020. Transient and stepwise ocean oxygenation during the late Ediacaran Shuram Excursion: Insights from carbonate $\delta^{238}U$ of northwestern Mexico. Precambrian Res. 344, 105741. https://doi.org/10.1016/j.precamres.2020.105741.
Li, J., Azmy, K., Kendall, B., 2022. The Mo- and U-isotope signatures in alternating shales and carbonate beds of rhythmites: A comparison and implications for redox conditions across the Cambrian-Ordovician boundary. Chem. Geol. 602, 120882. https://doi.org/10.1016/j.chemgeo.2022.120882.
Lindahl, P., Olszewski, G., Eriksson, M., 2021. Performance and optimisation of triple quadrupole ICP-MS for accurate measurement of uranium isotopic ratios. J. Anal. At. Spectrom. 36, 2164–2172. https://doi.org/10.1039/d1ja00177a.
Liu, M., Chen, D., Jiang, L., Stockey, R.G., Aseal, D., Zhang, B., Liu, K., Yang, X., Yan, D., Planavsky, N.J., 2022. Oceanic anoxia and extinction in the latest Ordovician. Earth Planet. Sci. Lett. 588, 117553. https://doi.org/10.1016/j.epsl.2022.117553.
Livermore, B.D., Connelly, J.N., Moynier, F., Bizzarro, M., 2018. Evaluating the robustness of a consensus $^{238}U/^{235}U$ value for U-Pb geochronology. Geochim. Cosmochim. Acta 237, 171–183. https://doi.org/10.1016/j.gca.2018.06.014.
Livermore, B.D., Dahl, T.W., Bizzarro, M., Connelly, J.N., 2020. Uranium isotope compositions of biogenic carbonates – Implications for U uptake in shells and the application of the paleo-ocean oxygenation proxy. Geochim. Cosmochim. Acta 287, 50–64. https://doi.org/10.1016/j.gca.2020.07.005.
Lloyd, N.S., Chenery, S.R.N., Parrish, R.R., 2009. The distribution of depleted uranium contamination in Colonie, NY, USA. Sci. Total Environ. 408, 397–407. https://doi.org/10.1016/j.scitotenv.2009.09.024.
Loss, R.D., Rosman, K.J.R., De Laeter, J.R., Curtis, D.B., Benjamin, T.M., Gancarz, A.J., Maeck, W.J., Delmore, J.E., 1989. Fission-product retentivity in peripheral rocks at the Oklo natural fission reactors. Gabon. Chem. Geol. 76, 71–84. https://doi.org/10.1088/2041-8205/735/2/L37.
Lounsbury, M., 1956. The Natural Abundances of the Uranium Isotopes. Can. J. Chem. 34, 259–264. https://doi.org/10.1139/v56-039.
Lu, X., Kendall, B., Stein, H.J., Li, C., Hannah, J.L., Gordon, G.W., Ove, J., Ebbestad, R., 2017. Marine redox conditions during deposition of Late Ordovician and Early Silurian organic-rich mudrocks in the Siljan ring district , central Sweden. Chem. Geol. 457, 75–94. https://doi.org/10.1016/j.chemgeo.2017.03.015.
Lu, X., Dahl, T.W., Zheng, W., Wang, S., Kendall, B., 2020. Estimating ancient seawater isotope compositions and global ocean redox conditions by coupling the molybdenum and uranium isotope systems of euxinic organic-rich mudrocks. Geochim. Cosmochim. Acta 290, 76–103. https://doi.org/10.1016/j.gca.2020.08.032.
Lu, X., Edwards, C.T., Kendall, B., 2023. No evidence for expansion of global ocean euxinia during the base Stairsian mass extinction event (Tremadocian, Early Ordovician). Geochim. Cosmochim. Acta 341, 116–131. https://doi.org/10.1016/j.gca.2022.11.028.
Maden, C., Trinquier, A., Fauré, A.L., Hubert, A., Pointurier, F., Rickli, J., Bourdon, B., 2018. Design of a prototype thermal ionization cavity source intended for isotope ratio analysis. Int. J. Mass Spectrom. 434, 70–80. https://doi.org/10.1016/j.ijms.2018.09.006.
Mänd, K., Lalonde, S.V., Robbins, L.J., Thoby, M., Paiste, K., Kreitsmann, T., Paiste, P., Reinhard, C.T., Romashkin, A.E., Planavsky, N.J., Kirsimäe, K., Lepland, A., Konhauser, K.O., 2020. Palaeoproterozoic oxygenated oceans following the Lomagundi–Jatuli Event. Nat. Geosci. 13, 302–306. https://doi.org/10.1038/s41561-020-0558-5.
Marin, R.C., Sarkis, J.E.S., Nascimento, M.R.L., 2013. The use of LA-SF-ICP-MS for nuclear forensics purposes: Uranium isotope ratio analysis. J. Radioanal. Nucl. Chem. 295, 99–104. https://doi.org/10.1007/s10967-012-1980-y.
Marquez, Ren T.C., Tissot, François L.H., 2022. COSMO: Double spike optimization for sample-limited analyses of isotopically anomalous materials. Chem. Geol. 612 (5), 121095. https://doi.org/10.1016/j.chemgeo.2022.121095.
Mathew, K., Mason, P., Voeks, A., Narayanan, U., 2012. Uranium isotope abundance ratios in natural uranium metal certified reference material 112-A. Int. J. Mass Spectrom. 315, 8–14. https://doi.org/10.1016/j.ijms.2012.02.005.
Mathew, K.J., O'Connor, G., Hasozbek, A., Kraiem, M., 2013. Total evaporation method for uranium isotope-amount ratio measurements. J. Anal. At. Spectrom. 28, 866–876. https://doi.org/10.1039/c2ja30321c.
McDonald, B.S., Partin, C.A., Sageman, B., Holmden, C., 2022. Uranium isotope reconstruction of ocean deoxygenation during OAE 2 hampered by uncertainties in fractionation factors and local U-cycling. Geochim. Cosmochim. Acta. https://doi.org/10.1016/j.gca.2022.05.010.
Meija, J., Coplen, T.B., Berglund, M., Brand, W.A., De Bièvre, P., Gröning, M., Holden, N.E., Irrgeher, J., Loss, R.D., Walczyk, T., Prohaska, T., 2016. Atomic weights of the elements 2013 (IUPAC Technical Report). Pure Appl. Chem. 88, 265–291. https://doi.org/10.1515/pac-2015-0305.
Merle, R., Amelin, Y., Yin, Q.Z., Huyskens, M.H., Sanborn, M.E., Nagashima, K., Yamashita, K., Ireland, T.R., Krot, A.N., Sieber, M.J., 2020. Exploring the efficiency of stepwise dissolution in removal of stubborn non-radiogenic Pb in chondrule U-Pb dating. Geochim. Cosmochim. Acta 277, 1–20. https://doi.org/10.1016/j.gca.2020.03.010.
Metzger, S.C., Rogers, K.T., Bostick, D.A., McBay, E.H., Ticknor, B.W., Manard, B.T., Hexel, C.R., 2019. Optimization of uranium and plutonium separations using TEVA and UTEVA cartridges for MC-ICP-MS analysis of environmental swipe samples. Talanta 198, 257–262. https://doi.org/10.1016/j.talanta.2019.02.034.
Metzger, S., Manard, B.T., Bostick, D.T., Ticknor, B.W., Rogers, K.T., McBay, E.H., Glasgow, D., Zirakparvar, N.A., Hexel, C., 2021. An Approach to Separating Pu, U, and Ti from High-Purity Graphite for Isotopic Analysis by MC-ICP-MS. J. Anal. At. Spectrom. 36 (6), 1150–1158. https://doi.org/10.1039/D1JA00079A.
Meyers, L.A., LaMont, S.P., Stalcup, A.M., Spitz, H.B., 2014. Uranium isotopic signatures measured in samples of dirt collected at two former uranium facilities. J. Radioanal. Nucl. Chem. 301, 307–313. https://doi.org/10.1007/s10967-014-3187-x.
Minteer, M., Winkler, P., Wyatt, B., Moreland, S., Johnson, J., Winters, T., 2007. Reliability of using $^{238}U/^{235}U$ and $^{234}U/^{238}U$ ratios from alpha spectrometry as qualitative indicators of enriched uranium contamination. Health Phys. 92, 488–495. https://doi.org/10.1097/01.HP.0000254847.21026.7c.
Mishra, S., Kasar, S., Takamasa, A., Veerasamy, N., Sahoo, S.K., 2019. Measurement of uranium distribution coefficient and $^{235}U/^{238}U$ ratio in soils affected by Fukushima dai-ichi nuclear power plant accident. J. Environ. Radioact. 198, 36–42. https://doi.org/10.1016/j.jenvrad.2018.12.019.
Montoya-Pino, C., Weyer, S., Anbar, A.D., Pross, J., Oschmann, W., van de Schootbrugge, B., Arz, H.W., 2010. Global enhancement of ocean anoxia during oceanic anoxic event 2: A quantitative approach using U isotopes. Geology 38, 315–318. https://doi.org/10.1130/G30652.1.
Murphy, M.J., Stirling, C.H., Kaltenbach, A., Turner, S.P., Schaefer, B.F., 2014. Fractionation of $^{238}U/^{235}U$ by reduction during low temperature uranium mineralisation processes. Earth Planet. Sci. Lett. 388, 306–317. https://doi.org/10.1016/j.epsl.2013.11.034.
Nakanishi, T., Higuchi, N., Nomura, M., Aida, M., Fujii, Y., 1996. Enrichment of U-232 by U(IV)-U(VI) redox ion exchange chromatography. J. Nucl. Sci. Technol. 33, 341–345. https://doi.org/10.1080/18811248.1996.9731914.
Neuilly, M., Bussac, J., Vendryes, G., Frejacques, C., Nief, G., Yvon, J., 1972. Sur l'existence, dans un passé reculé, d'une réaction en chaine naturelle de fissions dans le gisement d'uranium d'Oklo (Gabon). Compte Rendu l'Académie des Sci. 275, 1847–1849.
New Brunswick Laboratory, 2010. Certificate of Analysis, CRM 145 Uranyl (Normal) Nitrate Assay and Isotopic Solution: Argonne, Illinois, New Brunswick Laboratory. U. S. Department of Energy (2 p).
Nier, A.O., 1938. The Isotopic Constitution of Calcium, Titanium, Sulphur and Argon. Phys. Rev. 53, 282–286. https://doi.org/10.1103/PhysRev.53.282.
Nier, A.O., 1939. The isotopic constitution of uranium and the half-lives of uranium isotopes. Phys. Rev 55. https://doi.org/10.1103/PhysRev.55.150.
Nir-El, Y., 2000. Isotopic analysis of uranium in U_3O_8 by passive gamma-ray spectrometry. Appl. Radiat. Isot. 52, 753–757. https://doi.org/10.1016/S0969-8043(99)00240-7.
Nomura, M., Higuchi, N., Fujii, Y., 1996. Mass dependence of uranium isotope effects in the U(IV)-U(VI) exchange reaction. J. Am. Chem. Soc. 118, 9127–9130. https://doi.org/10.1021/ja954075s.
Noordmann, J., Weyer, S., Montoya-Pino, C., Dellwig, O., Neubert, N., Eckert, S., Paetzel, M., Böttcher, M.E., 2015. Uranium and molybdenum isotope systematics in modern euxinic basins: Case studies from the central Baltic Sea and the Kyllaren fjord (Norway). Chem. Geol. 396, 182–195. https://doi.org/10.1016/j.chemgeo.2014.12.012.
Noordmann, J., Weyer, S., Georg, R.B., Jöns, S., Sharma, M., 2016. $^{238}U/^{235}U$ isotope ratios of crustal material, rivers and products of hydrothermal alteration: new insights on the oceanic U isotope mass balance. Isotopes Environ. Health Stud. 52, 141–163. https://doi.org/10.1080/10256016.2015.1047449.
Oliveira, O.P., Sarkis, J.E.S., 2002. Isotope measurements in uranium using a quadrupole inductively coupled plasma mass spectrometer (ICPMS). J. Radioanal. Nucl. Chem. 253, 345–350. https://doi.org/10.1023/A:1020444814314.
Ostrander, C.M., Kendall, B., Gordon, G.W., Nielsen, S.G., Zheng, W., Anbar, A.D., 2022. Shale heavy metal isotope records of low environmental O_2 between two archean oxidation events. Front. Earth Sci. 10. https://doi.org/10.3389/feart.2022.833609.
Pan, W., Cao, M., Du, Y., Cheng, M., Zhou, Y., Algeo, T.J., Zhao, M., Thibault, N., Li, C., Wei, G., Dahl, T.W., 2021. Paired U and Mo isotope evidence for pervasive anoxia in the Cryogenian early interglacial ocean. Precambrian Res. 361, 106244. https://doi.org/10.1016/j.precamres.2021.106244.
Pappas, R.S., Ting, B.G., Paschal, D.C., 2003. A practical approach to determination of low concentration uranium isotope ratios in small volumes of urine. J. Anal. At. Spectrom. 18, 1289–1292. https://doi.org/10.1039/b305515a.
Parrish, R.R., Thirlwall, M.F., Pickford, C., Horstwood, M., Gerdes, A., Anderson, J., Coggon, D., 2006. Determination of $^{238}U/^{235U}$, $^{236}U/^{238}U$ and uranium concentration in urine using SF-ICP-MS and MC-ICP-MS: an interlaboratory comparison. Health Phys. 90, 127–138. Available at: https://doi.org/10.1097/01.HP.0000174809.43871.54.
Pazukhin, E.M., Rudya, K.G., 2002. Isotopic composition of uranium in lava-like fuel-containing masses from the fourth block and radioactive fallout of the chernobyl NPP service area. Radiochemistry 44, 621–625. https://doi.org/10.1023/A:1022348914071.
Peńkin, M., Boulyga, S., Dabbs, B., Fischer, D., Humphrey, M., Kochetkov, A., Koepf, A., Sturm, M., 2018. Isotopic composition of commercially available uranium chemicals and elemental analysis standards. J. Radioanal. Nucl. Chem. 316, 791–798. https://doi.org/10.1007/s10967-018-5740-5.
Peres, P., Hedberg, P.M.L., Walton, S., Montgomery, N., Cliff, J.B., Rabemananjara, F., Schuhmacher, M., 2013. Nuclear safeguards applications using LG-SIMS with automated screening capabilities. Surf. Interface Anal. 45, 561–565. https://onlinelibrary.wiley.com/doi/10.1002/sia.5015.

Phan, T.T., Gardiner, J.B., Capo, R.C., Stewart, B.W., 2018. Geochemical and multi-isotopic (87Sr/86Sr, $^{143}Nd/^{144}Nd$, $^{238}U/^{235}U$) perspectives of sediment sources, depositional conditions, and diagenesis of the Marcellus Shale, Appalachian Basin, USA. Geochim. Cosmochim. Acta 222, 187–211. https://doi.org/10.1016/j.gca.2017.10.021.

Pimentel-Galvan, M., Lau, K.V., Maher, K., Mukerji, T., Lehrmann, D.J., Altiner, D., Payne, J.L., 2022. Duration and Intensity of End-Permian Marine Anoxia. *Geochemistry*. Geophys. Geosystems 23, 1–19. https://doi.org/10.1029/2021gc010130.

Placzek, C.J., Heikoop, J.M., House, B., Linhoff, B.S., Pelizza, M., 2016. Uranium isotope composition of waters from South Texas uranium ore deposits. Chem. Geol. 437, 44–55. https://doi.org/10.1016/j.chemgeo.2016.05.008.

Pointurier, F., Pottin, A., Hubert, A., 2011. Application of nanosecond-UV laser ablation–inductively coupled plasma mass spectrometry for the isotopic analysis of single submicrometer-size uranium particles. Anal. Chem. 83, 7841–7848. https://pubs.acs.org/doi/10.1021/ac201596t.

Pointurier, F., Hubert, A., Pottin, A.C., 2013. Performance of laser ablation: Quadrupole-based ICP-MS coupling for the analysis of single micrometric uranium particles. J. Radioanal. Nucl. Chem. 296, 609–616. https://doi.org/10.1021/ac201596t.

Pöml, P., Burakov, B., Geisler, T., Walker, C.T., Grange, M.L., Nemchin, A.A., Berndt, J., Fonseca, R.O.C., Bottomley, P.D.W., Hasnaoui, R., 2013. Micro-analytical uranium isotope and chemical investigations of zircon crystals from the Chernobyl "lava" and their nuclear fuel inclusions. J. Nucl. Mater. 439, 51–56. https://doi.org/10.1016/j.jnucmat.2013.03.031.

Quemet, A., Maloubier, M., Dalier, V., Ruas, A., 2014. Development of an analysis method of minor uranium isotope ratio measurements using electron multipliers in Thermal Ionization Mass Spectrometry. Int. J. Mass Spectrom. 374, 26–32. https://doi.org/10.1016/j.ijms.2014.10.008.

Quemet, A., Maloubier, M., Ruas, A., 2016. Contribution of the Faraday cup coupled to 1012 Ω current amplifier to uranium 235/238 and 234/238 isotope ratio measurements by thermal ionization mass spectrometry. Int. J. Mass Spectrom. 404, 35–39. https://doi.org/10.1016/j.ijms.2016.04.005.

Rademacher, L.K., Lundstrom, C.C., Johnson, T.M., Sanford, R.A., Zhao, J., Zhang, Z., 2006. Experimentally determined uranium isotope fractionation during reduction of hexavalent U by bacteria and zero valent iron. Environ. Sci. Technol. 40, 6943–6948. https://doi.org/10.1021/es0604360.

Ranebo, Y., Eriksson, M., Tamborini, G., Niagolova, N., Bildstein, O., Betti, M., 2007. The use of SIMS and SEM for the characterization of individual particles with a matrix originating from a nuclear weapon. Microsc. Microanal. 13, 179–190. https://doi.org/10.1017/S1431927607070353.

Ranebo, Y., Hedberg, P.M.L., Whitehouse, M.J., Ingeneri, K., Littmann, S., 2009. Improved isotopic SIMS measurements of uranium particles for nuclear safeguard purposes. J. Anal. At. Spectrom. 24, 277–287. https://doi.org/10.1039/b810474c.

Richter, S., Goldberg, S.A., 2003. Improved techniques for high accuracy isotope ratio measurements of nuclear materials using thermal ionization mass spectrometry. Int. J. Mass Spectrom. 229, 181–197. https://doi.org/10.1016/S1387-3806(03)00338-5.

Richter, S., Alonso, A., De Bolle, W., Wellum, R., Taylor, P.D., 1999a. Isotopic "fingerprints" for natural uranium ore samples. Int. J. Mass Spectrom. 193, 9–14. https://doi.org/10.1016/S1387-3806(99)00102-5.

Richter, S., Alonso, A., Wellum, R., Taylor, P.D.P., 1999b. The isotopic composition of commercially available uranium chemical reagents. J. Anal. At. Spectrom. 14, 889–891. https://doi.org/10.1039/a900774a.

Richter, S., Alonso, A., Bolle, W., De, Kühn H., Verbruggen, A., Wellum, R., Taylor, P.D.P., 2005. Re-certification of a series of uranium isotope reference materials: IRMM-183, IRMM-184, IRMM-185, IRMM-186 and IRMM-187. Int. J. Mass Spectrom. 247, 37–39. https://doi.org/10.1016/j.ijms.2005.07.008.

Richter, S., Alonso, A., Truyens, J., Kühn, H., Verbruggen, A., Wellum, R., 2006. Certification report: REIMEP 18 inter-laboratory comparison for the measurement of uranium isotopic ratios in nitric acid solution. European Commission Joint Research Centre, Scientific and Technical Research Series: EUR 22244 EN. https://joint-research-centre.ec.europa.eu/system/files/2013-05/eur22244en.pdf.

Richter, S., Alonso-Munoz, A., Eykens, R., Jacobsson, U., Kuehn, H., Verbruggen, A., Aregbe, Y., Wellum, R., Keegan, E., 2008. The isotopic composition of natural uranium samples-Measurements using the new $n(^{233}U)/n(^{236}U)$ double spike IRMM-3636. Int. J. Mass Spectrom. 269, 145–148. https://doi.org/10.1016/j.ijms.2007.09.012.

Richter, S., Eykens, R., Kühn, H., Aregbe, Y., Verbruggen, A., Weyer, S., 2010. New average values for the $n(^{238}U)/n(^{235}U)$ isotope ratios of natural uranium standards. Int. J. Mass Spectrom. 295, 94–97. https://doi.org/10.1016/j.ijms.2010.06.004.

Richter, S., Kühn, H., Aregbe, Y., Hedberg, M., Horta-Domenech, J., Mayer, K., Zuleger, E., Bürger, S., Boulyga, S., Köpf, A., Poths, J., Mathew, K., 2011. Improvements in routine uranium isotope ratio measurements using the modified total evaporation method for multi-collector thermal ionization mass spectrometry. J. Anal. At. Spectrom. 26, 550–564. https://doi.org/10.1039/c0ja00173b.

Richter, S., Venchiarutti, C., Hennessy, C., Jacobsson, U., Bujak, R., Truyens, J., Aregbe, Y., 2018. Preparation and certification of the uranium nitrate solution reference materials series IRMM-2019 to IRMM-2029 for the isotopic composition. J. Radioanal. Nucl. Chem. 318, 1359–1368. https://doi.org/10.1007/s10967-018-6166-9.

Rodríguez-Alvarez, M.J., Sánchez, F., 1995. Behavior of uranium along Jucar River (Eastern Spain): Determination of $^{234}U/^{238}U$ and $^{235}U/^{238}U$ ratios. J. Radioanal. Nucl. Chem. Artic. 190, 113–120. https://doi.org/10.1007/BF02035642.

Roebbert, Y., Rosendahl, C.D., Brown, A., Schippers, A., Bernier-latmani, R., Weyer, S., 2021. Uranium isotope fractionation during the anoxic mobilization of noncrystalline U (IV) by ligand complexation. Environ. Sci. Technol. 55 (12), 7959–7969. https://doi.org/10.1021/acs.est.0c08623.

Romaniello, S.J., Herrmann, A.D., Anbar, A.D., 2013. Uranium concentrations and $^{238}U/^{235}U$ isotope ratios in modern carbonates from the Bahamas: Assessing a novel paleoredox proxy. Chem. Geol. 362, 305–316. https://doi.org/10.1016/j.chemgeo.2013.10.002.

Ronzani, A.L., Hubert, A., Pointurier, F., Marie, O., Clavier, N., Humbert, A.C., Aupiais, J., Dacheux, N., 2019. Determination of the isotopic composition of single sub-micrometer-sized uranium particles by laser ablation coupled with multi-collector inductively coupled plasma mass spectrometry. Rapid Commun. Mass Spectrom. 33, 419–428. https://doi.org/10.1002/rcm.8366.

Rosholt, J.N., Tatsumoto, M., 1970. Isotopic composition of uranium and thorium in Apollo 11 samples. Proc. Apollo 11 Lunar Sci. Conf. 2, 1499–1502.

Rosholt, J.N., Tatsumoto, M., 1971. Isotopic composition of thorium and uranium in Apollo 12 samples. In: Proceedings of the Second Lunar Science Conference, pp. 1577–1584.

Rosholt, J.N., Shields, W.R., Garner, E.L., 1963. Isotopic fractionation of uranium in sandstone. Science 139, 224–226. Available at: https://doi.org/10.1126/science.139.3551.224.

Rosholt, J.N., Butler, A.P., Garner, E.L., Shields, W.R., 1965. Isotope fractionation of uranium in sandstone, Powder River basin, Wyoming, and Slick Rock District, Colorado. Econ. Geol. 60, 199–213. https://doi.org/10.2113/gsecongeo.60.2.199.

Roth, E., 1977. The discovery and study of the nuclear reactor in Oklo. J. Radioanal. Chem. 37, 65–78. https://doi.org/10.1007/BF02520518.

Rovan, L., Štrok, M., 2019. Optimization of the sample preparation and measurement protocol for the analysis of uranium isotopes by MC-ICP-MS without spike addition. J. Anal. At. Spectrom. 34, 1882–1891. https://doi.org/10.1039/c9ja00144a.

Rudge, J.F., Reynolds, B.C., Bourdon, B., 2009. The double spike toolbox. Chem. Geol. 265, 420–431. https://doi.org/10.1016/j.chemgeo.2009.05.010.

Sahoo, S.K., Yonehara, H., Kurotaki, K., Fujimoto, K., Nakamura, Y., 2002. Precise determination of 235U/238U isotope ratio in soil samples by using thermal ionisation mass spectrometry. J. Radioanal. Nucl. Chem. 241–245. https://doi.org/10.1023/A:1015745717871.

Sahoo, S.K., Nakamura, Y., Shiraishi, K., Masuda, A., 2004. Accurate measurement of uranium isotope ratios in soil samples using thermal ionization mass spectrometry equipped with a warp energy filter. Int. J. Environ. Anal. Chem. 84, 919–926. https://doi.org/10.1080/03067310410001729015.

Sahoo, S.K., Yoshida, S., Tokonami, S., Yonehara, H., Tsygankov, N.Y., Zamostyan, P.V., 2009. Isotopic composition of uranium in soil and ground water samples collected around 30 km Chernobyl exclusion zone. Radioprotection 44, 785–790. https://doi.org/10.1051/radiopro/20095141.

Schauble, E.A., 2007. Role of nuclear volume in driving equilibrium stable isotope fractionation of mercury, thallium, and other very heavy elements. Geochim. Cosmochim. Acta 71, 2170–2189. https://doi.org/10.1016/j.gca.2007.02.004.

Schramel, P., 2002. Determination of ^{235}U and ^{238}U in urine samples using sector field inductively coupled plasma mass spectrometry. J. Chromatogr. B Anal. Technol. Biomed. Life Sci. 778, 275–278. https://doi.org/10.1016/S0378-4347(01)00462-5.

Senftle, F., Stieff, L., Cuttitta, F., Kuroda, P., 1957. Comparison of the isotopic abundance of U^{235} and U^{238} and the radium activity ratios in Colorado Plateau uranium ores. Geochim. Cosmochim. Acta 11, 189–193. https://doi.org/10.1016/0016-7037(57)90081-9.

Shibahara, Y., Kubota, T., Fujii, T., Fukutani, S., Takamiya, K., Konno, M., Mizuno, S., Yamana, H., 2016. Determination of isotopic ratios of plutonium and uranium in soil samples by thermal ionization mass spectrometry. J. Radioanal. Nucl. Chem. 307, 2281–2287. https://doi.org/10.1007/s10967-015-4551-1.

Shiel, A.E., Laubach, P.G., Johnson, T.M., Lundstrom, C.C., Long, P.E., Williams, K.H., 2013. No measurable changes in $^{238}U/^{235}U$ due to desorption-adsorption of U(VI) from groundwater at the Rifle, Colorado, integrated field research challenge site. Environ. Sci. Technol. 47, 2535–2541. https://doi.org/10.1021/es303913y.

Shiel, A.E., Johnson, T.M., Lundstrom, C.C., Laubach, P.G., Long, P.E., Williams, K.H., 2016. Reactive transport of uranium in a groundwater bioreduction study: Insights from high-temporal resolution $^{238}U/^{235}U$ data. Geochim. Cosmochim. Acta 187, 218–236. https://doi.org/10.1016/j.gca.2016.05.020.

Shimamura, T., Lugmair, G.W., 1981. U-isotopic abundances. Lunar and Planetary Science Conference 976–978.

Shimokaua, J., Kobayashi, F., 1970. Separation of uranium isotopes by chemical exchange. Isot. Isot. Environ. Heal. Stud. 6, 170–176. https://doi.org/10.1080/10256017008621706.

Shinonaga, T., Esaka, F., Magara, M., Klose, D., Donohue, D., 2008. Isotopic analysis of single uranium and plutonium particles by chemical treatment and mass spectrometry. Spectrochim. Acta - Part B At. Spectrosc. 63, 1324–1328. https://doi.org/10.1016/j.sab.2008.09.001.

Shollenberger, Q.R., Wittke, A., Render, J., Mane, P., Schuth, S., Weyer, S., Gussone, N., Wadhwa, M., Brennecka, G.A., 2019. Combined mass-dependent and nucleosynthetic isotope variations in refractory inclusions and their mineral separates to determine their original Fe isotope compositions. Geochim. Cosmochim. Acta 263, 215–234. https://doi.org/10.1016/j.gca.2019.07.021.

Smith, L.A., 1961. Variations in the uranium-235 content of fifteen ores., Oak Ridge Gaseous Diffusion Plant. Union Carbide Nuclear Company.

Snow, J.E., Friedrich, J.M., 2005. Multiple ion counting ICPMS double spike method for precise U isotopic analysis at ultra-trace levels. Int. J. Mass Spectrom. 242, 211–215. https://doi.org/10.1016/j.ijms.2004.11.024.

Sobotovich, E.V., Bondarenko, G.N., 2001. Isotopic composition of uranium in the products of accidental ejection from the chernobyl NPP. In: Radionuclides and Heavy Metals in Environment. Springer, Netherlands, Dordrecht, pp. 77–84. https://doi.org/10.1007/978-94-010-0993-5_12.

Song, Hue, Song, Haijun, Algeo, T.J., Tong, J., Romaniello, S.J., Zhu, Y., Chu, D., Gong, Y., Anbar, A.D., 2017. Uranium and carbon isotopes document global-ocean

redoxproductivity relationships linked to cooling during the Frasnian- Famennian mass extinction. Geology 45, 887–890. https://doi.org/10.1130/G39393.1.
Spano, T.L., Simonetti, A., Balboni, E., Dorais, C., Burns, P.C., 2017. Trace element and U isotope analysis of uraninite and ore concentrate: Applications for nuclear forensic investigations. Appl. Geochemistry 84, 277–285. https://doi.org/10.1016/j.apgeochem.2017.07.003.
Spivak-Birndorf, L.J., Bouvier, A., Benedix, G.K., Hammond, S., Brennecka, G.A., Howard, K., Rogers, N., Wadhwa, M., Bland, P.A., Spurný, P., Towner, M.C., 2015. Geochemistry and chronology of the bunburra rockhole ungrouped achondrite. Meteorit. Planet. Sci. 50, 958–975. https://doi.org/10.1111/maps.12443.
Stebelkov, V., Elantyev, I., Hedberg, M., Wallenius, M., Fauré, A.L., 2018. Determination of isotopic composition of uranium in the CMX-4 samples by SIMS. J. Radioanal. Nucl. Chem. 315, 417–423. https://doi.org/10.1007/s10967-017-5664-5.
Stefánka, Z., Katona, R., Varga, Z., 2008. Laser ablation assisted ICP-MS as a tool for rapid categorization of seized uranium oxide materials based on isotopic composition determination. J. Anal. At. Spectrom. 23, 1030–1033. https://doi.org/10.1039/b804199g.
Steiger, R.H., Jäger, E., 1977. Subcommission on geochronology: Convention on the use of decay constants in geo- and cosmochronology. Earth Planet. Sci. Lett. 36, 359–362. https://doi.org/10.1016/0012-821X(77)90060-7.
Stirling, C.H., Halliday, A.N., Porcelli, D., 2005. In search of live ^{247}Cm in the early solar system. Geochim. Cosmochim. Acta 69, 1059–1071. https://doi.org/10.1016/j.gca.2004.06.034.
Stirling, C.H., Halliday, A.N., Potter, E.K., Andersen, M.B., Zanda, B., 2006. A low initial abundance of ^{247}Cm in the early solar system and implications for r-process nucleosynthesis. Earth Planet. Sci. Lett. 251, 386–397. https://doi.org/10.1016/j.epsl.2006.09.023.
Stirling, C.H., Andersen, M.B., Potter, E.-K., Halliday, A.N., 2007. Low-temperature isotopic fractionation of uranium. Earth Planet. Sci. Lett. 264, 208–225. https://doi.org/10.1016/j.epsl.2007.09.019.
Stirling, C.H., Andersen, M.B., Warthmann, R., Halliday, A.N., 2015. Isotope fractionation of ^{238}U and ^{235}U during biologically-mediated uranium reduction. Geochim. Cosmochim. Acta 163, 200–218. https://doi.org/10.1016/j.gca.2015.03.017.
Stockey, R.G., Cole, D.B., Planavsky, N.J., Loydell, D.K., Frýda, J., Sperling, E.A., 2020. Persistent global marine euxinia in the early Silurian. Nat. Commun. 11, 1804. https://doi.org/10.1038/s41467-020-15400-y.
Stylo, M., Neubert, N., Roebbert, Y., Weyer, S., Bernier-Latmani, R., 2015a. Mechanism of Uranium Reduction and Immobilization in Desulfovibrio vulgaris Biofilms. Environ. Sci. Technol. 49, 10553–10561. https://doi.org/10.1021/acs.est.5b01769.
Stylo, M., Neubert, N., Wang, Y., Monga, N., Romaniello, S.J., Weyer, S., Bernier-Latmani, R., 2015b. Uranium isotopes fingerprint biotic reduction. Proc. Natl. Acad. Sci. U. S. A. 112, 5619–5624. https://doi.org/10.1073/pnas.1421841112.
Sus, F., Krtil, J., Bulovič, V., Klosová, E., Maksimovič, Z., 1979. Determination of isotopic composition and concentration of uranium, plutonium and neodymium by mass-spectrometric isotope dilution in the irradiated fuel of the Czechoslovak atomic power station A-1. J. Radioanal. Chem. 51, 143–151. https://doi.org/10.1007/BF02519932.
Suzuki, D., Saito-Kokubu, Y., Sakurai, S., Lee, C.G., Magara, M., Iguchi, K., Kimura, T., 2010. A new method for isotope ratio measurement of uranium in trace amount by thermal ionization mass spectrometry: The continuous heating method. Int. J. Mass Spectrom. 294, 23–27. https://doi.org/10.1016/j.ijms.2010.04.007.
Tamborini, G., 2004. SIMS analysis of uranium and actinides in microparticles of different origin. Microchim. Acta 145, 237–242. https://doi.org/10.1007/s00604-003-0160-8.
Tamborini, G., Betti, M., Forcina, V., Hiernaut, T., Giovannone, B., Koch, L., 1998. Application of secondary ion mass spectrometry to the identification of single particles of uranium and their isotopic measurement. Spectrochim. Acta Part B At. Spectrosc. 53, 1289–1302. https://doi.org/10.1016/S0584-8547(98)00121-9.
Tang, H., Liu, M.-C., McKeegan, K.D., Tissot, F.L.H., Dauphas, N., 2017. In situ isotopic studies of the U-depleted Allende CAI Curious Marie: Pre-accretionary alteration and the co-existence of ^{26}Al and ^{36}Cl in the early solar nebula. Geochim. Cosmochim. Acta 207, 1–18. https://doi.org/10.1016/j.gca.2017.03.001.
Tatsumoto, M., Rosholt, J.N., 1970. Age of the moon: An isotopic study of uranium-thorium-lead systematics of lunar samples. Science 167, 461–463. https://doi.org/10.1126/science.167.3918.461.
Tatsumoto, M., Shimamura, T., 1980. Evidence for live ^{247}Cm in the early solar system. Nature 286, 118–122. https://doi.org/10.1038/286118a0.
Taylor, R.N., Croudace, I.W., Warwick, P.E., Dee, S.J., 1998. Precise and rapid determination of ^{238}U/^{235}U and uranium concentration in soil samples using thermal ionisation mass spectrometry. Chem. Geol. 144, 73–80. Available at: https://doi.org/10.1016/S0009-2541(97)00118-6.
Telus, M., Dauphas, N., Moynier, F., Tissot, F.L.H., Teng, F.Z., Nabelek, P.I., Craddock, P. R., Groat, L.A., 2012. Iron, zinc, magnesium and uranium isotopic fractionation during continental crust differentiation: The tale from migmatites, granitoids, and pegmatites. Geochim. Cosmochim. Acta 97, 247–265. https://doi.org/10.1016/j.gca.2012.08.024.
Tissot, F.L.H., Dauphas, N., 2015. Uranium isotopic compositions of the crust and ocean: Age corrections, U budget and global extent of modern anoxia. Geochim. Cosmochim. Acta 167, 113–143. https://doi.org/10.1016/j.gca.2015.06.034.
Tissot, F.L.H., Ibañez-Mejia, M., 2021. Unlocking the Single-Crystal Record of Heavy Stable Isotopes. Elements 17 (6), 389–394. https://doi.org/10.2138/gselements.17.6.389.
Tissot, F.L.H., Dauphas, N., Grossman, L., 2016. Origin of uranium isotope variations in early solar nebula condensates. Sci. Adv. 2, e1501400. https://doi.org/10.1126/sciadv.1501400.
Tissot, F.L.H., Dauphas, N., Grove, T.L., 2017. Distinct ^{238}U/^{235}U ratios and REE patterns in plutonic and volcanic angrites: Geochronologic implications and evidence for U isotope fractionation during magmatic processes. Geochim. Cosmochim. Acta 213, 593–617. https://doi.org/10.1016/j.gca.2017.06.045.
Tissot, F.L.H., Chen, C., Go, B.M., Naziemiec, M., Healy, G., Bekker, A., Swart, P.K., Dauphas, N., 2018. Controls of eustasy and diagenesis on the ^{238}U/^{235}U of carbonates and evolution of the seawater (^{234}U/^{238}U) during the last 1.4 Myr. Geochim. Cosmochim. Acta 242, 233–265. https://doi.org/10.1016/j.gca.2018.08.022.
Tissot, F.L.H., Ibañez-Mejia, M., Boehnke, P., Dauphas, N., McGee, D., Grove, T.L., Harrison, T.M., 2019. ^{238}U/^{235}U measurement in single-zircon crystals: Implications for the Hadean environment, magmatic differentiation and geochronology. J. Anal. At. Spectrom. 34, 2035–2052. https://doi.org/10.1039/c9ja00205g.
Todorov, T.I., Xu, H., Ejnik, J.W., Mullick, F.G., Squibb, K., McDiarmid, M.A., Centeno, J. A., 2009. Depleted uranium analysis in blood by inductively coupled plasma mass spectrometry. J. Anal. At. Spectrom. 24, 189–193. https://doi.org/10.1039/b816058a.
Tolmachyov, S.Y., Kuwabara, J., Noguchi, H., 2004. Flow injection extraction chromatography with ICP-MS for thorium and uranium determination in human body fluids. J. Radioanal. Nucl. Chem. 261, 125–131. https://doi.org/10.1023/B:JRNC.0000030945.53499.1c.
Tostevin, R., Clarkson, M.O., Gangl, S., Shields, G.A., Wood, R.A., Bowyer, F., Penny, A. M., Stirling, C.H., 2019. Uranium isotope evidence for an expansion of anoxia in terminal Ediacaran oceans. Earth Planet. Sci. Lett. 506, 104–112. https://doi.org/10.1016/j.epsl.2018.10.045.
Trinquier, A., Maden, C., Fauré, A.L., Hubert, A., Pointurier, F., Bourdon, B., Schönbächler, M., 2019. More than five percent ionization efficiency by cavity source thermal ionization mass spectrometry for uranium subnanogram amounts. Anal. Chem. 91, 6190–6199. https://doi.org/10.1021/acs.analchem.9b00849.
Tripathi, R.M., Sahoo, S.K., Mohapatra, S., Lenka, P., Dubey, J.S., Puranik, V.D., 2013. Study of uranium isotopic composition in groundwater and deviation from secular equilibrium condition. J. Radioanal. Nucl. Chem. 295, 1195–1200. https://doi.org/10.1007/s10967-012-1992-7.
Tuli, J.K., 1995. Nuclear wallet cards. Brookhaven National Laboratory.
Uvarova, Y.A., Kyser, T.K., Geagea, M.L., Chipley, D., 2014. Variations in the uranium isotopic compositions of uranium ores from different types of uranium deposits. Geochim. Cosmochim. Acta 146, 1–17. https://doi.org/10.1016/j.gca.2014.09.034.
Varga, Z., 2008. Application of laser ablation inductively coupled plasma mass spectrometry for the isotopic analysis of single uranium particles. Anal. Chim. Acta 625, 1–7. https://doi.org/10.1016/j.aca.2008.07.012.
Varga, Z., Krachler, M., Nicholl, A., Ernstberger, M., Wiss, T., Wallenius, M., Mayer, K., 2018. Accurate measurement of uranium isotope ratios in solid samples by laser ablation multi-collector inductively coupled plasma mass spectrometry. J. Anal. At. Spectrom. 33, 1076–1080. https://doi.org/10.1039/c8ja00006a.
Veerasamy, N., Takamasa, A., Murugan, R., Kasar, S., Aono, T., Inoue, K., Fukushi, M., Sahoo, S.K., 2020. Chemical separation of uranium and precise measurement of ^{234}U/^{238}U and ^{235}U/^{238}U ratios in soil samples using multi collector inductively coupled plasma mass spectrometry. Molecules 25, 2138. https://doi.org/10.3390/molecules25092138.
Verbruggen, A., Alonso, A., Eykens, R., Kehoe, F., Kuhn, H., Richter, S., Aregbe, Y., 2008. Preparation and certification of IRMM-3636, IRMM-3636a and IRMM-3636b. JRC Scientific and Technical Reports.
Wall, J.D., Krumholz, L.R., 2006. Uranium reduction. Annu. Rev. Microbiol. 60, 149–166. https://doi.org/10.1146/annurev.micro.59.030804.121357.
Wang, X., Johnson, T.M., Lundstrom, C.C., 2015a. Isotope fractionation during oxidation of tetravalent uranium by dissolved oxygen. Geochim. Cosmochim. Acta 150, 160–170. https://doi.org/10.1016/j.gca.2014.12.007.
Wang, X., Johnson, T.M., Lundstrom, C.C., 2015b. Low temperature equilibrium isotope fractionation and isotope exchange kinetics between U(IV) and U(VI). Geochim. Cosmochim. Acta 158, 262–275.
Wang, X., Planavsky, N.J., Reinhard, C.T., Hein, J.R., Johnson, T.M., 2016. A cenozoic seawater redox record derived from ^{238}U/^{235}U in ferromanganese crusts. Am. J. Sci. 315, 64–83. https://doi.org/10.1016/j.gca.2018.07.024.
Wang, X., Planavsky, N.J., Hofmann, A., Saupe, E.E., De Corte, B.P., Philippot, P., LaLonde, S.V., Jemison, N.E., Zou, H., Ossa, F.O., Rybacki, K., Alfimova, N., Larson, M.J., Tsikos, H., Fralick, P.W., Johnson, T.M., Knudsen, A.C., Reinhard, C.T., Konhauser, K.O., 2018. A Mesoarchean shift in uranium isotope systematics. Geochim. Cosmochim. Acta 238, 438–452. https://doi.org/10.1016/j.gca.2018.07.024.
Wang, X., Ossa, F., Hofmann, A., Agangi, A., Paprika, D., Planavsky, N.J., 2020. Uranium isotope evidence for Mesoarchean biological oxygen production in shallow marine and continental settings. Earth Planet. Sci. Lett. 551, 116583. https://doi.org/10.1016/j.epsl.2020.116583.
Wang, W., Zhang, F., Shen, S., Bizzarro, M., Garbelli, C., Zheng, Q., Zhang, Y., Yuan, D., Shi, Y., Cao, M., Dahl, T.W., 2022. Constraining marine anoxia under the extremely oxygenated Permian atmosphere using uranium isotopes in calcitic brachiopods and marine carbonates. Earth Planet. Sci. Lett. 594, 117714. https://doi.org/10.1016/j.epsl.2022.117714.
Warneke, T., Croudace, I.W., Warwick, P.E., Taylor, R.N., 2002. A new ground-level fallout record of uranium and plutonium isotopes for northern temperate latitudes. Earth Planet. Sci. Lett. 203, 1047–1057. https://doi.org/10.1016/S0012-821X(02)00930-5.
Wasserburg, G.J., Papanastassiou, D.A., Nenow, E.V., Bauman, C.A., 1969. A Programmable Magnetic Field Mass Spectrometer with On-Line Data Processing. Rev. Sci. Instrum. 40, 288–295. https://doi.org/10.1063/1.1683921.

Wei, G.Y., Planavsky, N.J., Tarhan, L.G., Chen, X., Wei, W., Li, D., Ling, H.F., 2018. Marine redox fluctuation as a potential trigger for the Cambrian explosion. Geology 46, 587–590. https://doi.org/10.1130/G40150.1.

Wei, G.Y., Planavsky, N.J., Tarhan, L.G., He, T., Wang, D., Shields, G.A., Wei, W., Ling, H. F., 2020. Highly dynamic marine redox state through the Cambrian explosion highlighted by authigenic $\delta^{238}U$ records. Earth Planet. Sci. Lett. 544, 116361. https://doi.org/10.1016/j.epsl.2020.116361.

Wei, G., Planavsky, N.J., He, T., Zhang, F., Stockey, R.G., Cole, D.B., Lin, Y., Ling, H., 2021. Global marine redox evolution from the late Neoproterozoic to the early Paleozoic constrained by the integration of Mo and U isotope records. Earth-Science Rev. 214, 103506. https://doi.org/10.1016/j.earscirev.2021.103506.

Weyer, S., Anbar, A.D., Gerdes, A., Gordon, G.W., Algeo, T.J., Boyle, E.A., 2008. Natural fractionation of $^{238}U/^{235}U$. Geochim. Cosmochim. Acta 72, 345–359. https://doi.org/10.1016/j.gca.2007.11.012.

White, D.A., Elrick, M., Romaniello, S., Zhang, F., 2018. Global seawater redox trends during the Late Devonian mass extinction detected using U isotopes of marine limestones. Earth Planet. Sci. Lett. 503, 68–77. https://doi.org/10.1016/j.epsl.2018.09.020.

Xiao, G., Jones, R.L., Saunders, D., Caldwell, K.L., 2014. Determination of $^{234}U/^{238}U$, $^{235}U/^{238}U$ and 236U/238U isotope ratios in urine using sector field inductively coupled plasma mass spectrometry. Radiat. Prot. Dosimetry 162, 618–624. https://doi.org/10.1093/rpd/ncu023.

Yamamoto, M., Kawabata, Y., Murata, Y., Komura, K., 2002. Variation of uranium isotopic composition in soil within the JCO grounds from the 30 September 1999 criticality accident at JCO, Tokai-mura, Japan. Health Phys. 83, 197–203. https://doi.org/10.1097/00004032-200208000-00005.

Yamamoto, K., Asanuma, H., Takahashi, H., Hirata, T., 2021. In situ isotopic analysis of uranium using a new data acquisition protocol for 10^{13}ohm Faraday amplifiers. J. Anal. At. Spectrom. 36, 668–675. https://doi.org/10.1039/d0ja00498g.

Yang, S., Liu, Y., 2016. Nuclear field shift effects on stable isotope fractionation: a review. Acta Geochim. 35, 227–239. https://doi.org/10.1007/s11631-016-0109-3.

Yang, S., Kendall, B., Lu, X., Zhang, F., Zheng, W., 2017. Uranium isotope compositions of mid-Proterozoic black shales: Evidence for an episode of increased ocean oxygenation at 1.36 Ga and evaluation of the effect of post-depositional hydrothermal fluid flow. Precambrian Res. 298, 187–201. https://doi.org/10.1016/j.precamres.2017.06.016.

Yomogida, T., Esaka, F., Magara, M., 2017. Chemical state and isotope ratio analysis of individual uranium particles by a combination of micro-Raman spectroscopy and secondary ion mass spectrometry. Anal. Methods 9, 6261–6266. https://doi.org/10.1039/c7ay01815k.

Zeiri, O., Fruchter, N., Elish, E., Gizbar, H., Shamir, D., Sedgi, I., 2021. Determination of Uranium Isotopic Ratio by ICP-OES Using Optimal Sensitivity Position Analysis. Anal. Chem. 93, 5123–5128. https://doi.org/10.1021/acs.analchem.0c04842.

Zhang, X.Z., Esaka, F., Esaka, K.T., Magara, M., Sakurai, S., Usuda, S., Watanabe, K., 2007. Application of Inductively Coupled Plasma Mass Spectrometry to the determination of uranium isotope ratios in individual particles for nuclear safeguards. Spectrochim Acta - Part B At. Spectrosc. 62, 1130–1134. https://doi.org/10.1016/j.sab.2007.06.013.

Zhang, F., Algeo, T.J., Romaniello, S.J., Cui, Y., Zhao, L., Chen, Z.Q., Anbar, A.D., 2018a. Congruent Permian-Triassic $\delta^{238}U$ records at Panthalassic and Tethyan sites: Confirmation of global-oceanic anoxia and validation of the U-isotope paleoredox proxy. Geology 46, 327–330. https://doi.org/10.1130/G39695.1.

Zhang, F., Romaniello, S.J., Algeo, T.J., Lau, K.V., Clapham, M.E., Richoz, S., Herrmann, A.D., Smith, H., Horacek, M., Anbar, A.D., 2018b. Multiple episodes of extensive marine anoxia linked to global warming and continental weathering following the latest Permian mass extinction. Sci. Adv. 4, 1–10. https://doi.org/10.1126/sciadv.1602921.

Zhang, F., Xiao, S., Kendall, B., Romaniello, S.J., Cui, H., Meyer, M., Gilleaudeau, G.J., Kaufman, A.J., Anbar, A.D., 2018c. Extensive marine anoxia during the terminal Ediacaran Period. Sci. Adv. 4, eaan8983. https://doi.org/10.1126/sciadv.aan8983.

Zhang, F., Algeo, T.J., Cui, Y., Shen, J., Song, H., Sano, H., Rowe, H.D., Anbar, A.D., 2019a. Global-ocean redox variations across the Smithian-Spathian boundary linked to concurrent climatic and biotic changes. Earth-Science Rev. 195, 147–168. Available at: https://doi.org/10.1016/j.earscirev.2018.10.012.

Zhang, F., Xiao, S., Romaniello, S.J., Hardisty, D., Li, C., Melezhik, V., Pokrovsky, B., Cheng, M., Shi, W., Lenton, T.M., Anbar, A.D., 2019b. Global marine redox changes drove the rise and fall of the Ediacara biota. Geobiology 17, 594–610. https://doi.org/10.1111/gbi.12359.

Zhang, F., Dahl, T.W., Lenton, T.M., Luo, G., Shen, S., Algeo, T.J., Planavsky, N., Liu, J., Cui, Y., Qie, W., Romaniello, S.J., Anbar, A.D., 2020a. Extensive marine anoxia associated with the Late Devonian Hangenberg Crisis. Earth Planet. Sci. Lett. 533, 115976. Available at: https://doi.org/10.1016/j.epsl.2019.115976.

Zhang, F., Lenton, T.M., del Rey, Á., Romaniello, S.J., Chen, X., Planavsky, N.J., Clarkson, M.O., Dahl, T.W., Lau, K.V., Wang, W., Li, Z., Zhao, M., Isson, T., Algeo, T. J., Anbar, A.D., 2020b. Uranium isotopes in marine carbonates as a global ocean paleoredox proxy: A critical review. Geochim. Cosmochim. Acta.

Zhang, F., Shen, S., Cui, Y., Lenton, T.M., Dahl, T.W., Zhang, H., Feng, Zheng Q., Wang, W., Krainer, K., Anbar, A.D., 2020c. Two distinct episodes of marine anoxia during the Permian-Triassic crisis evidenced by uranium isotopes in marine dolostones. Geochim. Cosmochim. Acta 287, 165–179. Available at: https://doi.org/10.1016/j.gca.2020.01.032.

Zhang, F., Stockey, R.G., Xiao, S., Shen, S., Dahl, T.W., Wei, G.Y., Cao, M., Li, Z., Kang, J., Cui, Y., Anbar, A.D., Planavsky, N.J., 2022. Uranium isotope evidence for extensive shallow water anoxia in the early Tonian oceans. Earth Planet. Sci. Lett. 583, 117437. https://doi.org/10.1016/j.epsl.2022.117437.

Zhao, H., Algeo, T.J., Liu, Y., Chen, Z.Q., Zhang, L., Hu, Z., Li, Z., 2020. Lower Triassic carbonate δ238U record demonstrates expanded oceanic anoxia during Smithian Thermal Maximum and improved ventilation during Smithian-Spathian boundary cooling event. Palaeogeogr. Palaeoclimatol. Palaeoecol. 539, 109393. https://doi.org/10.1016/j.palaeo.2019.109393.

Zoriy, M.V., Kayser, M., Izmer, A., Pickhardt, C., Becker, J.S., 2005. Determination of uranium isotopic ratios in biological samples using laser ablation inductively coupled plasma double focusing sector field mass spectrometry with cooled ablation chamber. Int. J. Mass Spectrom. 242, 297–302. https://doi.org/10.1016/j.ijms.2004.10.026.